CANADIAN THESES

THÈSES CANADIENNES

NOTICE

The quality of this microfiche is heavily dependent upon the quality of the original thesis submitted for microfilming. Every effort has been made to ensure the highest quality of reproduction possible.

If pages are missing, contact the university which granted the degree.

Some pages may have indistinct print especially if the original pages were typed with a poor typewriter ribbon or if the university sent us an inferior photocopy.

Previously copyrighted materials (journal articles, published tests, etc.) are not filmed.

Reproduction in full or in part of this film is governed by the Canadian Copyright Act, R.S.C. 1970, c. C-30. Please read the authorization forms which accompany this thesis.

AVIS

La qualité de cette microfiche dépend grandement de la qualité de la thèse soumise au microfilmage. Nous avons tout fait pour assurer une qualité supérieure de reproduction.

S'il manque des pages, veuillez communiquer avec l'université qui a conféré le grade.

La qualité d'impression de certaines pages peut laisser à désirer, surtout si les pages originales ont été dactylographiées à l'aide d'un ruban usé ou si l'université nous a fait parvenir une photocopie de qualité inférieure.

Les documents qui font déjà l'objet d'un droit d'auteur (articles de revue, examens publiés, etc.) ne sont pas microfilmés.

La reproduction, même partielle, de ce microfilm est soumise à la Loi canadienne sur le droit d'auteur, SRC 1970, c. C-30. Veuillez prendre connaissance des formules d'autorisation qui accompagnent cette thèse.

THIS DISSERTATION HAS BEEN MICROFILMED EXACTLY AS RECEIVED

LA THÈSE A ÉTÉ MICROFILMÉE TELLE QUE NOUS L'AVONS REÇUE

Canadä

182

PERMISSION TO MICROFILM — AUTORISATION DE MICROFILMER

• Please print or type — Écrire en lettres moulées ou dactylographier

Full Name of Author — Nom complet de l'auteur

JOHN ROBERT PRADKO

Date of Birth — Date de naissance	Country of Birth — Lieu de naissance
3 Feb 1959	United States

Permanent Address — Résidence fixe

5500 Woodmire Drive
Utica, Michigan 48087
U.S.A.

Title of Thesis — Titre de la thèse

THE ELECTROCHEMISTRY OF BILIRUBIN

University — Université

University of Alberta

Degree for which thesis was presented — Grade pour lequel cette thèse fut présentée

M. Sc.

Year this degree conferred — Année d'obtention de ce grade	Name of Supervisor — Nom du directeur de thèse
1983	B. Stanley Pons

Date	Signature
23 June 1983	John R. Pradko

NL-91 (4/77)

THE UNIVERSITY OF ALBERTA

THE ELECTROCHEMISTRY OF BILIRUBIN

by

JOHN ROBERT PRADKO

A THESIS

SUBMITTED TO THE FACULTY OF GRADUATE STUDIES AND RESEARCH

IN PARTIAL FULFILMENT OF THE REQUIREMENTS FOR THE DEGREE

OF MASTER OF SCIENCE

DEPARTMENT OF CHEMISTRY

EDMONTON, ALBERTA

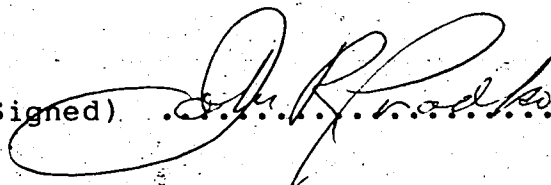FALL, 1983

THE UNIVERSITY OF ALBERTA

RELEASE FORM

NAME OF AUTHOR   John Robert Pradko

TITLE OF THESIS   The Electrochemistry of Bilirubin

DEGREE FOR WHICH THESIS WAS PREPARED   M.Sc.

YEAR THIS DEGREE GRANTED   1983

Permission is hereby granted to THE UNIVERSITY OF ALBERTA LIBRARY to reproduce single copies of this thesis and to lend or sell such copies for private, scholarly or scientific research purposes only.

The author reserves other publication rights, and neither the thesis nor extensive extracts from it may be printed or otherwise reproduced without the author's written permission.

(Signed) ....

PERMANENT ADDRESS

5500 Woodmire Drive,
Utica, Michigan   48087
U.S.A.
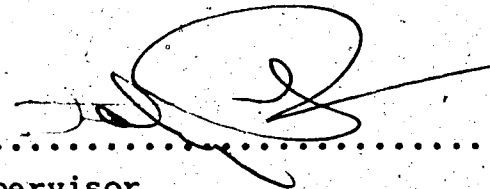
DATE ..23 June 83...

THE UNIVERSITY OF ALBERTA

FACULTY OF GRADUATE STUDIES AND RESEARCH

The undersigned certify that they have read, and
recommend to the Faculty of Graduate Studies and Research,
for acceptance, a thesis entitled THE ELECTROCHEMISTRY OF
BILIRUBIN
submitted by JOHN ROBERT PRADKO in partial fulfilment of the
requirements for the degree of Master of Science.

....
Supervisor

.....Susan Kaufman.....

.....James A. Plambeck.....

DATE June 22, 1983

It is the theory which decides

what we can observe

-Albert Einstein

ABSTRACT

The electrochemistry of bilirubin IX-α in N,N-dimethylformamide (DMF) has been investigated. The oxidation and reduction waves for bilirubin, biliverdin, and purpurin are identified. Using conventional electrochemical techniques, the behavior of this molecule in acidic and basic media is also reported. A detailed investigation was undertaken to determine the mechanism for the electrochemical oxidation of bilirubin. Using conventional modulated specular reflectance spectroscopy (MSRS) along with the recently described ac reflectance technique - sinusoidally modulated alternating current reflectance spectroscopy (SMACRS), the spectra of a number of intermediates have been recorded.

The production of biliverdin during the photo-oxidation of bilirubin is also examined. By monitoring the current, the efficiency of this process in DMF is reported.

I would like to thank my friend and research director Dr. B. Stanley Pons for the opportunity to conduct this research. His guidance, support, and encouragement has contributed greatly to the completion of this work.

I would also like to thank Dr. Jerome F. McAleer - a true scientist and optimist. His interest, inspiration, enthusiasm, and helpful discussions are all truly appreciated.

Special thanks go to Annabelle Wiseman who was able to reduce my sometimes crude handwritten versions to legible typescript.

Finally, I wish to thank my family and friends for their support and interest in this work.

TABLE OF CONTENTS

*****

xii

CHAPTER 1

INTRODUCTION

1.1 INTRODUCTORY REMARKS

Bilirubin is a waste product and apparently of no practical use to the body. Despite this, scientific interest in this bile pigment has been very keen. This interest has been prompted by the fact that bilirubin in high concentrations is a poison. A great deal of work has dealt solely with characterization of the molecule [1-3]. There have also been numerous investigations as to the nature of the biochemical agents which catalyze its formation [4-5]. Recognition of the fact that visible light radiation causes a reduction of bilirubin concentration in blood serum has initiated a large volume of research in this area. The physical aspects [6], mechanisms [7], and products involved in this phenomenon were explored [8-11]. More recently the metabolic [12] and pharmacologic [13] traits have been investigated. Methods of detection and assay procedures for bilirubin have been continually suggested and improved [14-16].

1

While electrochemical methods have proven invaluable in elucidating electron transfer mechanisms and identifying reaction intermediates in many types of organic redox reactions, in recent years few publications have dealt directly with the electrochemistry of bilirubin. This point is less suprising when one examines a typical cyclic voltammogram of the molecule in nonaqueous solvents. Recent advances in electrochemical and spectroelectrochemical techniques, however, now permit precise studies of such complicated electrochemical reactions, and the application of some of these are demonstrated herein.

My interest in bilirubin stems from the apparent interference which the molecule exerts on the oxidative phosphorylation process in the cell mitochondria [17]. By inhibiting the normal cell metabolism, the clinical condition known as kernicterus may eventually result. It is thus of practical interest to initiate a study of the oxidative electrochemistry of this molecule in nonaqueous solvents with a view of adding to the understanding of this serious metabolic interference.

1.2 ~ORIGIN AND CATABOLISM OF BILIRUBIN

The life span of a newborn infant's red blood cell is
shorter than that of an adult's.. As the senescent cells
and their fragments become sequestered in the
reticuloendothelial system, the hemoglobin molecule is
split into two fragments: (1) globin, which enters the
protein metabolic pool and (2) heme, which is further
catabolized. The first step in the degradative process is
the oxidation of the α-carbon methene link of heme by an
enzyme known as heme α-methyl oxygenase [18,19], and the
release of this carbon atom as carbon monoxide. The
cyclic tetrapyrrole formed is immediately converted to an
open-chain tetrapyrrole known as biliverdin IX-α (Figure
1). The latter undergoes enzymatic reduction to
bilirubin. Most of the bilirubin is eventually
transported to the liver, where it is converted
enzymatically into a water soluble diglucuronide (Figure
1), and excreted via the bile into the duodenum [20]. The
diglucuronide is hydrolized in the lower portion of the
intestinal tract to glucuronic acid and bilirubin. The
bilirubin is finally converted by the bacterial flora to a
variety of products: urobilinogen, stercobilinogen,
urobilin and stercobilin. This process is shown
diagramatically in Figure 2.

(a) Biliverdin IX − α

(b) Bilirubin IX − α

(c) Bilirubin IX − α
diglucuronide

GL = glucuryl

Figure 1

Fate of Bilirubin during the Catabolism of A Red Blood Cell
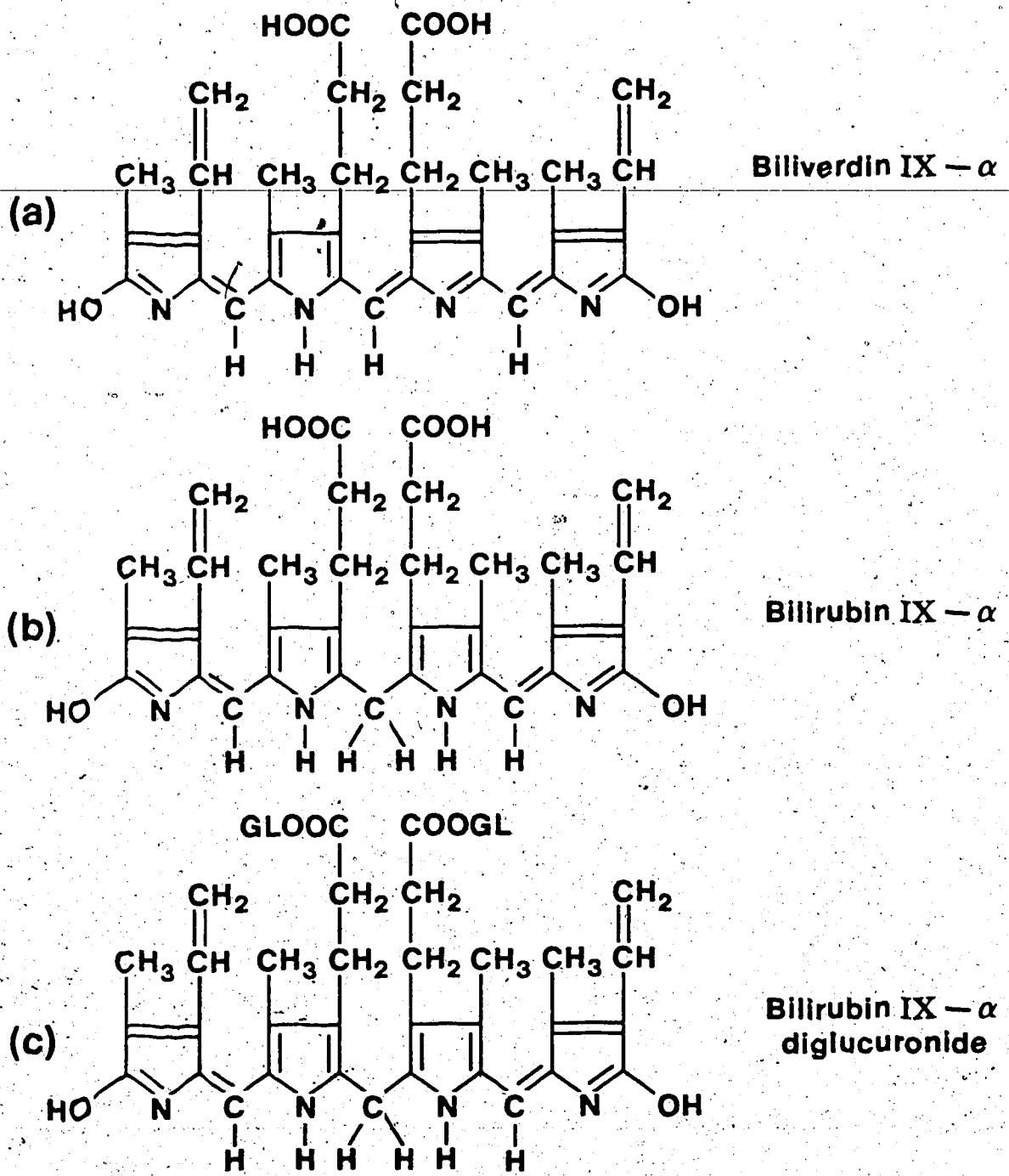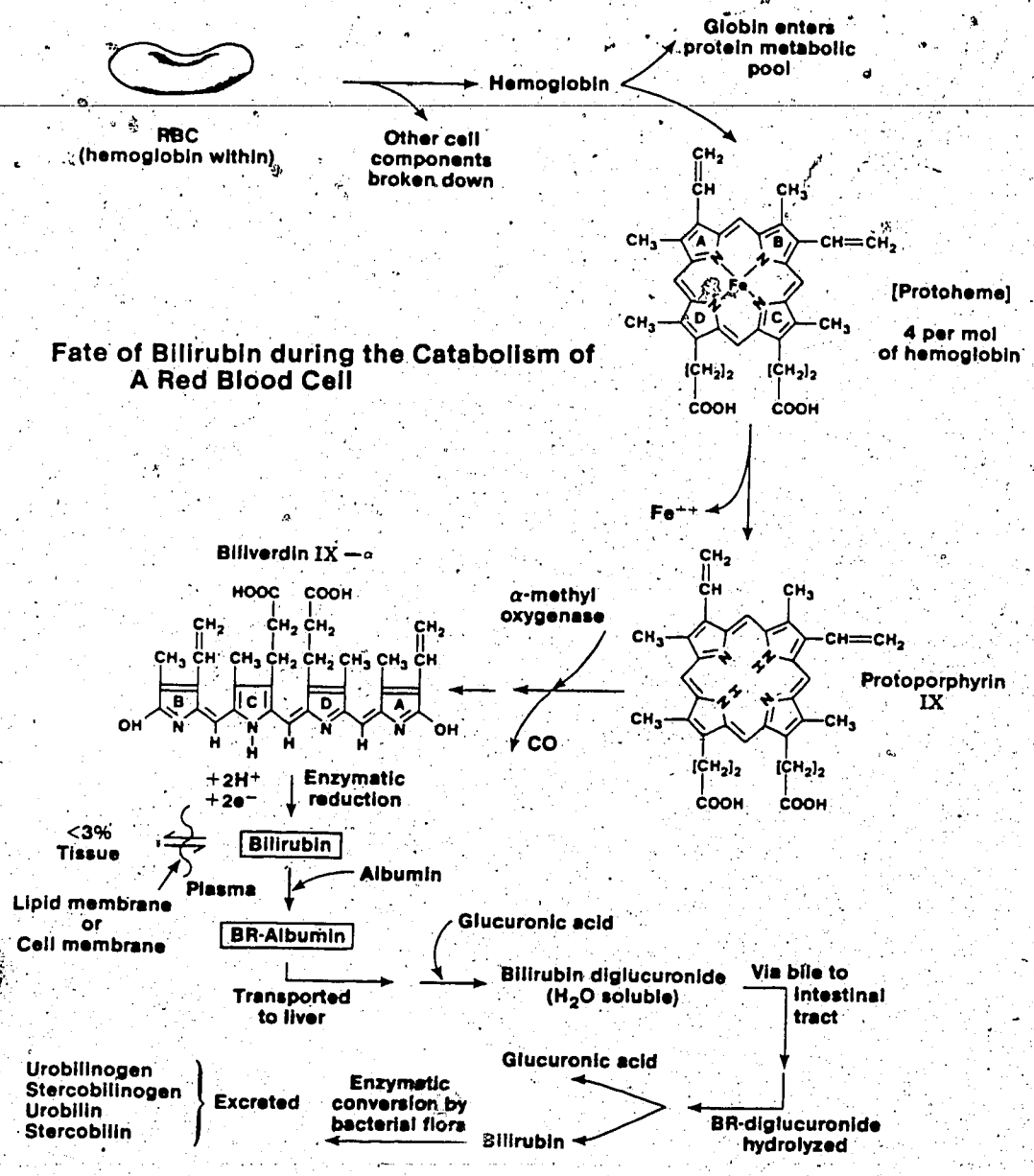
Figure 2

1.3 HISTORY OF BILIRUBIN RESEARCH

Bilirubin was first isolated in crystalline form by Virchow in 1847 [21], and was given its name by Stadeler in 1864 [22]. Its structure was determined by Siedel and Fisher in 1933 [23], and confirmed via total synthesis by Fisher and Plieninger in 1943 [24]. Much of the basic chemistry of this pigment was investigated during the 1940's by the Fisher school [25]. Since that time there have been more than 3000 publications dealing with bilirubin and of these about 400 specifically with some aspect of the chemistry or biochemistry of the molecule. The majority of attention has been directed towards formation, complexation, and photochemistry.

1.4 GENERAL CHEMICAL PROPERTIES OF BILIRUBIN

The chemical structure of bilirubin is shown in Figure 1. It is evident from the structure that by interchanging the substituents on the pyrrole rings, a number of structural isomers of bilirubin can be formed (Figure 3). Few of these many possible entities are known. The only natural isomer is the IX-α. This isomer is so designated because it is derived from ferriprotoporphyrin IX (Figure 2), via cleavage of the porphyrin ring at the α-bridge position.

Bilirubin Isomers

Bilirubin III — α

Bilirubin IX — α

Bilirubin XIII — α
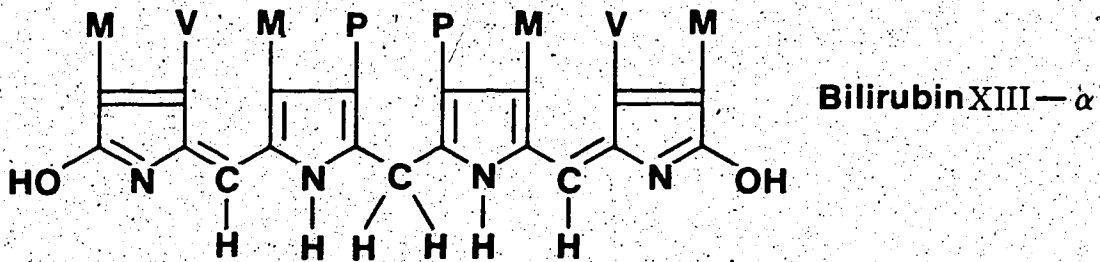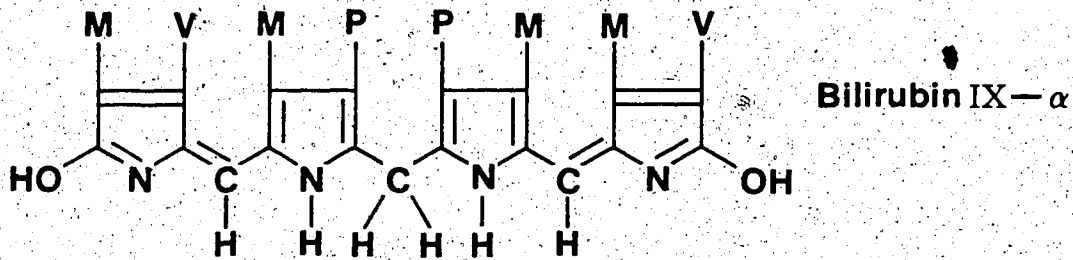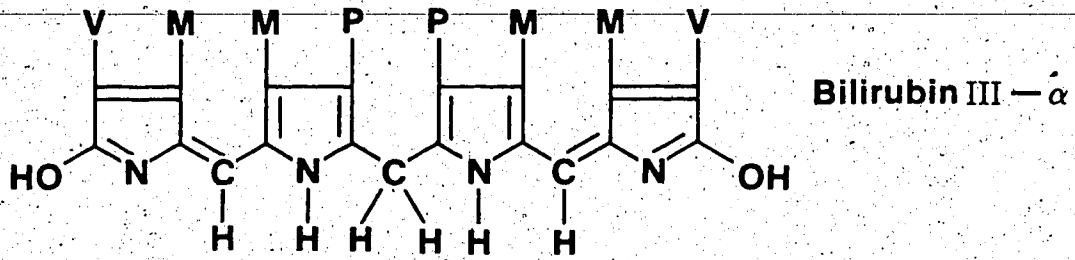
M = methyl, V = vinyl, P = propionic acid

Figure 3

Bilirubin is a stable solid which crystallizes readily from chloroform-methanol solutions. Commercial preparations of the bile pigment, which are generally obtained from animal (oxen) bile, or gallstones may contain other isomers of bilirubin (created during processing) or non-bilirubin material as impurities [26]. Bilirubin which is isomerically homogeneous is easy to purify [27]. The removal of unwanted isomers has been accomplished on a small scale and only by employing thin-layer chromatography [28]. Pure bilirubin is soluble in several organic solvents (e.g. chloroform, methylene chloride, pyridine, dimethylsulfoxide (DMSO), DMF), and is practically insoluble in petroleum ether, methanol or water. Its slight solubility in water increases with pH but is essentially zero below pH 7.0.

The primary chemical properties of bilirubin are somewhat predictable on the basis of its structure. As is shown in Figure 4, the molecule contains two carboxylic acid side-chains (weakly acidic) which should readily form esters. On the lactam positions of the end rings there is a further pair of weakly acidic protons which would be expected to ionize only in strongly alkaline solutions. The central pyrrole rings would be expected to be weakly basic and should support protonation in strong acids. Bilirubin contains a number of double bonds which should

Reducible

Reducible

Reducible

Acidic

HOOC COOH

CH₂ CH₂

CH₂ CH₂

O

N–H

N–H

N–H

N–H

O

Weakly Acidic

Weakly Basic

Weakly Acidic
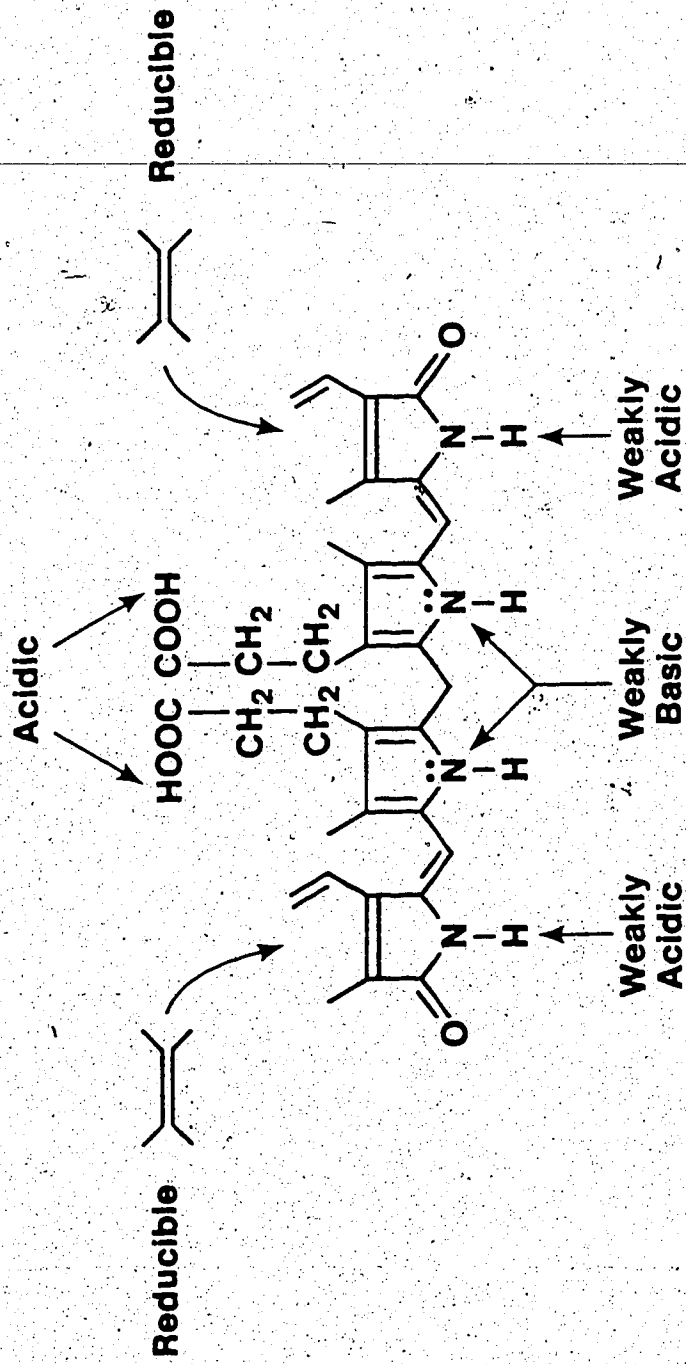
Bilirubin IX–α Functional Groups

Figure 4

be reducible, especially those in the side-chains which are sterically more accessible to reducing agents, and those on the ring ends. The two central aromatic pyrrole rings are expected to be more resistant to reduction. Bilirubin can be thought of as being composed of a pair of dipyrrylmethenes and a dipyrrylmethane. The dipyrrylmethane segment is much less stable and the methane carbon is regarded as the least bonded point in the molecule. The dipyrrylmethane segment may be attacked by electrophiles, and undergoes cleavage about the central $-CH_2-$ bridge in the presence of strong acids. The dipyrrylmethene segments which contain the conjugated π electron systems are responsible for the yellow color of the pigment.

Bilirubin can be readily reduced using sodium amalgam or catalytically hydrogenated using palladium or charcoal [29]. Referring to Figure 5, the hydrogens add two by two, first at the exo-vinyl group (site #1) and then at the endo-vinyl group (site #2). This results in the formation of mesobilirubin. Bilirubin can be further reduced at site #3 which yields colorless urobilinogen, and finally at site #4 producing stercobilinogen. The latter reactions occur in the gut and are catalyzed by bacterial enzymes of the gut flora [30].
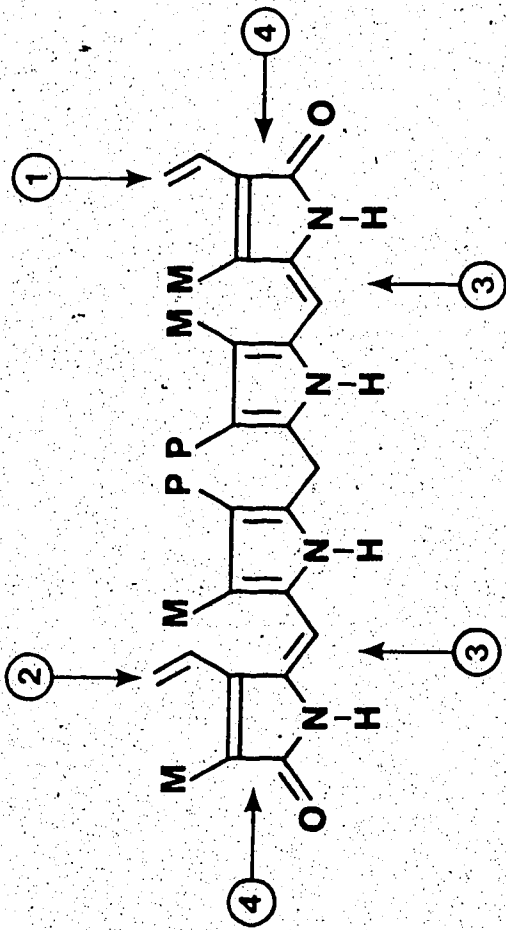
Bilirubin $\xrightarrow{1,2}$ Meso-bilirubin

$\xrightarrow{3}$ Urobilirubin

$\downarrow$ 4

Stercobilinogen

H_2/Pd, Na/Hg — CHEMICALLY

(Gut Flora) — ENZYMATICALLY

Hydrogenation Reduction of Bilirubin IX—α

Figure 5

Bilirubin undergoes a variety of oxidative reactions, a few of which are depicted in Figure 6. When treated with strong oxidizing agents such as potassium permanganate or chromic acid, bilirubin rapidly cleaves forming monopyrrole units. The use of less powerful oxidizing agents such as ferric chloride leads to gentle dehydrogenation of the central bridge producing the fully conjugated biliverdin. The latter oxidant is commonly used for the preparation of biliverdin [31]. The use of benzoquinone and acetic acid in DMSO also works very well [32]. In the dark and in the absence of any other oxidizing agents, bilirubin undergoes spontaneous oxidation with atmospheric oxygen [33]. The auto-oxidation process occurs at a negligible rate in chloroform, but becomes quite pronounced in aqueous alkaline solutions. The mechanism of auto-oxidation has not been determined, but can be easily inhibited by adding oxygen scavengers such as ascorbic acid or EDTA to the reaction solution [34]. A fourth oxidative path is photo-oxidation. This reaction has drawn a great deal of attention due to its medical application in the control of neonatal jaundice. Photodegradation of bilirubin occurs quite rapidly when light of wavelengths 420-460 nm is incident on the molecule. The predominant mechanism appears to be an oxygenation process, whereby bilirubin
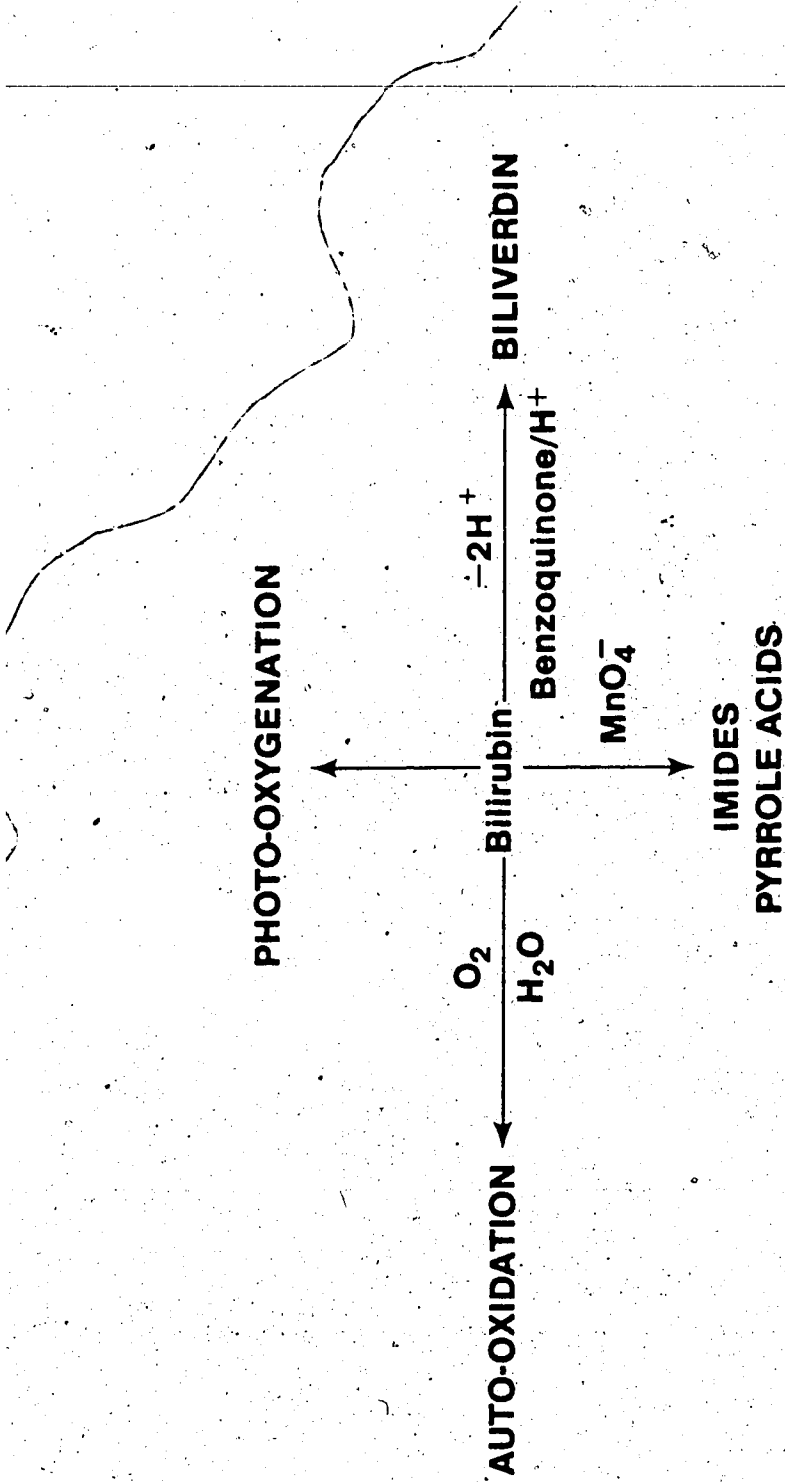
Several Oxidative Reactions of Bilirubin IX — α

Figure 6

acts as a photosensitizer which results ultimately in its own destruction [35]. The overall mechanism is as follows [36]:

Bilirubin + hv → Bilirubin*

Bilirubin* + O_2 → Bilirubin + O_2*

Bilirubin + O_2* → [Bilirubin·O_2*] → Products
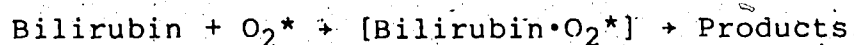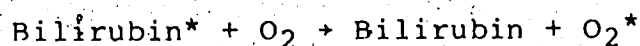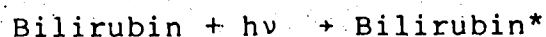
1.5 ELECTROCHEMISTRY OF BILIRUBIN

In his first paper on bilirubin, Van Norman [37] proposed that the purity of bilirubin for use as a clinical standard may be determined through the electrochemical technique of coulometry. His study consisted of monitoring the cyclic voltammetry and visible spectrum of a bilirubin solution during electrolysis. As the electrolysis progressed the cyclic voltammetry indicated that the peak height of the bilirubin oxidation wave decreased. Simultaneous spectra of aliquots indicated that the bilirubin absorbance at λ_{max} = 453 nm diminished as the biliverdin absorbance at λ_{max} = 384 and 650 nm increased in magnitude. The solution of bilirubin was electrolyzed at a constant potential of 0.65 V vs the standard calomel electrode (SCE). The solution was pre-electrolyzed at 0.80 V before addition of the bilirubin, and a background correction of charge per unit time was

made before and after the electrolysis. The calculated

value for the number of electrons passed per bilirubin.

molecule yielded 1.96 ± 0.06. Based on an n value of 2,

controlled potential coulometric analysis of five samples

of bilirubin in DMF gave the theoretical value within

±3%. These results suggest that controlled potential

coulometry may be used as a possible alternative in the

evaluation of the purity of bilirubin as a clinical

standard.

Van Norman also investigated the acid-base properties

of bilirubin in DMF [38]. Titration of bilirubin with

either picric acid or hydrochloric acid showed that it had

no affinity for protons. Titration of bilirubin with the

base tetramethylguanidine (TMG) showed two breaks in the

titration curve. They occurred at 1:1 and 2:1

TMG:bilirubin molar ratios. The spectrum of bilirubin

changed with the addition of base: a bathochromic shift

from 453 nm to 463 nm occurred. The oxidative voltammetry

also showed a change: as base was added, the neutral

bilirubin was quantitatively converted to the dianion.

The two-electron wave at 0.70 V vs SCE shifts to 0.40 V.

The biliverdin oxidation wave appears unchanged. Van

Norman believes that under neutral conditions in DMF,

bilirubin exists as the neutral molecule and thus

maintains intramolecular hydrogen bonding. The neutral

molecule thus maintains a relatively high oxidation

potential and appears inert to complexation. With the

quantitative neutralization of two acidic protons, the

oxidation potential drops to 0.40 V vs SCE. The site of

oxidation of the dianion still appears to be at the

central methene bridge since it was shown to lose two

electrons to form biliverdin as does the neutral

molecule. The removal of two hydrogens seems to disrupt

intra-ring hydrogen bonding and leads to steric changes

which leaves the methene bridge more prone to oxidation.

Therefore the potential shift for oxidation between the

neutral and dianion forms is to be expected. The author

also notes that the chemical oxidation sequence of

bilirubin known as the Gmelin sequence can be directly

observed electrochemically, although he is only able to

report the electrochemical production of the first three

products (see Figure 7).

Cyclic voltammetry, controlled potential coulometry,

and thin layer techniques have been applied to the

electro-reduction and electro-oxidation of bilirubin at

mercury and gold electrodes in DMSO [39,40]. These

workers have shown that bilirubin reduction occurs at two

different sites within the molecule. A thin layer cell

study produced a voltammetric response characteristic of

an e.c.e. mechanism for the oxidation of bilirubin to

Gmelin color sequence observed during biliruin oxidation

M V M P P M M V   **Bilirubin   Yellow**
                   biladiene a,c

$-2e^-$

M V M P P M M V   **Biliverdin   Green**
                   bilatriene

$-2e^-$

M V M P P M M V   **Purpurin   Purple**
                   biladiene -a,b-one-c

$-2e^-$

M V M P P M M V   **Choletellin   Yellow**
                   biladiene -b-one-a,c
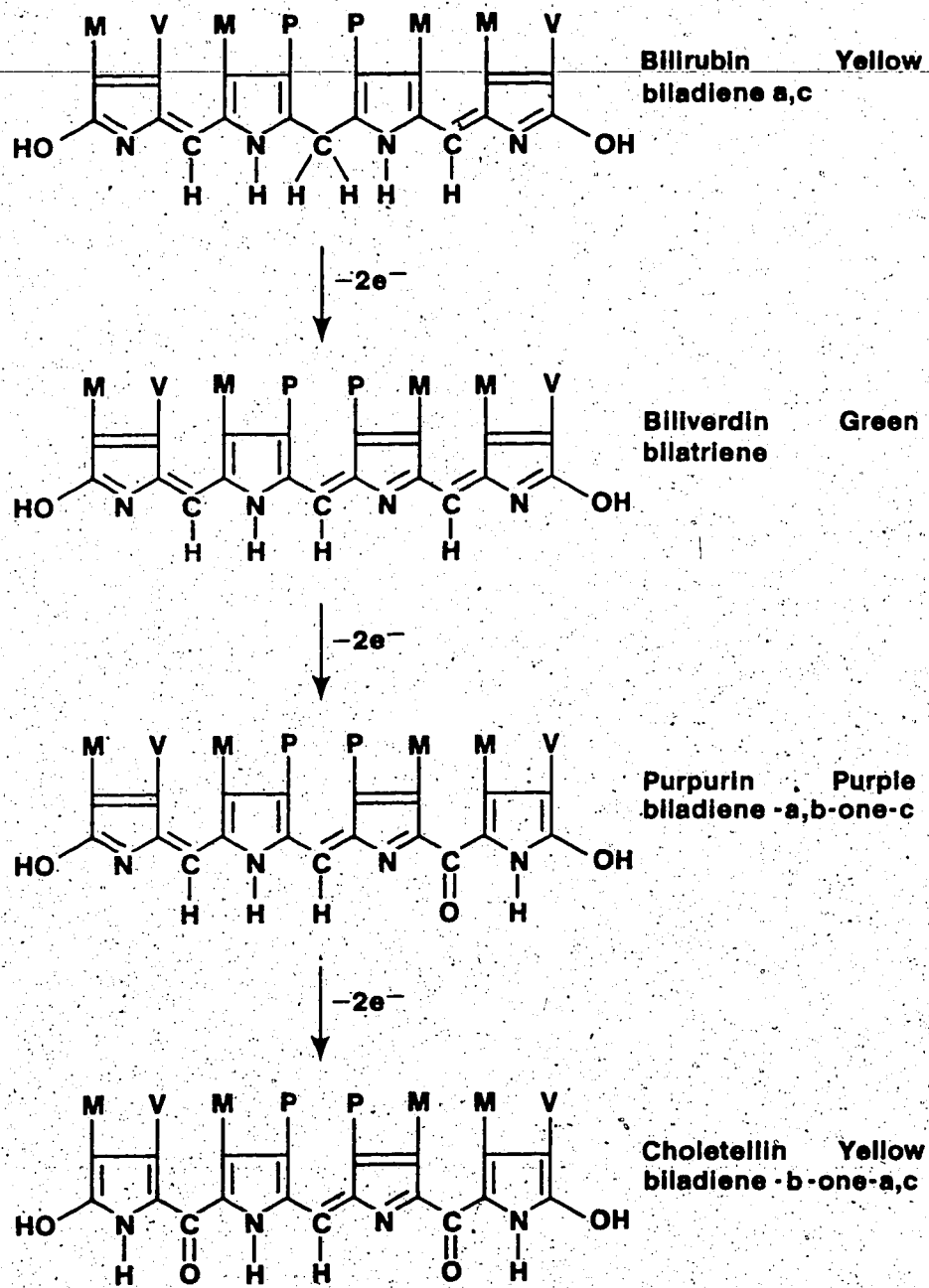
Figure 7

biliverdin. They could not distinguish between an I-I
(two irreversible electro-oxidation steps) or R-I (a
reversible electro-oxidation followed by an irreversible
one). They prefer however an e.e.c. mechanism whereby the
nitrogens on the second and third pyrrole rings each lose
an electron, followed by the rapid loss of two protons
giving rise to the product biliverdin. These authors also
studied the effect of changing pH on the reduction of
bilirubin in aqueous media. They showed that the
reduction in neutral solution results in three waves: (1)
a reversible adsorption prewave, followed by (2) a
reversible two electron wave which was pH dependent, and
(3) a one electron irreversible wave. In basic solution
they observed only two waves. The first was again
attributed to an adsorption prewave, and the second was a
three electron wave believed to be the result of the
coalescence of the second and third waves which were
detected in the neutral solution. No proposed mechanism
has been made to explain these observations.

Further work on the oxidative electrochemistry of
bilirubin has appeared recently [41]. Using a Pt working
electrode in DMF with 0.1 M KClO$_4$ and 300 μM bilirubin,
these workers observed three oxidation peaks at 0.37 V,
0.59 V, and 0.72 V, vs SCE. The first peak is attributed
to oxidation of the dianion of bilirubin, the second peak

a two electron oxidation of bilirubin to biliverdin, and the third peak oxidation of biliverdin. A cyclic voltammogram of pure biliverdin confirms the latter. With regard to reduction, biliverdin displayed two reduction waves at -0.95 V and -1.20 V. A cathodic voltammogram of bilirubin confirms that the wave at -0.95 V is the reduction of biliverdin to bilirubin and the wave at -1.20 V is the subsequent reduction of bilirubin. It should be noted that the solvent in this experiment was not pure. We will show herein that proper distillation of DMF leads to the disappearance of the first oxidation wave due to the removal of any basic impurities which enhance conversion to the deprotonated (more easily oxidized) species.

1.6 THE PHOTOCHEMISTRY OF BILIRUBIN

It is known that irradiation of jaundiced infants with broad spectrum visible light, or more monochromatic light of wavelengths near the 450 nm region has two major effects [42]. Areas of the skin as well as the underlying tissue exposed to the light become bleached. The concentration of bilirubin in the serum also diminishes. These two effects are due to two processes: (1) the conversion of bilirubin to unidentified compounds which are more readily excreted [43,44], and (2) stimulation of

the hepatic excretion of albumin-free bilirubin [44,45].
The relative contributions of the two processes to the
overall result are unknown.

The complete mechanism of phototherapy is still
unknown. It is reasonable to suppose, however, that the
initial event in the process is absorption of light by
bilirubin in peripheral tissues leading to the formation
of excited-state bilirubin molecules. If this is true
then the biochemical mechanism which leads to the observed
phototherapeutic effects must depend on the behavior of
this excited species. The excited bilirubin molecule may
undergo one of three processes as shown in Figure 8. It
may simply decay to the ground state and transfer most of
its photochemically obtained energy to the surrounding
tissue (thermal deactivation). Excited bilirubin may also
transfer its energy of excitation to some other molecule
(quenching) resulting in ground state bilirubin and an
excited quencher molecule. Third, it may undergo a
chemical reaction with itself or some other metabolite
resulting in formation of photoproducts.

There are five known photochemical reactions in which
bilirubin participates. A brief discussion of each is
given here along with a discussion of the degree to which
each would be expected to occur in the body during
phototherapy.
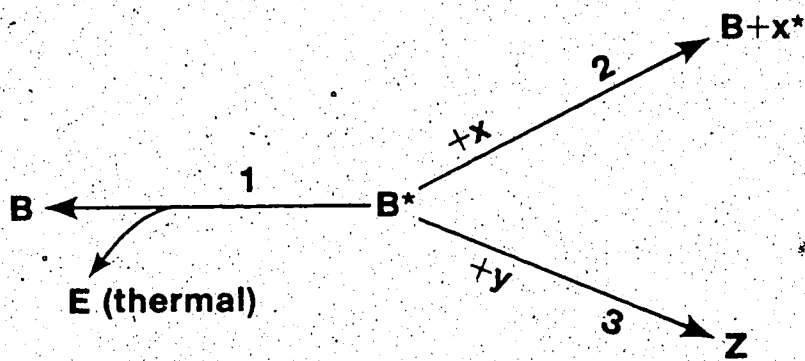
Expected reaction pathways of triplet state excited Bilirubin (B*)

1) conversion to ground state
2) quenching
3) chemical reaction

Figure 8

1.6.1 Conversion to 443 nm Pigment

When solutions of bilirubin in aqueous albumin or serum solutions are irradiated with a mercury lamp, the pigment is partially converted to a compound which absorbs at 443 nm [46]. The yield is greatest when albumin is present. The compound is believed to be the same as that isolated by Kapitulnik [47]. This compound has never been detected in vivo during phototherapy.

1.6.2 Photoisomerization

The photoisomerization products of bilirubin have been identified [48]. The overall reaction is believed to be a free radical process, and is most easily detected under anaerobic conditions. The III-α and XIII-α isomer have never been detected in vivo during phototherapy. The only natural isomer appears to be the IX-α isomer.

1.6.3 Photoaddition

When bilirubin is irradiated in the presence of alcohols or thiols, photoaddition to the exovinyl group occurs [49]. An ionic mechanism involving the first excited state of bilirubin has been proposed. The reaction is slow unless oxygen is removed from the solution.

1.6.4 Photo-oxidation to Biliverdin

Although the yield is very low, the formation of biliverdin during irradiation of bilirubin is well known. The yield is maximized by using large starting concentrations and nonpolar solvents [50,51]. It appears to be a free radical process, and as such should be favored by the in situ binding of albumin to biliverdin [52].

1.6.5 Photo-oxygenation

Photo-oxygenation has been the most extensively studied photochemical reaction of bilirubin. In the presence of air and light, bilirubin decomposes. The major products of this reaction (Figure 9) have been shown to be mono- and dipyrrolic compounds [51,53]. The mechanism involves photosensitized formation of singlet oxygen by bilirubin followed by rapid reaction of singlet oxygen with bilirubin (54). Bilirubin is a poor singlet oxygen sensitizer; thus by adding better sensitizers such as certain porphyrins or methylene blue, the reaction can be accelerated. Singlet oxygen appears to attack bilirubin via 1,4 addition across the pyrrole rings and/or by 1,2 addition to the bridge double bonds.

Photo-Oxygenation Products
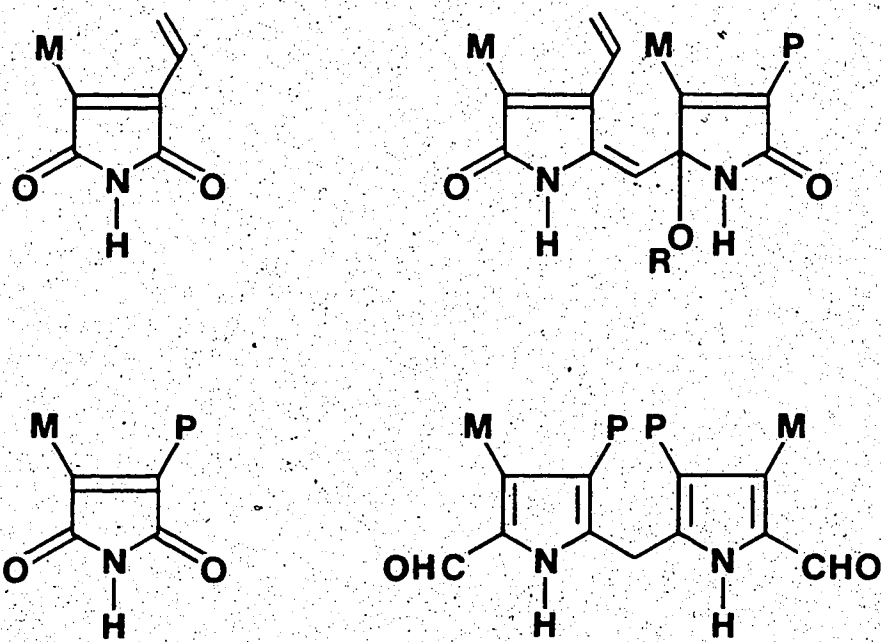
R = H or CH$_3$
P = CH$_2$–CH$_2$–COOH
M = CH$_3$

Figure 9

1.6.6 Summary

The first four photochemical reactions appear to be slow processes, three of these being free-radical processes and the other possibly an ionic one. The first three are inhibited by the presence of oxygen. The fifth, however, is a fast nonradical process which requires oxygen. The evidence has shown that bilirubin, like many dye molecules, can undergo both radical and nonradical reactions. Based on the present knowledge one would expect only photo-oxygenation to occur to an appreciable extent during phototherapy. Since oxygen is far more soluble in nonpolar and lipoprotein media than in water [55], it is likely that bilirubin found in the fatty tissues will undergo photo-oxygenation much more easily than bilirubin in the serum. In addition, bilirubin in the fatty tissue is in general much closer to the skin surface than is the serum bilirubin. The present concensus is that photo-oxygenation of bilirubin is primarily responsible for the skin bleaching and formation of excretable photoproducts. What about the other effect of phototherapy, i.e. the decrease in serum bilirubin? At present a mechanism to explain this has not been put forth. Since covalent bonds would be neither made nor broken, the process probably does not involve chemical reaction of the excited state bilirubin molecule. One

possibility may be some type of photodissociation from
binding sites via isomerization or a conformational change
of bilirubin.

THEORETICAL CONSIDERATIONS OF THE TECHNIQUES EMPLOYED

2.1 INTRODUCTION

For the past fifteen years there has been rapid growth in the utilization of spectroscopic techniques for in situ monitoring of electrochemical reactions which occur at the electrode-solution interphase during electrolysis. Progress has been realized in the study of adsorption [56-58], double layer structure [59], metal deposition [60], reaction kinetics [61-63], film formation [64], and identification of reaction intermediates [65]. Reflectance spectroscopy is, in general, (depending on the system under investigation) extremely sensitive to the changes which occur in the interphase. Concentrations as little as 10^{-13} mol-cm^{-2} of electrochemically generated species have been detected [66,67].

Specular reflection spectroscopy monitors the change in intensity of the reflected beam between two electrode potential states. Reflection spectroscopy is easy to perform and is in general a very flexible and rapid technique for observing intermediates.

The first technique used to monitor an absorbing species during an electrochemical reaction was internal reflection spectroscopy [68,69]. An attribute of this technique is that one is not hindered by having to pass light through strongly absorbing reaction solutions before it contacts the electrode surface. The technique is limited by the availability of suitable electrodes, i.e. they must be conductive and optically transparent to light in the optical frequency range under investigation. Thin metal films deposited onto optically transparent substrates, and the use of some semiconductor materials as electrodes have helped circumvent the problem [69,70]. The mathematical treatment of the experimental results is in general difficult to apply.

Another popular technique has been conventional transmission spectroscopy employing optically transparent electrodes (OTE) [69,70]. The conventional use of this technique is not suitable for the detection of short lived intermediates due to the extremely small perturbations involved in the total transmitted beam caused by the intermediate species, which as stated earlier may only be present in typical steady state concentrations of 10^{-13} mol-cm^{-2}. More specifically, OTE's often have high resistances which may not be corrected for by efficient cell design. This can result in uneven potential

distribution across the electrode distorting the electrochemical currents under investigation. OTE's also absorb a significant fraction of the incident radiation.

Modulated specular reflectance spectroscopy (MSRS) has been successful in overcoming the problems associated with the other spectroscopic techniques. MSRS has the greatest sensitivity of the group, and can be used in the ultraviolet [71], visible [72], and infrared [73] spectral regions. For the elucidation of an electrochemical reaction mechanism where homogeneous reactions of the intermediates, products, or reactants may precede or follow the electron transfers, the use of the following general plan is recommended [74].

I) Perform conventional dc and ac cyclic voltammetric, chronoamperometric and coulometric electrochemical experiments on the system.

II) Perform modulated reflectance spectroscopy as a function of wavelength simultaneously with the electrochemistry to obtain an absorption spectrum of the intermediates and products at the various potentials.

III) Obtain absorbance/time transients at the absorption peak wavelengths with the same experimental apparatus in order to kinetically follow the formation and decay of the absorbing species.

IV) If possible, prepare by independent methods the
intermediates and/or products for conventional
electrochemical and spectroscopic studies for positive
identification of suspected species.

V) Isolate final products of the reaction.

Ideally, one will be able to obtain an absorption
spectrum for each of the intermediates and products along
with the kinetic behavior. Often the details of the
kinetics and/or reaction mechanism may not be elucidated
with a single technique because of one or more possible
schemes giving rise to identical results for that
technique. The addition of data from a completely
different physical technique performed on the same time
scale often allows for differentiation of the
alternatives.

2.2 REFLECTANCE THEORY

The expected response to an MSRS experiment can be
derived via the following considerations. For an
electrode process with no homogeneous kinetic
complications

$$O + ne^- \rightarrow R \tag{1}$$
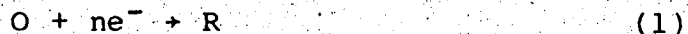
the absorbance-time profile has been shown by Kuwana [75]
to be

$$A(t) = \frac{\epsilon_r}{nFA} \int_0^t i(t) \, dt \qquad (2)$$

for a transmission optically transparent electrode
experiment. $A(t)$ is the absorbance, ϵ_r is the molar
extinction coefficient of the reduced species, F is the
Faraday, n is the number of electrons involved in the
reaction, A is the electrode surface area and $i(t)$ is the
current response as a function of time. When both the
oxidized and reduced species absorb at the wavelength of
the incident radiation, then $\Delta\epsilon$ [76] must be substituted
into Equation (2), where $\Delta\epsilon = \epsilon_r - \epsilon_{ox}$; i.e. the
difference in molar absorptivity of the redox pair. The
optical path for a MSRS experiment is depicted in Figure
10. Since the beam passes through the diffusion layer
twice at an angle of incidence θ, the absorbance must be
corrected for non-perpendicular transmission. From Figure
10 we see that the actual optical path is $2x/\cos\theta$ where x
is the perpendicular distance coordinate from the
electrode surface; thus the absorbance will be

$$A(t) = \frac{2\Delta\epsilon}{nFA \cos\theta} \int_0^t i(t) \, dt \qquad (3)$$

The coordinate system used in
specular reflectance spectroscopy.

$$q = \frac{2X}{\cos \theta}$$

**Incident
Radiation**

**Reflected
Radiation**

θ

X

q/2

Electrode Interface
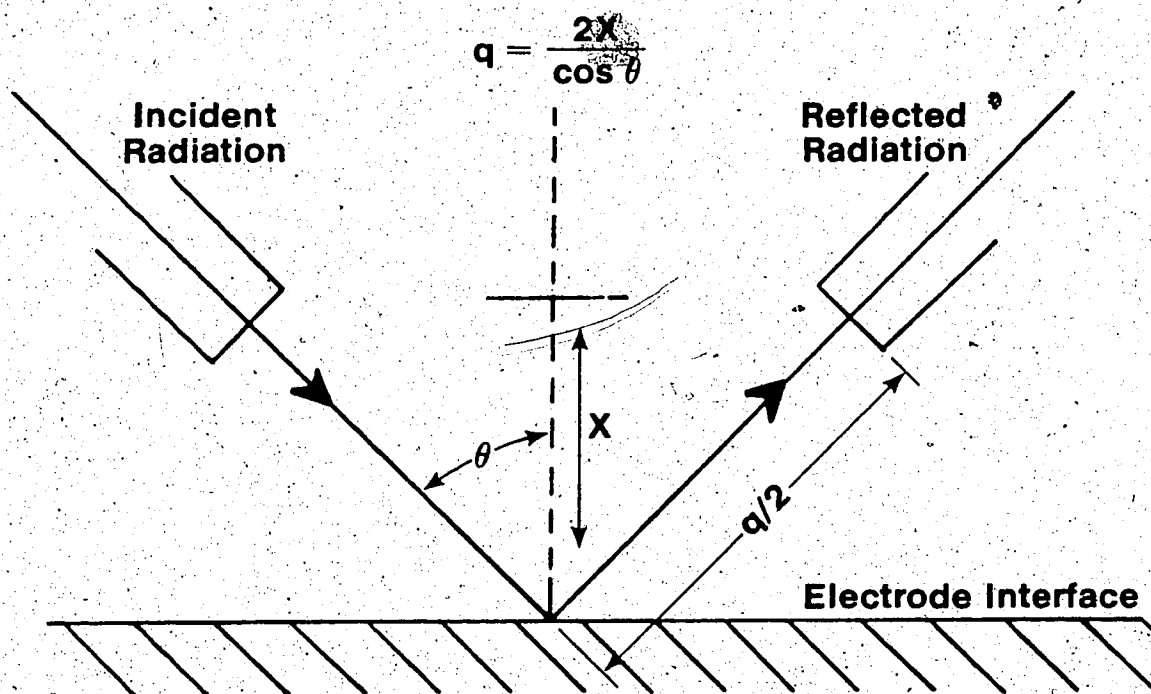
Figure 10

We choose to measure the change in reflectance as the normalized value

$$\Delta R/R = (R_1 - R_0)/R_0 \qquad (4)$$

R_1 is the time dependent reflectance at potential E_1 (where the faradaic process of interest occurs), and R_0 is the reflectance at the base potential E_0, where no faradaic process involving the substrate occurs. We note that

$$1 + \Delta R/R = 1 + (R_1 - R_0)/R_0 = R_1/R_0 \qquad (5)$$

letting $R = R_0$ by normal convention. From Beer's law

$$A(t) = -\log R_1/R_0 = (-1/2.303)\ln R_1/R_0 \qquad (6)$$

Thus

$$A(t) = (-1/2.303)\ln (\Delta R/R + 1) \qquad (7)$$

or

$$\ln (\Delta R/R + 1) = -2.303 \, A(t)$$

Thus from Equation (3)

$$\ln (\Delta R/R + 1) = -2.303\left(\frac{2\Delta\varepsilon}{nFA \cos\theta} \int_0^t i(t) \, dt\right)$$

$$= \frac{-4.606 \, \Delta\varepsilon}{nFA \cos\theta} \int_0^t i(t) \, dt \qquad (8)$$

For small values of $\Delta R/R$, the logarithmic term is Taylor expanded to

$$\ln (\Delta R/R + 1) \cong \Delta R/R \qquad (9)$$

This approximation is quite valid since $\Delta R/R$ in our experiments is $10^{-3} - 10^{-6}$, and the second term in the expansion is quadratic in $\Delta R/R$. Using this approximation, we finally arrive at the working equation

$$\Delta R/R = \frac{-4.606 \, \Delta\varepsilon}{nFA \cos\theta} \int_0^t i(t) \, dt \qquad (10)$$

2.3 SINUSOIDALLY MODULATED AC REFLECTANCE SPECTROSCOPY

Recently a powerful new spectroelectrochemical technique has been developed in this laboratory [77]. The technique has been termed SMACRS - Sinusoidally Modulated AC Reflectance Spectroscopy. It has been shown that if a small amplitude sinusoidal perturbation is superimposed on

a slowly varying cyclic potential ramp applied to an electrode, the output of a lock-in amplifier monitoring a photodetector collecting the light beam reflected from the active electrode surface mirrors the <u>charging current-corrected</u> ac voltammetric response. This technique provides both the qualitative and quantitative information of ac voltammetry, along with the species resolution advantage of spectroscopic observation. The selectivity attainable with SMACRS has made it especially useful in the deconvolution of overlapping voltammetric waves as is the case exhibited in bilirubin voltammetry. It is extremely useful for qualitative diagnosis of complicated reaction schemes.

As was previously stated, SMACRS was employed herein only as a qualitative tool for the investigation of the bilirubin oxidation mechanism. Only a brief discussion of the theory is given here; details are given elsewhere [77-79]. As was derived for general modulated specular reflectance spectroscopy:

$$-\Delta R/R = \frac{4.606 \; \Delta \varepsilon}{nFA \; \cos\theta} \int_0^t i(t) \; dt \qquad (11)$$

For a quasi-reversible electrode process, the fundamental harmonic current resulting from the superposition of a small ac sinusoidal wave on some dc bias potential is given by [78]

$$I(\omega t) = I_{rev} \ F(t) \ G(\omega) \ \sin \ (\omega t + \emptyset) \qquad (12)$$

Here, $F(t)$ and $G(\omega)$ are functions which take into account the effects of non-nernstian behavior on the dc and ac time scales respectively. ω is the angular frequency, t is the time, I_{rev} is the fundamental harmonic faradaic current component:

$$I_{rev} = \frac{n^2 F^2 A \ C_{ox}^b \ \omega^{1/2} \ D_{ox}^{1/2} \ \Delta E}{4RT \ \cosh^2 (j/2)} \qquad (13)$$

$$\emptyset = \cot^{-1} \ (1 + (2\omega)^{1/2}/\lambda) \qquad (14)$$

$$\lambda = k_s \ (e^{-\alpha j} + e^{\beta j})/(D_{ox}^\beta D_r^\alpha)^{1/2} \qquad (15)$$

$$j = nF \ (E_{dc} - E_r^{1/2})/RT \qquad (16)$$

α is the transfer coefficient, $\beta = (1-\alpha)$, E_{dc} is the bias potential, and $E_r^{1/2}$ is the half wave potential. We see that the fundamental alternating component of the reflectance response can be found by substitution of Equation (12) into (10):

$$-R(\omega t) = \frac{4.606 \ \Delta\varepsilon}{nFA \ \cos\theta} I_{rev} F(t)G(\omega) \int_0^t \sin(\omega t + \emptyset)d(t) \qquad (17)$$

using the normal assumption that F(t) remains constant with respect to the ac time scale. R(ωt) is now defined as the normalized reflectance parameter:

$$R(\omega t) = \Delta R/R \ (\omega t) \qquad (18)$$

After integration of Equation (17) we are left with

$$R(\omega t) = \frac{4.606 \ \Delta\varepsilon}{\omega \ nFA \ \cos\theta} I_{rev} F(t)G(\omega)\cos(\omega t + \emptyset) \qquad (19)$$

The ratio of the magnitude of the fundamental harmonic current to the corresponding reflectance parameter is given by

$$\left|\frac{I(\omega t)}{R(\omega t)}\right| = \frac{nFA \ \omega \ \cos\theta}{4.606 \ \Delta\varepsilon} \qquad (20)$$

This is the relation that may be used for the determination of extinction coefficients or n values. It should be noted that at any given frequency, the alternating reflectance is just a multiple of the corresponding alternating current. Hence the mathematical treatment of ac voltammetry also applies to the data obtained from a SMACRS experiment. The inherent

sensitivity associated with this type of reflectance measurement, along with its simplicity, makes SMACRS a very attractive spectroelectrochemical tool.

2.4 DC CYCLIC VOLTAMMETRY

For most potential sweep methods, the electrode potential is changed linearly with time, so that the potential may be written as .

$$E = E_i + vt \tag{21}$$

where E_i is the initial potential, and v is the potential sweep rate in $V-s^{-1}$, and t is the time in seconds. Unidirectional or cyclic sweeps between two limiting potential values may be employed. For very slow potential sweeps the reaction

$$O + ne^- \rightleftharpoons R \tag{22}$$
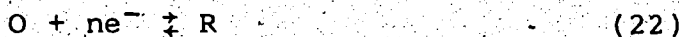
will show current-potential plots which one would expect from the theory of steady state experiments. As v is increased a peak will appear in the I-E curve, becoming more and more prominent. The peak is caused by both the rapid depletion of reactant concentration in the diffusion

layer, and by the high mass transfer rates caused by the imposition of a non-steady state. If the rate of electron transfer is sufficiently high so a nernstian equilibrium can be maintained at the electrode surface (a reversible reaction scheme), then the peak current density for a cathodic response of reaction (22) is given by [80] as

$$I_p = 2.72 \times 10^5 \, n^{3/2} \, D_0^{1/2} \, \nu^{1/2} \, C_0^{\infty} \qquad \text{at } 25°C \qquad (23)$$

C_0^{∞} is the concentration of the oxidized species in the bulk solution, D_0 is the diffusion coefficient of the oxidized species, and the other terms are as previously defined. The peak potential will be independent of sweep rate and is related to the polarographic half wave potential $(E_{1/2})$ by

$$E_p = E_{1/2} - .029/n \text{ Volts} \qquad (24)$$

If the reaction under investigation is sufficiently slow compared with the potential sweep rate, then the surface concentration of O and R will no longer follow nerstian values. Instead of obeying Equation (23) the I_p will approach the following at large sweep speeds [81]:

$$I_p = 2.99 \times 10^5 \, n(\alpha n_\alpha)^{1/2} \, D_0^{1/2} \, C_0^{\infty} \, \nu^{1/2} \qquad \text{at } 25°C \qquad (25)$$

and

$$E_p - E_{p/2} = .048/an_\alpha \text{ Volts} \qquad (26)$$

$$E_p = E_O^{\ominus} - \frac{RT}{an_\alpha F} \left[0.78 + 0.5 \ln \left(\frac{an_\alpha D_O F\nu}{RT} \right) - \ln k_O^{\ominus} \right] \qquad (27)$$

where $E_O^{\ominus}$ is the standard electrode potential, n_α is the

number of electrons transferred prior to and during the

rate determining step, $k_O^{\ominus}$ is the rate constant for

electron transfer at the standard electrode potential, R

is the gas constant and T is the absolute temperature.

The other terms are identical to those previously

mentioned. By plotting peak height, shape, and position

as a function of sweep speed, then α, n_α, and $k_O^{\ominus}$ can be

determined. The most immediate qualitative difference

between this and the reversible case is that here the peak

potential is dependent on the sweep rate: there is a

$30/an_\alpha$ mV shift per decade in sweep rate.

Providing R is stable, a reverse sweep back to the

initial potential will produce a second peak equal in

height but opposite in sign. This peak corresponds to the

opposite reaction (oxidation of R). The peak allows for

the measurement of a new kinetic parameter, the peak

separation ΔE_p. For a fast reversible process ΔE_p is

found to be 0.059/n V, and is independent of sweep speed. When the sweep rate is increased to the point where nernstian equilibrium is not able to be maintained, then ΔE_p will begin to increase with ν; the shape and position of the peaks will depend again on α, ν, and k_o^σ.

Although quantitative data can be obtained from cyclic voltammetry, its major use has been in the rapid qualitative elucidation of reaction mechanisms. Cyclic voltammetry allows for observation of a system over a wide potential range. In a single experiment, intermediates can be directly observed, and their possible identification implied by the potential at which they oxidize or reduce. One can often gain immediate information about the reaction mechanism from peak separation, peak height ratios, the absence of reversible peaks, the appearance of new peaks on the subsequent scans, etc.

There are two main experimental factors that must be considered while interpreting cyclic voltammetric responses: iR_u drop and charging current. For a properly designed cell and a highly conducting solution the scan rate is practically limited to about 50 V-s^{-1}; more often the limit is much less. iR_u drop is explained in detail in the next section. However, it should be mentioned here that it will cause distortions of the peaks, and may shift

the potentials. This trouble is more pronounced at higher sweep rates since a larger current results. The effects of iR_u is very similar to those caused by a small k_o^0 value, i.e. an irreversible electron transfer reaction. These effects may be distinguished by comparison with a known reversible system using the same cell and electrolyte.

The problem of charging current is due solely to a nonfaradaic process. It is caused by a reorganization of the ions in the electrical double layer in response to the changing electrode potential. The magnitude of the charging current is directly proportional to dE/dt, i.e. the sweep rate, v. As the sweep rate is increased the charging current will increasingly mask the faradaic current since the former increases as v and the latter as $v^{1/2}$. Correction is usually made by subtraction of the current obtained in an identical cell not containing the electroactive species.

2.5 AC CYCLIC VOLTAMMETRY

Cyclic ac voltammetry was used as a tool for the investigation of electrode processes during bilirubin oxidation. This technique is powerful because it retains the best features of two complimentary methods, conventional ac and dc cyclic voltammetry.

Heterogeneous kinetic reversibility is characterized in the dc cyclic experiment by a forward and reverse current peak separation of $59.2/n$ mV at $25°C$ regardless of potential sweep rate. In the ac experiment, reversibility is manifested in superimposed forward and reverse waves, and by half height peak widths of $90/n$ mV regardless of scan rate. The chemical stability of the reduced form is demonstrated in the dc experiment by a peak current ratio $i_{p,r}/i_{p,f}$ of unity, where $i_{p,r}$ is the reverse sweep peak intensity, and $i_{p,f}$ is the forward sweep peak intensity. For charge transfer reversibility the same ratio determined in the ac experiment is used. The advantage to the ac cyclic experiment is that a good flat baseline is present from which accurately measured currents are available. This reference is not easily found in dc voltammetric experiments in general.

When dc reversibility does not hold, then the situation can become quite complex. The mean surface concentrations at a given dc potential tend to depend on the way in which that potential is reached. The surface concentrations at any E_{dc} will differ on the forward and reverse scans, thus we can expect the corresponding traces to differ in the ac voltammogram. In the dc cyclic voltammogram, an increasingly slow electron transfer causes greater splitting of the forward and reverse peaks

since larger activation potentials are needed to cause

charge transfer. This peak separation is also caused by

the fact that the surface concentrations undergo the

transition from nearly pure "O" to virtually pure "R" in

different potential regions for the two scan directions.

Since the ac voltammogram shows a response only in the

potential regions where an electron transfer takes place,

we can expect the ac voltammogram to show split peaks that

are aligned with the forward and reverse dc voltammetric

half wave potentials when the dc scan rate is very slow

and k_o^o is large. It has been shown that a crossover

potential exists, where the forward and reverse scans

yield the same response. The potential where this exists

is rigorously shown [82] to lie at

$$E_{co} = E_{1/2} + RT/nF \ln (\alpha/1-\alpha) \qquad (28)$$

All terms are as previously defined. This equation is

often used for the evaluation of the charge transfer

coefficient. The system under investigation will

generally dictate the degree to which quantitative

information can be obtained.

CHAPTER 3

EXPERIMENTAL

3.1 SPECTROELECTROCHEMISTRY

MSRS was utilized to obtain absorbance spectra of the
intermediates involved in a given electrochemical
reaction. To do this a phase sensitive detection system
was employed. A scanning monochromator running typically
at 10 $Å-s^{-1}$ is slow enough to assure that the absorption
maxima of the species are not distorted. The other
typical instrumental parameters are listed in Table 1.
Under those conditions a steady state spectrum of the
given species was observed. The spectra obtained were
consistent with those spectra built from a transient
method described in the next section.

3.1.1 Optimization

The pulse length at the working electrode must be
properly chosen. If the pulse is too short, then
intermediate formation may be outrun by the experiment.
The modulation frequency must not be 60 Hz or any low odd
harmonic thereof due to excessive line noise coupling to
the optical signal. Proper grounding must also be

45

Table 1. Typical MSRS conditions for bilirubin oxidation.

Substrate Concentration	$-$ 1.0 mM
Reference Electrode	$-$ Ag/Ag$^+$ (0.1 M) in DMF
	$-$ 0.10 M Supporting Electrolyte
Modulation Frequency	$-$ 40 Hz
Modulation Pulse Height	$-$ -1.20 V to $+0.20$ V
Phase Sensitive Detector Sensitivity	$-$ 1.0 mV/V
Phase Sensitive Time Constant	$-$ 1 s
Recorder Sensitivity $-$ X	$-$ 250 mV cm^{-1}
Y	$-$ 250 mV cm^{-1}

---

assured. Ground loops can cause a great deal of noise and unreliability. When the system is working properly only white noise from the photomultiplier tube (PMT) should be observed on an oscilloscope display. The potential limits at the working electrode should be from a non-faradaic region to an upper limit 200 mV beyond the peak potential observed on a cyclic voltammogram. Under these conditions one is pulsing from an unreactive potential to a potential where the reaction is completely diffusion controlled. The concentration profiles of the reactant and products are thus defined by known equations or can be predicted from simulation techniques.

3.2 MSRS INSTRUMENTATION

MSRS can best be described with the help of a block diagram of the apparatus, Figure 11. Light from a high intensity mercury xenon lamp was passed through a high throughput GCA MacPherson 201 monochromator to select the wavelength of choice. Depending on the application the light may (adsorption studies) or may not (homogeneous studies) be polarized before being reflected off the working electrode. The potential of the working electrode was controlled by a Hi-Tek DT2101 potentiostat and PPR1 waveform generator. The reflected light was collected and then focussed onto a photodetector. The output of the

Instrumentation for MSRS
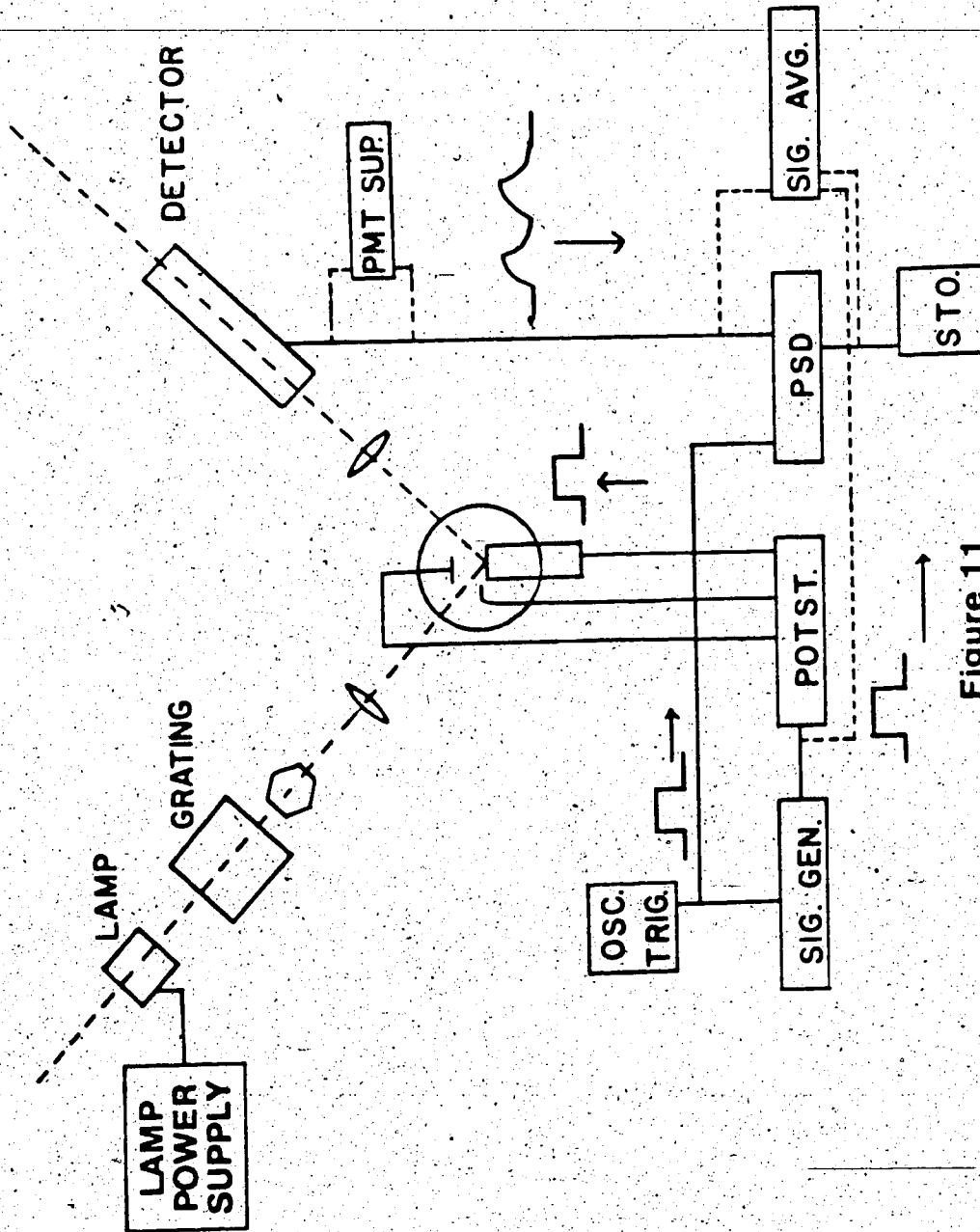
Figure 11

photodetector was then amplified and fed into a signal
recovery system. This was either a phase sensitive
detector/lock-in amplifier if spectra were being recorded
or a digital signal averager for transient recordings.
The electrochemical process was perturbed repetitively by
modulating the electrode potential with a square wave, a
triangular sweep or some other appropriate repetitive
profile. The signal recovery system ignores the average
steady state output of the photodetector and locks onto
the small optical absorption component fluctuating in step
with the applied reference modulation. This component
corresponds to the small changes, ΔR, in the reflectivity
of the working electrode at the two potentials. When the
wavelength is altered as in the case of scanning modulated
reflectance spectroscopy, the light intensity of the
source also changes. Thus, it was necessary to normalize
the reflectance to the background at all wavelengths. If
a photomultiplier was being used as a detector, this could
be accomplished by an optical feedback system which
adjusted the PMT power supply to maintain a preselected
constant dc anode current. The output was thus $\Delta R/R$.
When a photodiode was being used, this adjustment was not
possible, and the background dc reflectivity of the
electrode, R, had to be noted for each wavelength.
Finally the output of the signal recovery system, ΔR, was

normalized by dividing by the average electrode
reflectivity at each wavelength and all results are quoted
as the relative reflectivity change, $\Delta R/R$.

3.3 TRANSIENT RECORDINGS OF ELECTROCHEMICALLY INDUCED

INTERMEDIATES

The absorbance transients of the intermediates were
digitally stored in a Hi-Tek 512 word, 10 bit signal
averager. The instrument was triggered by a Hi-Tek PPR1
waveform generator such that transient recording would
begin at the same time that the electrode was pulsed into
the potential region E_1 (oxidation of the substrate). The
data acquisition time was adjusted to include the
absorbance decay when the pulse was terminated. In some
cases, in order to observe only chemical kinetic control
after the initial pulse, the system was open circuited at
the end of the pulse rather than pulsing back to E_0. This
was accomplished by inserting a mercury-wetted reed relay
circuit in the secondary electrode lead. The relay was
triggered to open circuit by a TTL pulse from the waveform
generator which was available at the end of the main
pulse. The waveform timing sequence is shown below.

Working electrode potential
WRT reference

Waveform generator trigger
for averager

Waveform generator trigger
for reed relay

Signal averager status

off on   off on
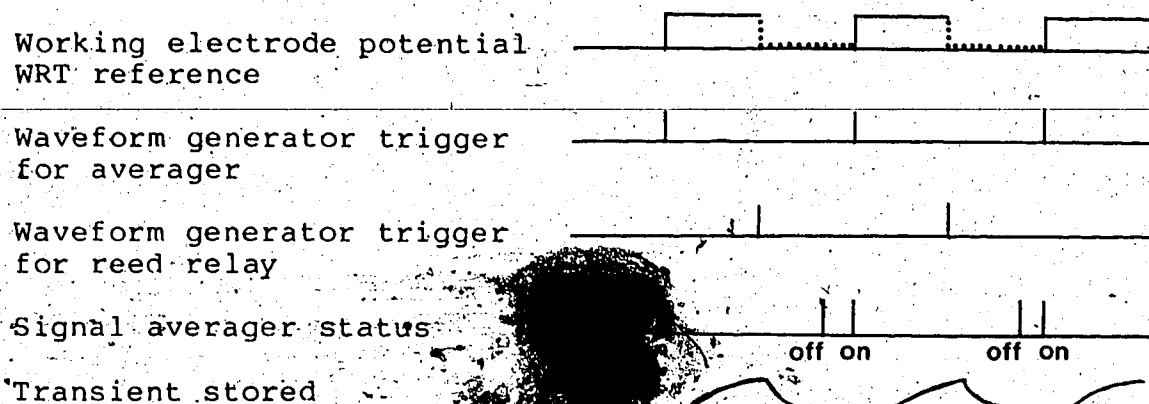
Transient stored

Most transients consisted of a 1-50 ms electrode

pulse, and a 100-500 ms open circuit. Delay times of up

to 16 s were employed in order for sufficient time to

elapse to restore the cell to essentially original

conditions. The number of cycles averaged would dictate

sensitivity; between 1 and 512 cycles typically were

averaged and digitally stored.

The wavelengths chosen for transient studies were

determined from the absorbance maxima obtained from the

scanning method described in the previous section. The

spectrum built from transients can be compared to that

obtained by the scanning method. This is accomplished by

collecting transients at a variety of wavelengths and

noting the magnitude of absorbance at a given time. These

"point by point" spectra gave the same maxima as those

found from the scanning method. These, however, are time

resolved and of quantitative value.

3.4   SMACRS INSTRUMENTATION

The instrumentation for SMACRS is shown in Figure 12.   Light from a 200 W Hg-Xe lamp was passed through a GCA MacPherson 201 monochromator, and then focussed onto the electrode surface in a conventional reflectance cell (see Figure 12).   After reflection, the light was focussed onto the window of a RCA 31000M photomultiplier tube.   The PMT was powered by a high voltage source, and the output circuit contained a current feedback loop so that $\Delta R/R$ could be measured directly by a PAR model HR-8 lock-in amplifier.   The reference signal for the lock-in amplifier was taken as the actual potential applied to the working electrode, which was available between the working electrode and reference electrode.   The high impedence reference electrode was isolated by a high input impedence voltage follower at the reference electrode.   The output was recorded on a Hewlett-Packard 7045A recorder.

3.5   VOLTAMMETRY INSTRUMENTATION

Cyclic voltammetry was performed using a Hi-Tek DT2101 potentiostat and a Hi-Tek PPR1 waveform generator.   The voltammograms were recorded on either a HR-2000 x-y recorder or a Hewlett-Packard 7045A

Instrumentation for SMACRS
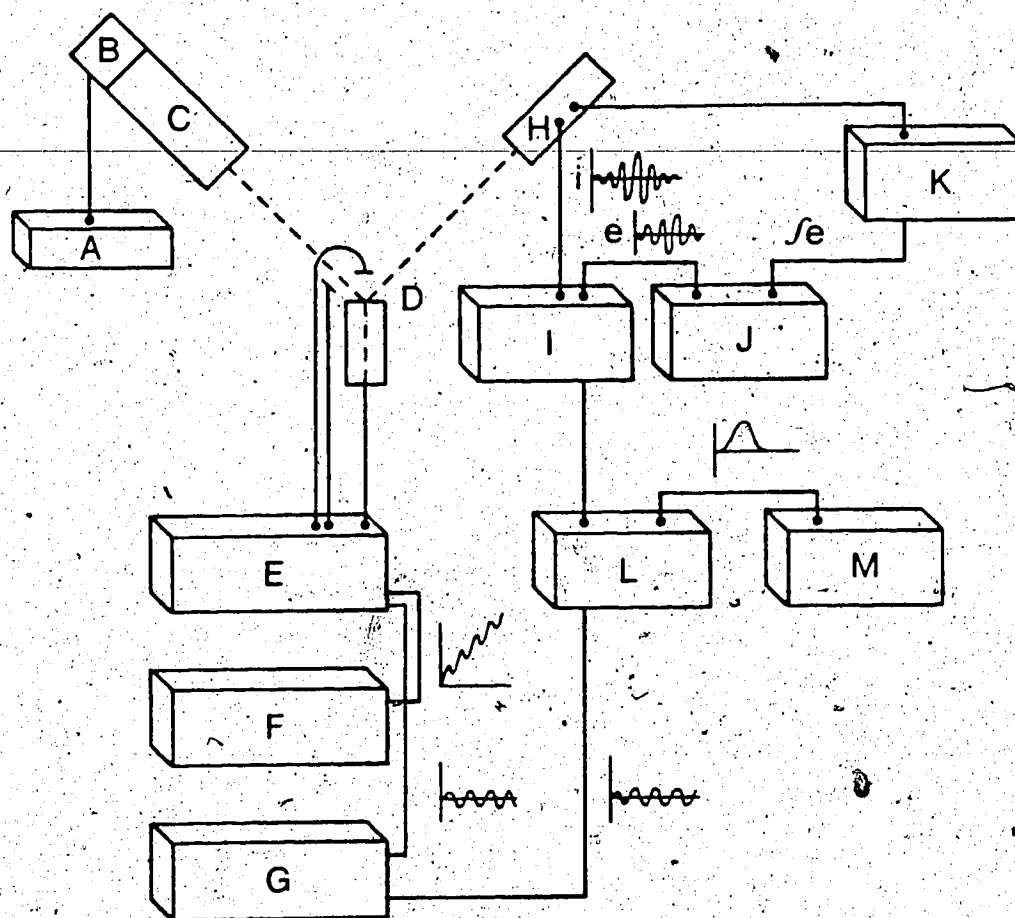
A. Power supply for lamp.
B. Lamp
C. Monochromator
D. Electrochemical cell
E. Potentiostat
F. Waveform generator
G. Oscillator
H. PMT
I. Current follower
J. Integrator
K. PMT high voltage source
L. Lock-in Amplifier
M. Recorder

Figure 12

recorder. For rapid scan voltammetry, i.e. sweep rates greater than 4 V-s^{-1}, a Hi-Tek AA1 512 word signal averager was used.

The kinetic cell used is shown in Figure 13. The Pt wire working electrode was 1.0 cm in length and 0.1 cm^2 in area. The secondary electrode consisted of a Pt basket placed concentrically around the working electrode. The cell voltages are referenced to Ag/Ag$^+$ (0.1 M) in DMF. The reference electrode was isolated from the working compartment by a Luggin probe and glass frits. Reported potentials are inclusive of junction potentials.

3.6 ELECTROCHEMICAL CELL PARAMETERS

There are six basic factors which should be considered when employing a cell for electrochemical experiments. I) It must be possible to accurately measure the potential at the working electrode. To accomplish this, a three-electrode cell should be used. The current is passed between the working electrode and the secondary electrode. A Luggin reference probe placed very close to the working electrode surface is used to monitor the potential at the working electrode with respect to the unpolarizable reference electrode. II) The current density must be constant over the entire area of the working electrode. This is accomplished providing

Cell Configuration Used For Electrokinetic Measurements
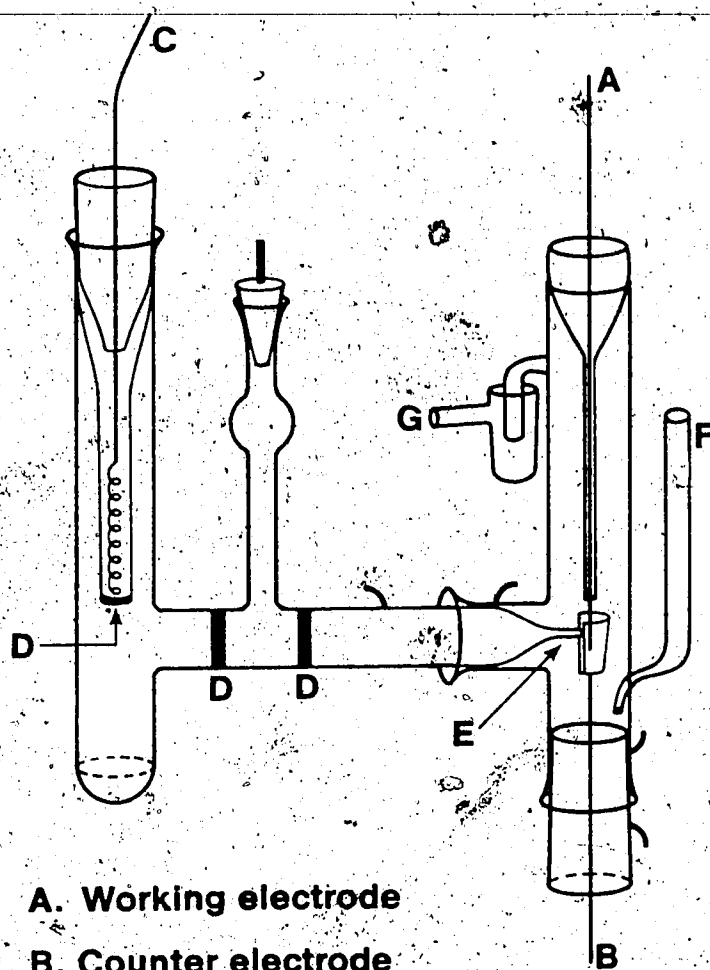
A. Working electrode

B. Counter electrode

C. Reference electrode

D. Frit

E. Luggin

F. Gas Inlet

G. Gas Exit

Figure 13

every point on the working electrode is equidistant from the secondary electrode. In practice this is not a large problem; however, it should be remembered that an improperly placed Luggin probe will interfere with the uniformity of the current distribution. III) The design of the cell should conform to the model used to develop the theory of the experiment. For example, the cell geometry may define conditions for simple linear diffusion, spherical diffusion, cylindrical diffusion, etc. IV) The reactions at the secondary electrode must in no way interfere with the processes at the working electrode. The area of the secondary electrode is always chosen to be much larger than the working electrode. In doing so the current can only be limited by the processes at the working electrode. If a species is produced at the secondary electrode which may react at the working electrode, a frit or membrane may be necessary to separate the two electrode processes. This is usually not a problem for short timescale experiments. V) It is desirable to place the working and secondary electrodes as close as possible to minimize cell resistance. This reduces resistive heating of the cell solution. VI) The shape and placement of the Luggin probe is directly related to the difference between the potential which the probe monitors and the potential which actually exists at

the working electrode. The difference is iR_u, where R_u is the uncompensated resistance of the solution between the electrode and the Luggin tip, and i is the current flowing through the cell. Moving the Luggin closer to the electrode will minimize this problem. However, a second problem is introduced: "shielding" of the working electrode which was discussed in II. The best compromise is that the Luggin tip be placed 2d away from the working electrode where d is the diameter of the tip. Since shielding and iR_u drop are reciprocal effects there is an optimal location where the two effects are maximally offset [83].

3.7 OPTICAL CELLS

3.7.1 The Reflectance Cell

For MSRS, SMACRS, and transient recordings, the same cell was used. The cell consisted of three electrodes: a Pt working electrode, a Pt secondary electrode and an Ag/Ag$^+$ (0.1 $\underline{M}$) reference electrode. The cell is shown in Figure 14. It was constructed of Pyrex glass with two quartz windows at right angles to each other (see Figure 10 for the optical path through the cell). The cell volume was 100 mL. The working electrode was mounted in the cell such that it was centered directly in front of the optical windows. The working electrode was

58
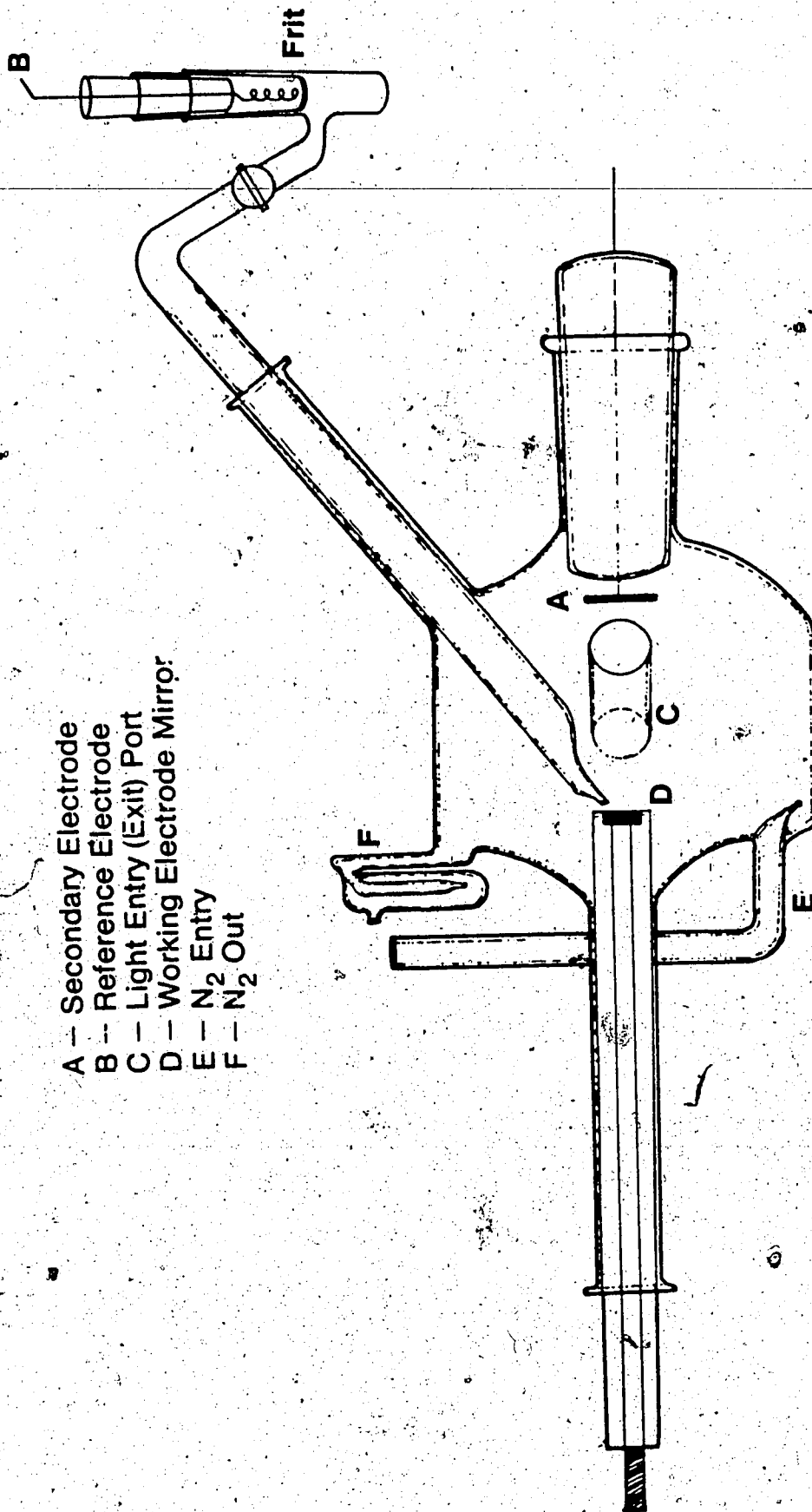
A — Secondary Electrode
B — Reference Electrode
C — Light Entry (Exit) Port
D — Working Electrode Mirror
E — N₂ Entry
F — N₂ Out

Frit

B

A

C

D

E

F

Optical Cell Used For Modulated Reflectance Experiments
Figure 14

constructed by mounting a highly polished Pt cylinder onto

the end of a long brass cylinder. This unit was then

heat-shrink fitted into a hollow Kel-F cylinder, so that

the assembly was inert to acids and organic solvents. The

electrode face was polished with the aid of a mandril.

Decreasing sizes of alumina polishing compound were used,

the last being 0.05 µm diameter. The secondary electrode

was placed in the cell 30 mm in front of and parallel to

the working electrode. It was fabricated from a 10 mm

diameter Pt disc.

3.7.2 The Photochemical Cell

The optical cell used for photoelectrochemical

experiments is shown in Figure 15. This cell

configuration was employed to electrochemically measure

the production of biliverdin during the photo-oxidation of

bilirubin. Light passed through the quartz window at the

front of the cell for a given period of time. Any

biliverdin which was photochemically produced was then

electrochemically reduced back to bilirubin by applying

the proper potential to the working electrode. The

working electrode consisted of a Pt mini-electrode located

directly behind the optical window. The counter electrode

was placed 30 mm directly behind the working electrode and

consisted of a 10 mm diameter Pt loop. The reference

electrode was separated from the working electrode by a

Electrochemical Cell For Photo-Oxidation Electrochemical Reduction Studies

Reference Compartment

Secondary Electrode

Gas Ports

Window

Luggin Capillary

Working Electrode Inserted Here

Side View

Clamping Nut

Working Electrode

Platinum Disc

KEL–F Sleeve

Brass Shaft

O–Ring
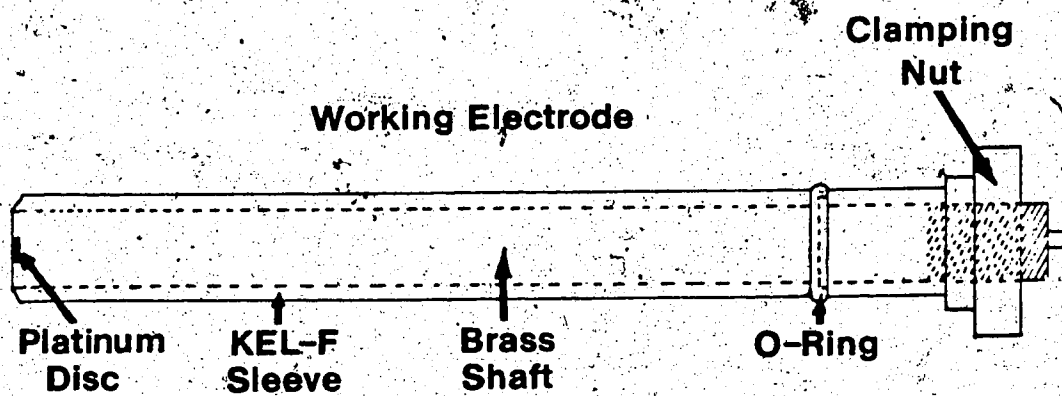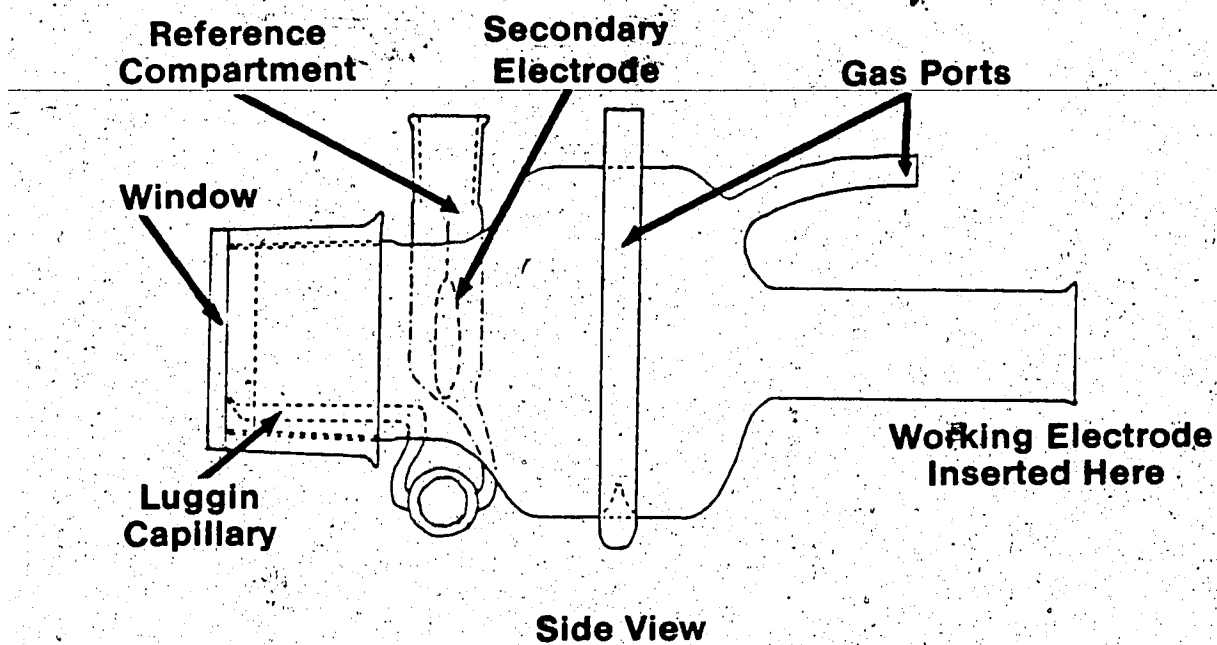
Figure 45

Luggin probe. The cell was constructed of Pyrex and held 50 mL of solution.

3.7.3 The Electrolysis Cells

Bulk electrolyses were carried out in a specially designed glass cell (Figure 16A). The working compartment was 50 mL. The working electrode consisted of a Pt mesh separated from the secondary electrode by two glass frits. The reference electrode compartment was separated from the working compartment by a Luggin probe and a wet stopcock. The reference electrode was identical to that used for voltammetry. For small scale electrolysis a prep-cell was utilized (Figure 16B). This cell was employed for rapid production of bilirubin oxidation products, which is possibly due to its large electrode area to solution volume ratio.

3.7.4 The Spectral Electrolysis Cell

Often it is desirable to obtain a gross spectrum of a product or intermediate being created at an electrode surface in a quick and easy manner. In the past optically transparent thin layer electrode (OTTLE) cells have been employed. They have, however, a serious drawback in nonaqueous solvents. It is difficult in these cells to obtain a voltammogram of quality sufficient to resolve the potential at which the species under investigation is

Diagram of Electrolysis Cells Used For Biliverdin/Purpurin Production
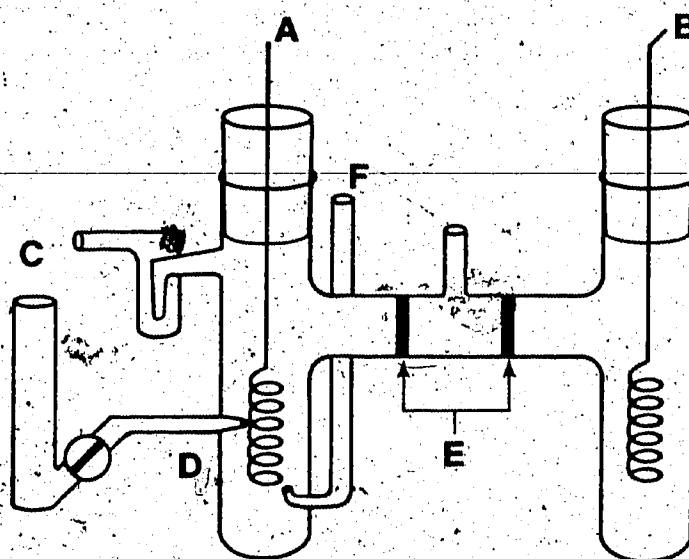
(A) Bulk Cell

(B) Prep Cell

A. Working electrode
B. Secondary electrode
C. Reference compartment
D. Luggin probe
E. Glass frits
F. Gas port
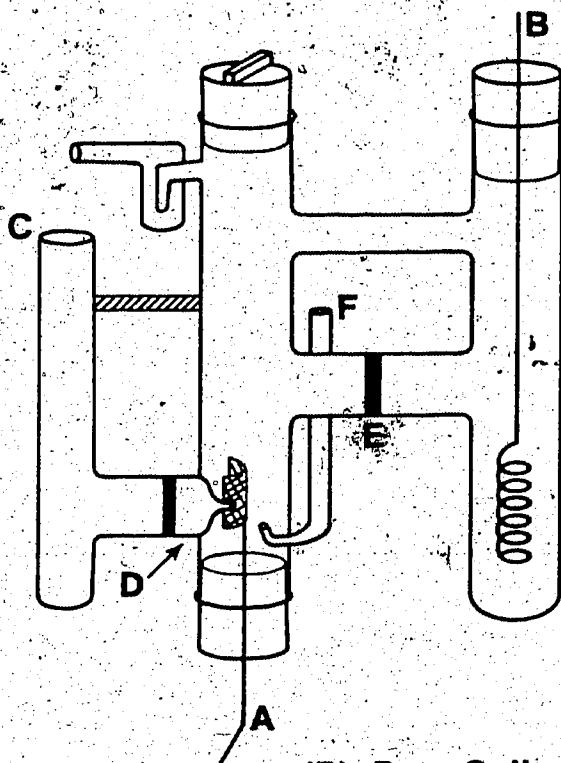
Figure 16

produced. This is caused mainly by the poor electrode geometry and high resistance. The secondary and reference electrodes are located externally, and the current distribution is very poor at the minigrid. These cells are constructed using two glass plates which sandwich a gold or platinum minigrid working electrode, and are held together with epoxy glue. There can be a problem in solvents such as DMSO which readily dissolve this glue. A new cell was designed [84] so that these two limitations were effectively eliminated. The cell and mount are shown in Figure 17. The working and secondary electrodes were Pt; the former a mesh, and the latter a pair of straight wires symmetrically placed parallel to the working electrode and located between the plates. The two quartz plates were 3 mm thick. The separation was <.2 mm. The cell was mounted in a Teflon boat which held 5 mL of solution. Capillary action drew the solution up between the plates. Three holes were located on the top of the mount. They allowed for placement of the Luggin probe, and the purge gas inlet and outlet. The entire unit fit inside the sample compartment of a Cary model 14 spectrometer. The cell was aligned such that the optical path passed directly through the center of the working electrode mesh. The electrode leads and the gas line were also fed into the sample compartment. With a

Thin Layer Optical Cell
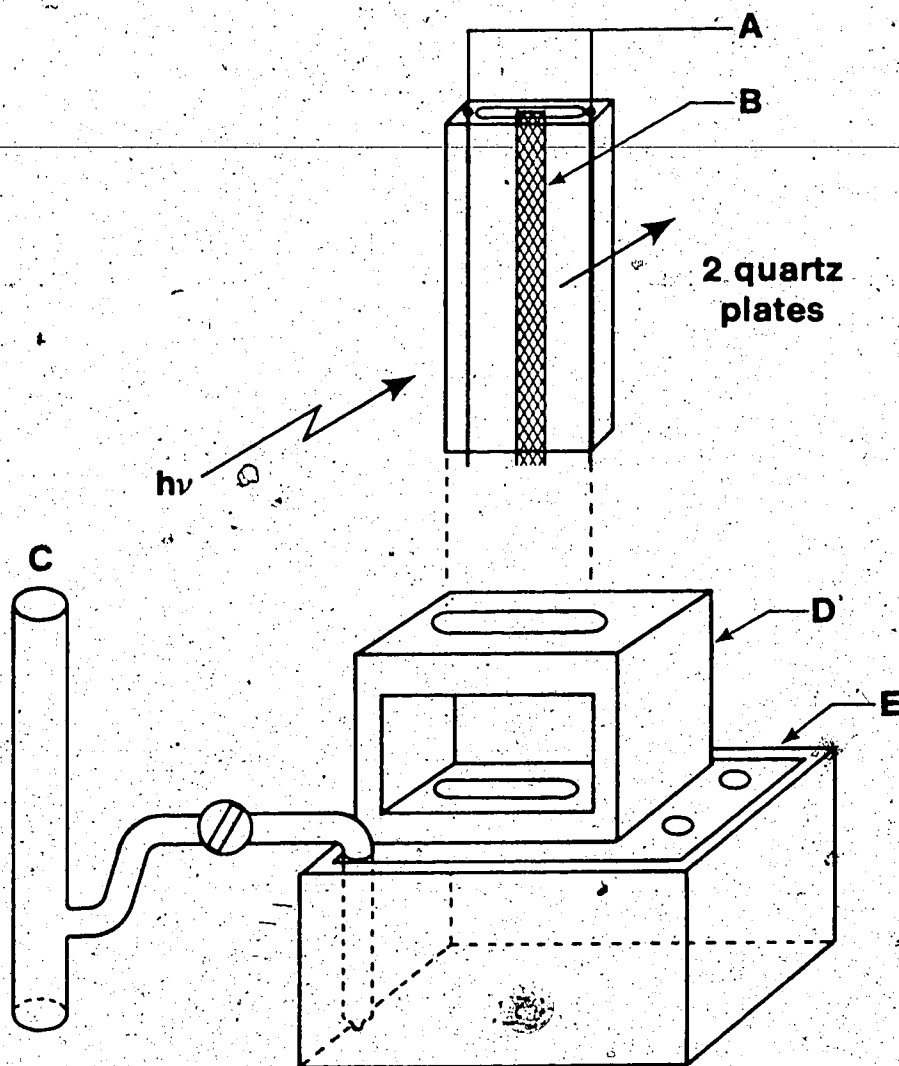
A. Secondary electrode (2 wires)

B. Working electrode (grid)

C. Reference compartment

D. Teflon solution boat

E. Gas ports

Figure 17

potentiostat, waveform generator and a recorder, it was
then possible to obtain a voltammogram of high quality and
monitor spectral changes as a function of potential.

3.8 PREPARATIONS

3.8.1 Bilirubin Purification

Due to poor analytical response to the simpler
physical tests of purity, such as the fact that bilirubin
has no melting point, and that chromatography is
inadequate to assure purity on the 99% level, a better
criterion of purity for this compound is usually based on
spectroscopic response.

Purification of commercial bilirubin was performed by
the following procedure. Commercial bilirubin was
dissolved in chloroform by boiling 5-15's while under
reflux. A concentration of .80-1.00 mg-mL^{-1} was
obtained. The solution was then cooled to room temp-
erature. A column of anhydrous sodium sulphate which had
been wrapped externally with aluminum foil to prevent
photochemical degradation was used to separate the
impurities. Impurities such as biliverdin and mono- and
dipyrroles remained on the column [27]. Approximately 60%
of the volume of the eluent was then removed by
distillation. Crystallization began spontaneously. Care
must be taken at this stage because if crystallization

proceeds too rapidly, occlusion occurs and the volume of chloroform has to then be doubled to once again dissolve all the crystals. The solution while still hot was filtered through a hot water funnel. It was then cooled to -20°C for 24 h and an equal volume of diethyl ether which had also been cooled was added which served to bring out some of the remaining bilirubin. The precipitate was collected by filtration, and washed with diethyl ether until the ether was uncolored. The precipitate was dried in vacuo at room temperature, in the dark. The yield was 50-55%.

3.8.2 Preparation of Pure Biliverdin

Biliverdin is the first isolatable product following the oxidation of heme [85]. It can also be obtained by the chemical/electrochemical oxidation of bilirubin. Use of this compound would obviously be invaluable in the mechanistic study of bilirubin oxidation, thus the most practical synthesis for this verdin in pure form was sought out. As previously mentioned several chemical methods for the production of biliverdin exist [86-88]. These procedures, however, all lead to substantial amounts of verdinoid by-products such as the III-α, and XIII-α isomers, which are a result of acid catalyzed isomeric scrambling of the initially pure bilirubin IX-α isomer. Purification of biliverdin is difficult and time

consuming. The typical method involves esterification and then TLC [89].

Another method for the preparation of biliverdin has been employed by Manitto and Monti [90]. In our laboratory this method has proved to be the most efficient in terms of low cost of materials and total time expended. Purified bilirubin was used as a starting material. Only traces of the III-α and XIII-α isomer were present. Following the bilirubin purification, 300 mg was then added to 400 mg of tetrachloro-1,4-benzoquinone, along with 570 mg of picric acid and 20 mL of t-butanol. This mixture was then added to 500 mL of ethanol-free chloroform. The solution was purged with argon for 15 m. After being properly sealed, the flask was stored in the dark for 6-8 d. As oxidation progressed the solution changed from orange to dark green in color. When the oxidation was complete the chloroform was evaporated in vacuo. To the product 100 mL of methanol-benzene (5:100 v/v) was added. After stirring, the green precipitate was collected. This precipitate which is a 1:1 complex of biliverdin and picric acid was then washed with benzene. The yield of this complex was usually between 75-95 mg. To remove the picric acid, the complex was dissolved in 4 mL of DMSO. This solution was added to 300 mL of ethyl acetate, placed into a separatory funnel and washed with

distilled water until the aqueous phase appeared colorless. This usually required ten extractions. The ethyl acetate solution which contained the pure biliverdin was then filtered, and the product was dried _in vacuo_. 40-50 mg (20% yield), of pure biliverdin was obtained. The purity was checked using TLC. The eluting system was methanol-benzene (5:100). One green spot migrated with R_f = 0.23. A visible spectrum showed peaks at 650 nm and 384 nm in DMF.

3.8.3 Preparation of Biliverdin Electrochemically.

Biliverdin was also produced following the same procedure as that for electrolytic purpurin production described in the next section. The precursor was pure bilirubin. The conversion was determined to be complete by spectroscopic monitoring.

3.8.4 Preparation of Purpurin.

Purpurin was prepared by controlled potential electrolysis. Pure biliverdin was used as the substrate. Typically 2 mg was dissolved in a minimum amount of DMF (~5 mL). The solution was placed into the working compartment of the electrolysis cell and brought to a workable volume using acetonitrile. The acetonitrile provides two functions: (1) it increases the volume so that the entire working electrode is covered for maximum

electrolysis efficiency and (2) upon completion of electrolysis it is easily removed in vacuo to provide a concentrated final product. The supporting electrolyte was 0.1 M tetrabutylammonium tetrafluoroborate. A cyclic voltammogram of the substrate was taken to determine the half-wave potential of 0.23 V. The potential at the working electrode was then chosen to be 150 mV positive of the half-wave potential. The current through the cell was integrated. Oxygen was bubbled through the solution, and periodic spectra of the solution were taken to monitor the conversion. Upon completion of the reaction (2 C-(mol of substrate)$^{-1}$) the solution was concentrated by vacuum evaporation of solvent.

3.8.5 Preparation of Supporting Electrolyte

Tetra-n-butylammonium tetrafluoroborate (TBAF) was prepared using a modified method of Lund and Iverson [91]. The supporting electrolyte was prepared in one mol quantities. 340 g of tetrabutylammonium hydrogen sulfate was dissolved in 750 mL of distilled water. This solution was filtered, and then placed into a 6 L separatory funnel. 110 g of sodium tetrafluoroborate was dissolved in 650 mL of distilled water, filtered, and added to the separatory funnel. Upon mixing, the tetra-n-butylammonium tetrafluoroborate immediately precipitated. 500 mL of crushed ice was added to the precipitate and the mixture

was then thoroughly shaken. 150 mL of methylene chloride

was then added to the separatory funnel. After thorough

mixing the methylene chloride-TBAF layer was allowed to

separate. This layer was isolated, filtered, and added to

900 mL of ice-cold anhydrous diethyl ether. The TBAF was

allowed to precipitate for 15 m, filtered, and then

redissolved in 150 mL of methylene chloride. The TBAF was

recrystallized two more times, and then dried in vacuo at

60°C for 72 h. An 80% yield was obtained.

CHAPTER 4

RESULTS

4.1 VOLTAMMETRY

Cyclic voltammetry was performed on bilirubin and biliverdin. The kinetic cell used is shown in Figure 13. For all dc and ac voltammetry the DMF solution was 0.50 mM in bilirubin and 0.15 M TBAP. The potentials are referenced to Ag/AgI (0.1 M). The dry DMF solutions were saturated with argon for 15 m prior to the experiments. A positive sweep at 0.10 V·s^{-1} is shown in Figure 18A. This sweep from -0.40 V to 0.60 V and back exhibits four waves located at -0.21 V, 0.10 V, 0.24 V, and 0.47 V. A negative sweep (Figure 18B) from 0.00 V to -2.30 V exhibits one prominent wave at -1.55 V, and two smaller oxidation waves at -1.00 V and -0.21 V.

Figure 19 shows the bipolar voltammetry of bilirubin. When the potential sweep was initiated in the positive direction oxidation waves at 0.10 V, and -1.00 V along with reduction waves at -0.88 V, -1.35 V, and -1.55 V are observed. Figure 19B shows the voltammetric response when the potential sweep was initiated in the

A

0.47V

0.24V

0.10V

i (A.U.)

−0.21V

−0.40V   E   +0.60V

−2.30V   −1.55V   −1.00   0

B

−i (A.U.)
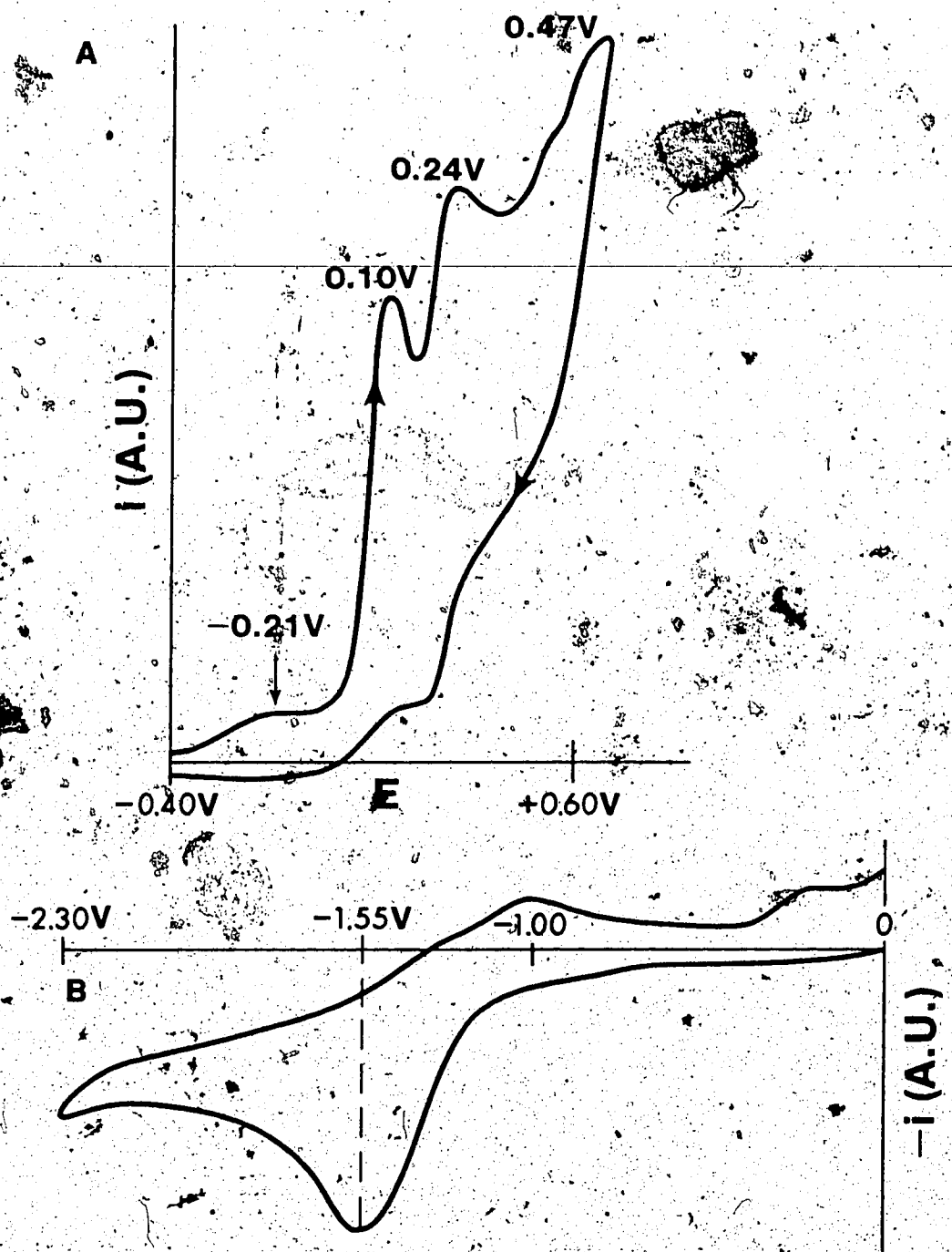
Voltammetry of 0.5 mM bilirubin in DMF with 0.15 M
TBAF and Ag/Ag$^+$ (0.1 M) reference electrode. Sweep
rate is 0.10 V s^{-1}.

Figure 18

A

i (A.U.)

−1.35V
−1.55V
−0.88V
−1.00V
0.15V

B

i (A.U.)

−1.35V
−1.00V
−1.55V
−0.88V
0.15V

Figure 19

**Voltammetry of bilirubin as a function of sweep
direction. A) positive first, B) negative first
Parameters are given in Figure 18**

negative direction. The reduction waves at -0.88 V and -1.35 V are observed to be the result to some oxidation process since they do not appear until the electrode potential has been swept positive.

Figures 20 and 21 show the voltammetric response of biliverdin. For a positive sweep (Figure 20A) two oxidation waves at 0.24 V and 0.47 V are observed. A negative sweep exhibits two reduction waves at -1.35 V and -1.55 V. The same sweep using biliverdin dihydrochloride (commercially obtained, Figure 20C) has two basic differences: 1) the appearance of a wave at -0.90 V and 2) the coalescing of the -1.35 V and -1.55 V waves into one broad wave from -1.35 to -1.55 V.

The bipolar voltammetry for biliverdin is shown in Figure 21. All of the previously observed waves are present regardless of the initial direction of the sweep, with the exception of that at -0.88 V. This wave was only present after the potential has been first swept to positive potentials.

Figure 22 shows the voltammetric changes which occur when base (tetrabutylammonium hydroxide) was added to a 0.5 mM solution of bilirubin. When cycling from -0.40 V to 0.40 V at 0.10 V-s^{-1}, the oxidation wave at -0.21 V increases quantitatively with base addition and the peak at 0.10 V decreases in height. The third oxidation wave at 0.24 V was unaffected by the addition of base.

Voltammetry of 0.5 mM biliverdin in DMF with 0.15 M TBAF and Ag/Ag$^+$ (0.1 M) reference electrode. Sweep rate is 0.10 V s^{-1}.
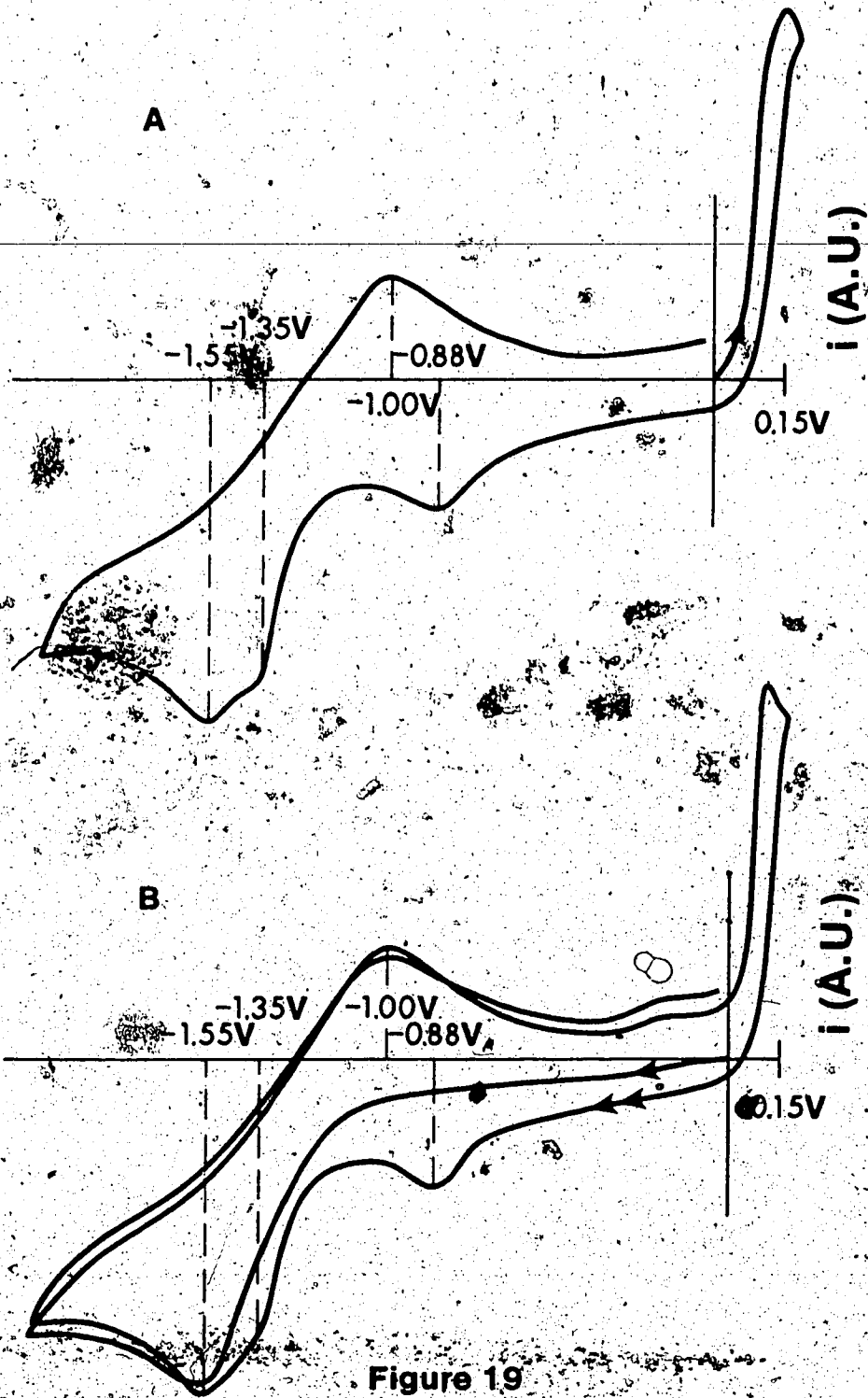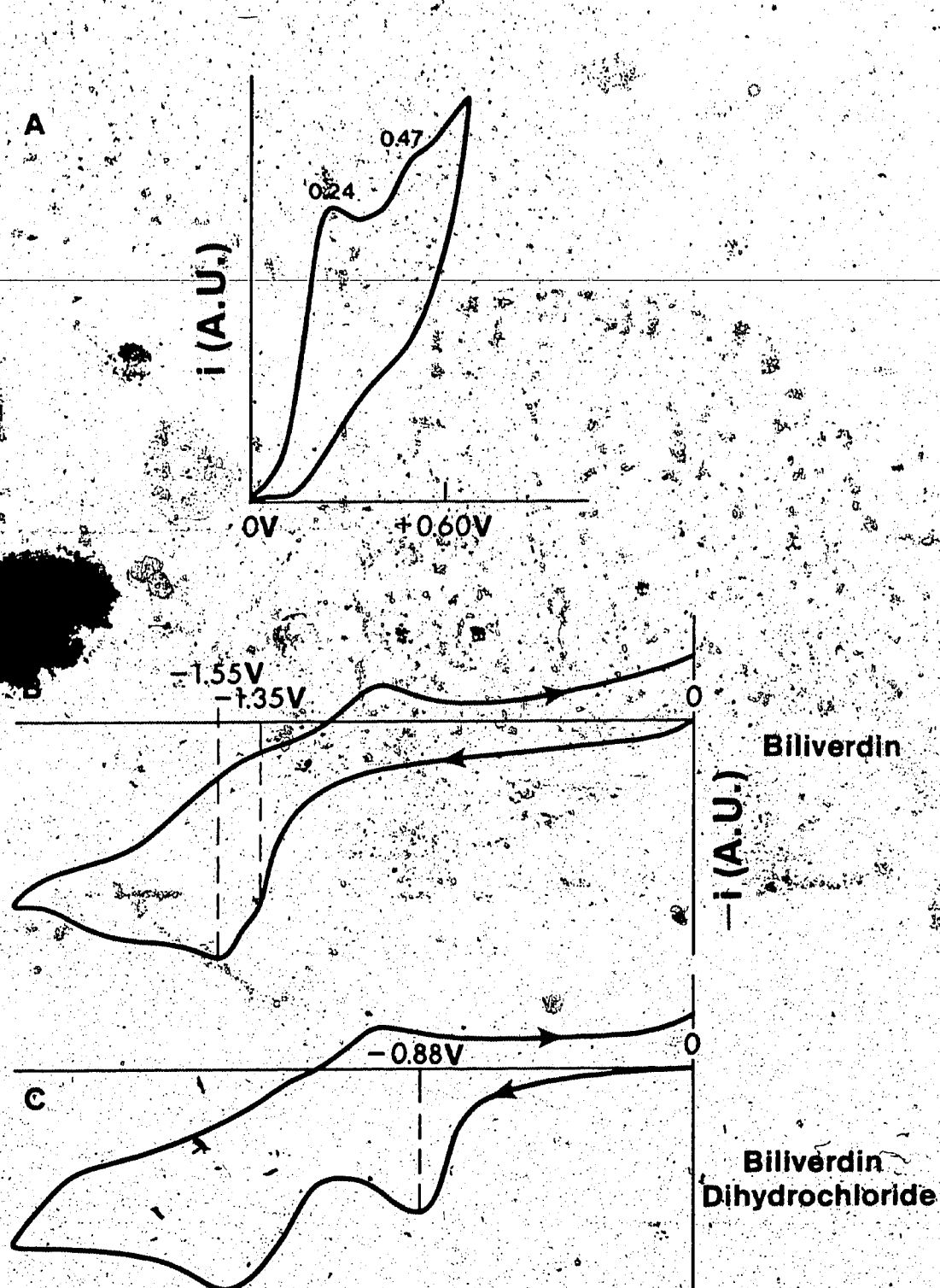
Figure 20
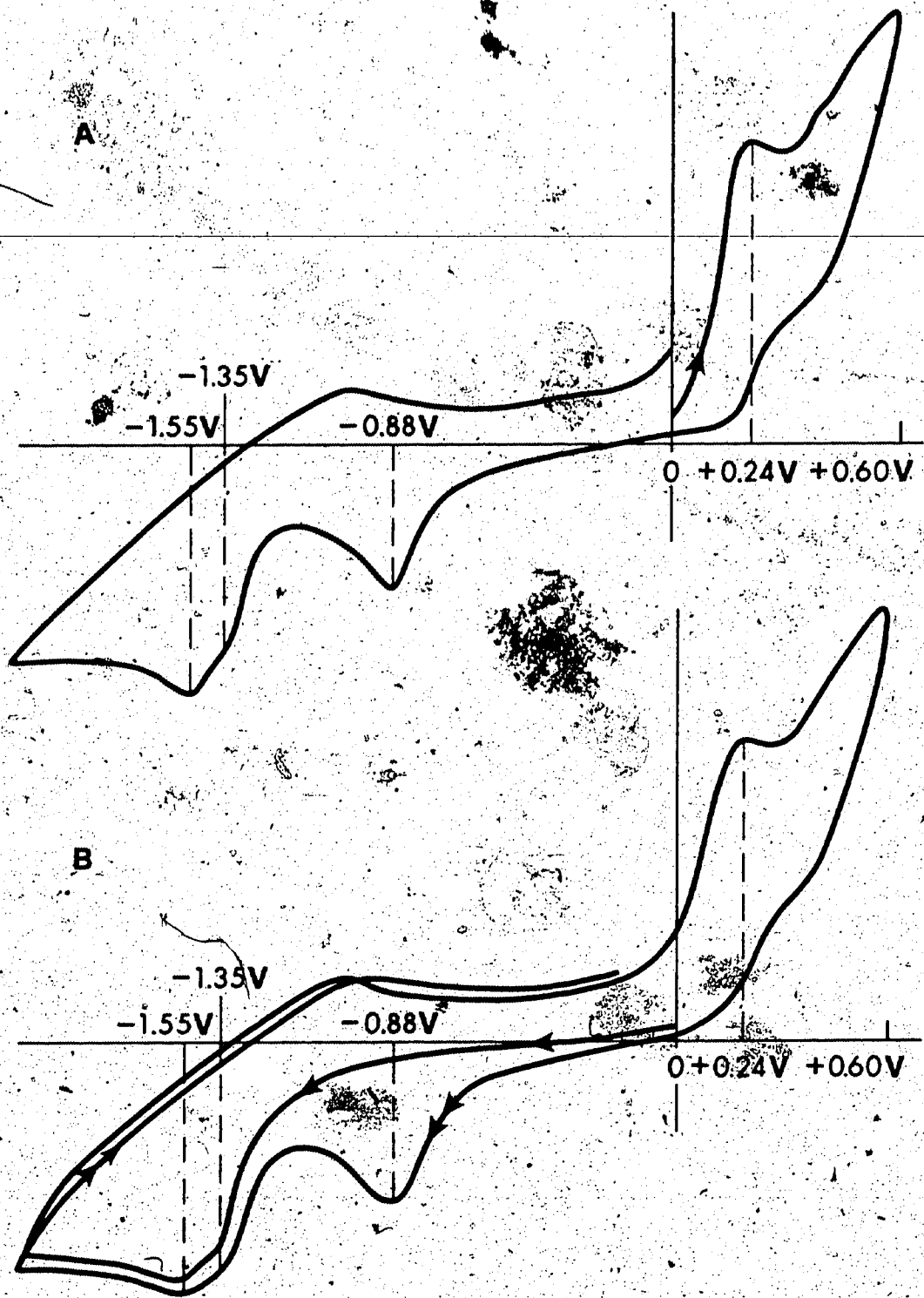
Voltammetry of 0.5 mM biliverdin as a function of sweep direction A) positive first, B) negative first. Parameters are the same as Figure 20. Figure 21

A   B   C   D

i (A.U.)

−0.4v 0v +0.4v

E
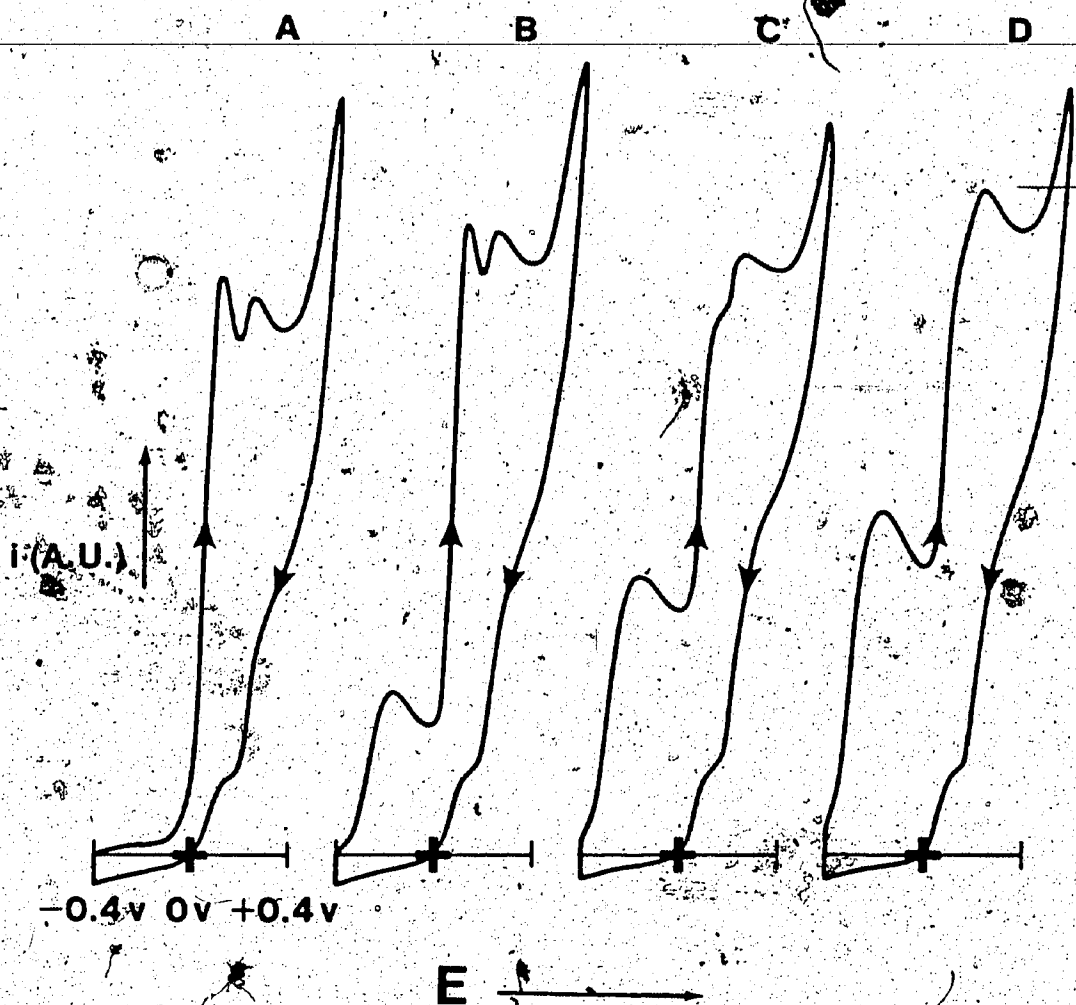
Voltammetric changes of a 0.5mM bilirubin solution in DMF with 0.15 M TBAF as tetrabutylammonium hydroxide is added. Sweep rate is 0.10 V sec^{-1} and the reference electrode is Ag/Ag$^+$ (0.1M)

Figure 22

The effect of acid additions on a 0.8 mM solution of bilirubin is shown in Figure 23. A plot of i_p vs $v^{1/2}$ for the 0.10 V oxidation wave exhibits a decrease in slope as the concentration of acid increases.

Figure 24 displays the effect of repetitive cycling about -1.20 V to 0.14 V. The sweep rate was 0.15 V-s^{-1}. As the cycling progressed three distinct changes are noted: 1) the oxidation wave at 0.11 V decreased slightly and then reaches an equilibrium value, 2) the reduction wave at -0.88 V rapidly increases in height and also reaches an equilibrium value, 3) the oxidation wave at -0.82 V increases in height and also reaches an equilibrium value. This wave was present in neutral and basic solutions but disappears under acidic conditions.

The effect of cutting short the voltammetric cycle between -1.20 V and 0.14 V is shown in Figure 25. Starting in the negative direction the reduction and oxidation waves at -0.88 V and -0.82 V are absent. After sweeping to 0.14 V and then coming negative again both of the previous waves are present. However, the species responsible for these waves was consumed rapidly since a repetitive negative sweep starting from -0.50 V shows the complete disappearance of these waves.

Iρ vs. $V^{1/2}$ as a function of acid concentration on the 0.10 V oxidation peak.

Iρ (μA)

A. 0 mM acid
B. 0.001 mM acid
C. 0.01 mM acid
D. 0.1 mM acid
E. 0.5 mM acid
F. 1.0 mM acid
G. 20.0 mM acid

Slopes:
A. 2.94
B. 2.83
C. 2.74
D. 2.55
E. 2.49
F. 2.22
G. 1.82

$V^{1/2}$
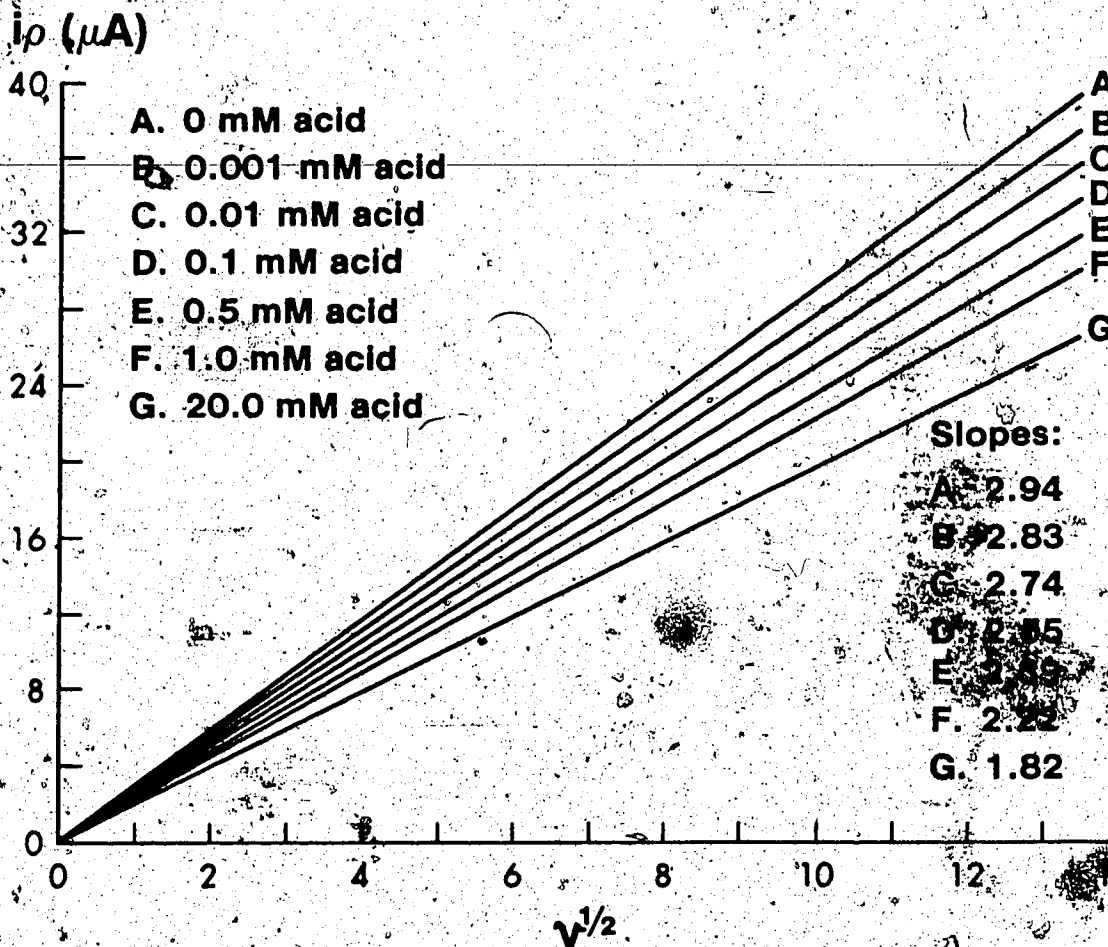
Conditions: 0.8 mM bilirubin
DMF solvent
Ag/Ag⁺ reference electrode (0.1 M)
0.15 M TBAF
potential limits 0.00 V to 0.50 V

Figure 23
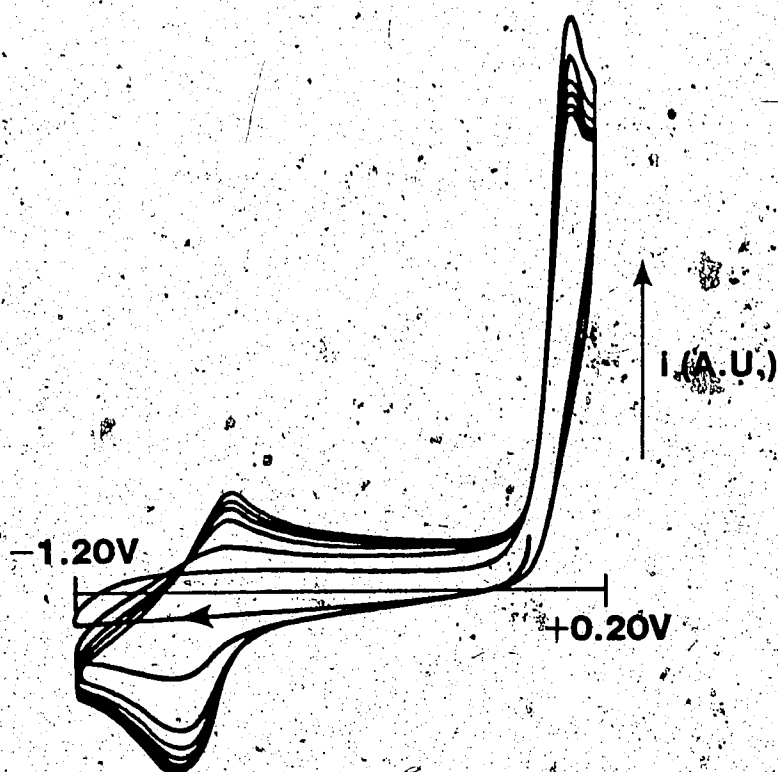
Effect of repetitive cycling about −1.20 — +0.14V
on a 0.5mM solution of bilirubin.
The potential is referenced to Ag/Ag⁺ (0.1M).
Supporting electrolyte 0.15M TBAF.
Sweep rate is 0.15 V.sec⁻¹.

Figure 24

i (A.U.)

−1.20V

+0.20V
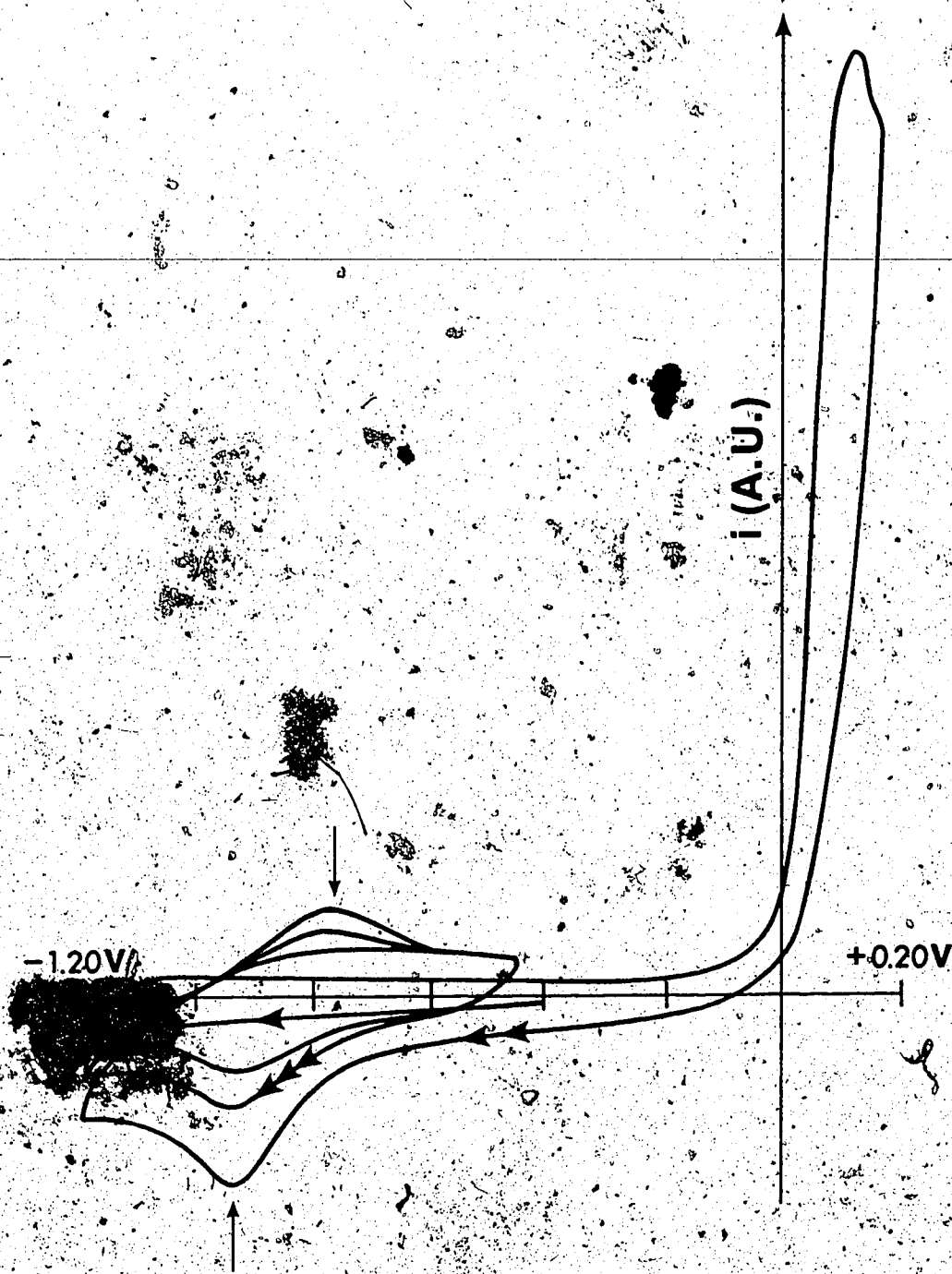
Attenuated Voltammetric Cycling about −1.20V
and +0.14V in a 0.5 mM solution of bilirubin in
DMF with 0.15 M TBAF, using an Ag/Ag$^+$ (0.1M)
reference electrode. Scan rate is 0.10 V s^{-1}

Figure 25

4.2 AC VOLTAMMETRY

The ac voltammetry of bilirubin is shown in Figure 26. As the frequency increases, i(ωt) at 0.20 V increases for biliverdin oxidation. The ac current for bilirubin oxidation at 0.10 V only increases as the frequency was decreased. On the reverse sweep the same trend in the bilirubin/biliverdin waves occur.

4.3 CONVENTIONAL SPECTRA

The visible spectra of bilirubin and its oxidation products - biliverdin, purpurin, and choletellin - are displayed in Figure 27A-D. These oxidation products were produced by controlled potential electrolysis using the thin layer optical cell shown in Figure 17. The single peak at 453 nm characteristic of bilirubin is shown in Figure 27A. After four minutes of electrolysis at 0.12 V the peaks at 384 nm and 670 nm appear, indicating the production of biliverdin (Figure 27B). Increasing the potential to 0.25 V forces the appearance of two new peaks at 336 nm and 550 nm (Figure 27C). Finally at 0.51 V spectral peaks at 312 nm and 487 nm appear (Figure 27D).

Figure 28 shows the spectral changes which occur when biliverdin was subjected to 0.5 mM picric acid. Figure 28A shows the substrate peaks at 380 nm and 650 nm.
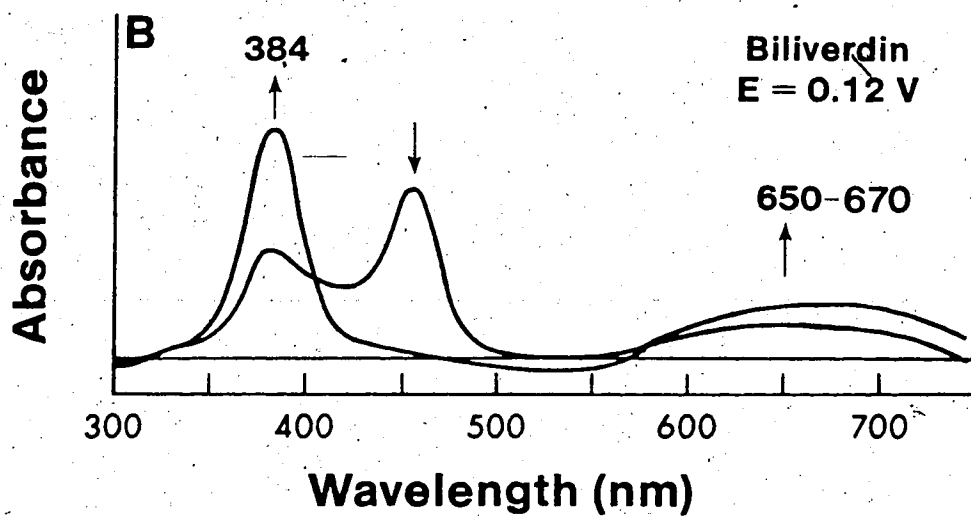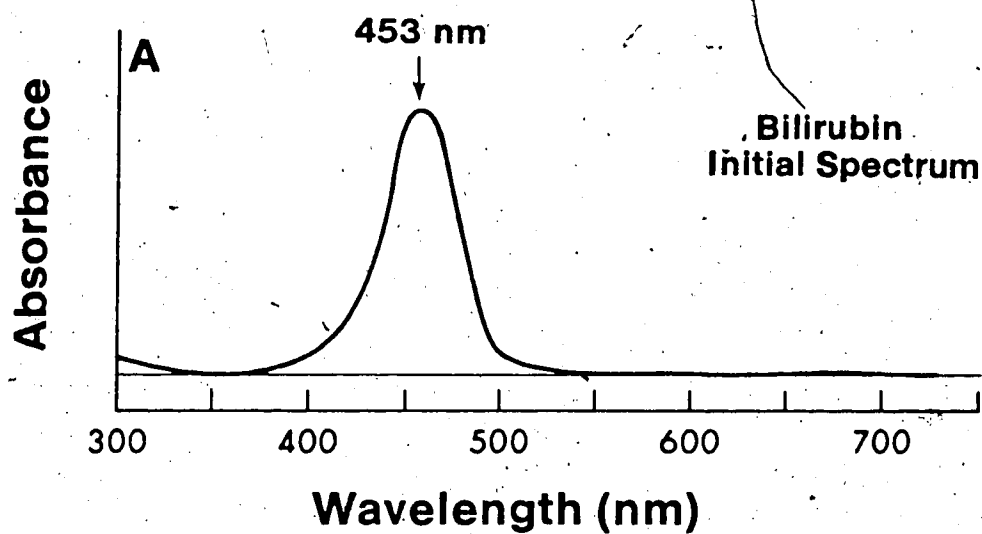
300 Hz

150 Hz

50 Hz

0.5 mM bilirubin in DMF
with 0.15M TBAF.
Ag/Ag$^+$ (0.1M) reference
electrode,
dc ramp 0.005 V sec^{-1},
ac oscillation 0.005 V.p.p.
sine wave

25 Hz

13 Hz

$I(\omega t)$
A.U.

0 V   +0.40V
E

Figure 26

Figure 27a-b

1) Spectra after 30 seconds
2) Spectra after 4 minutes;potentials are
   referenced to Ag/Ag$^+$ (0.1 M)

C

336nm

Purpurin
E = 0.25V

550

1

2

300   400   500   600   700

D

312 nm

Choletellin
E = 0.51V

487

1

2

300   400   500   600   700

Wavelength (nm)
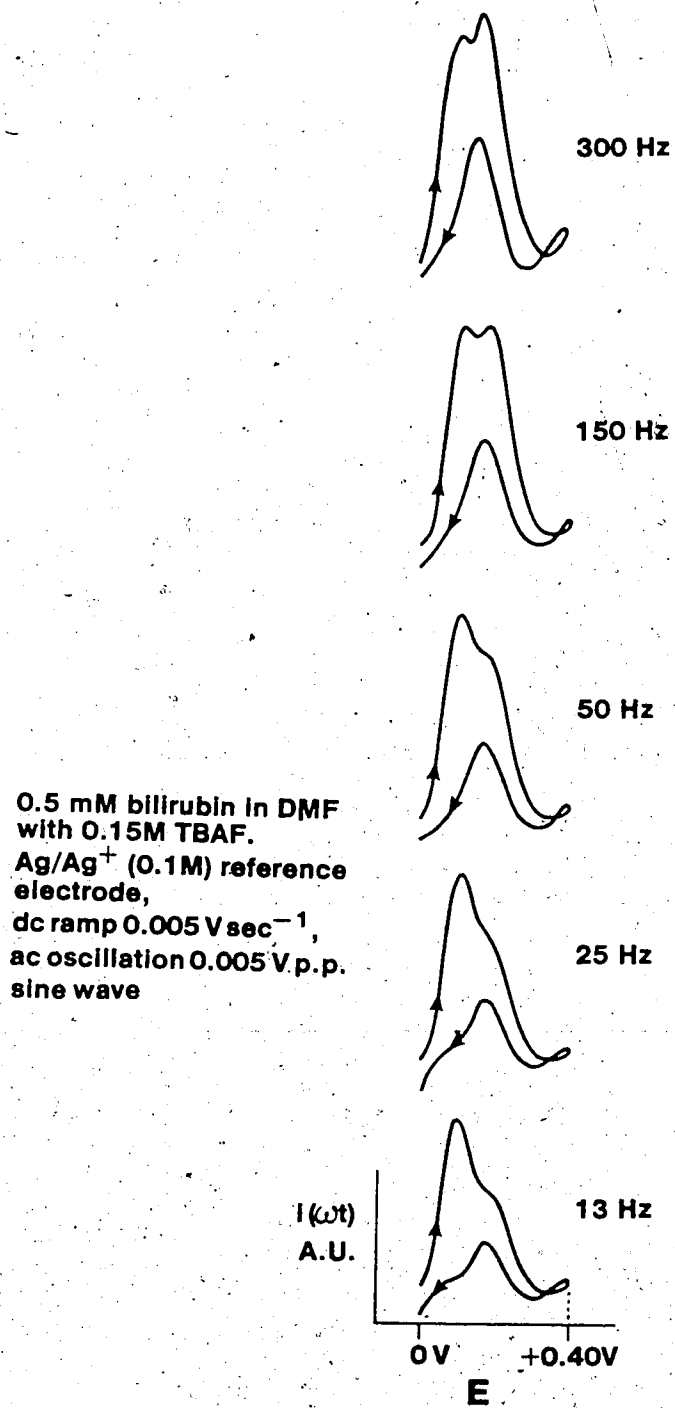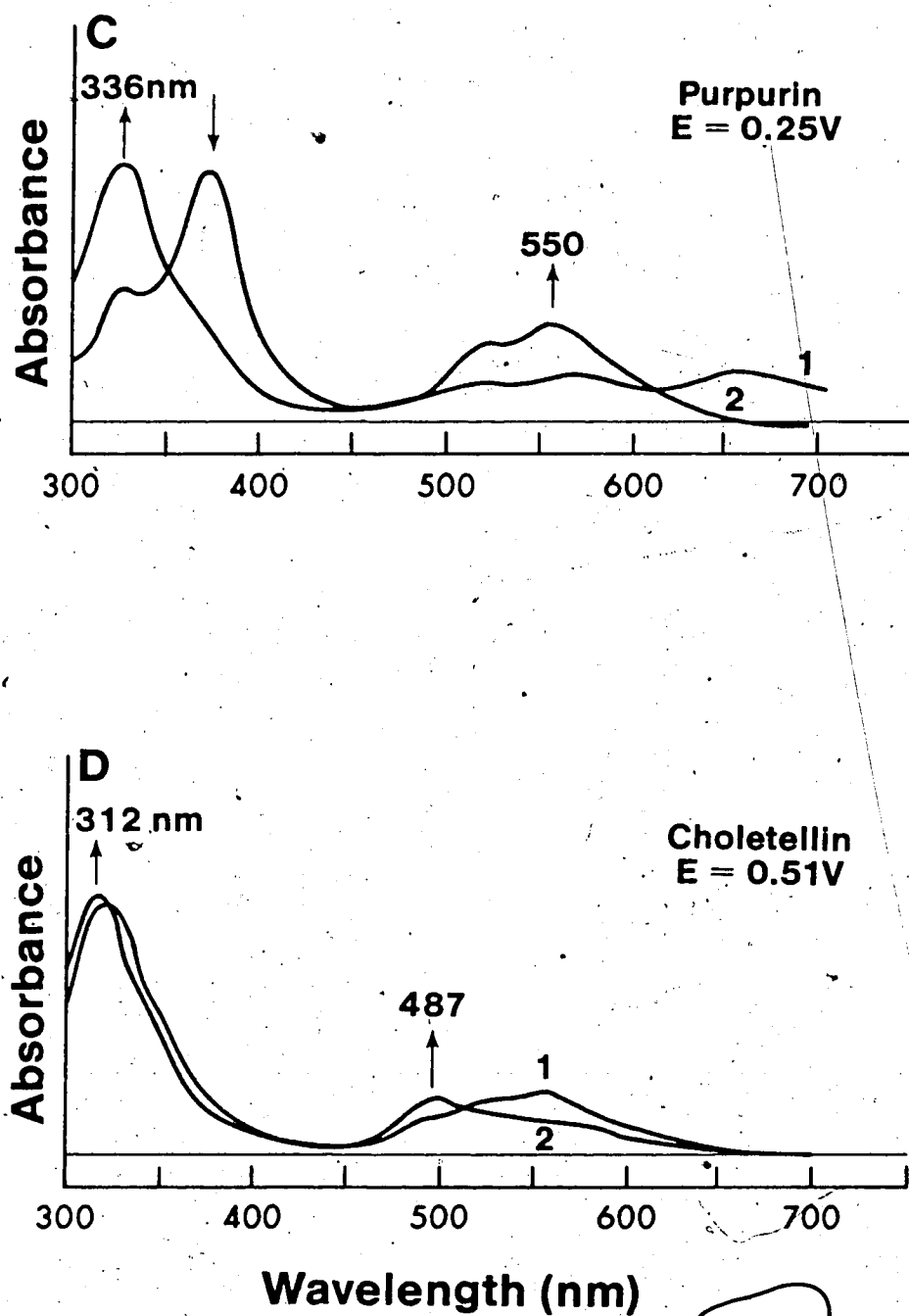
1) Spectra after 30 seconds
2) Spectra after 4 minutes
Potentials are referenced to Ag/Ag$^+$ (0.1 M)

Figure 27c-d
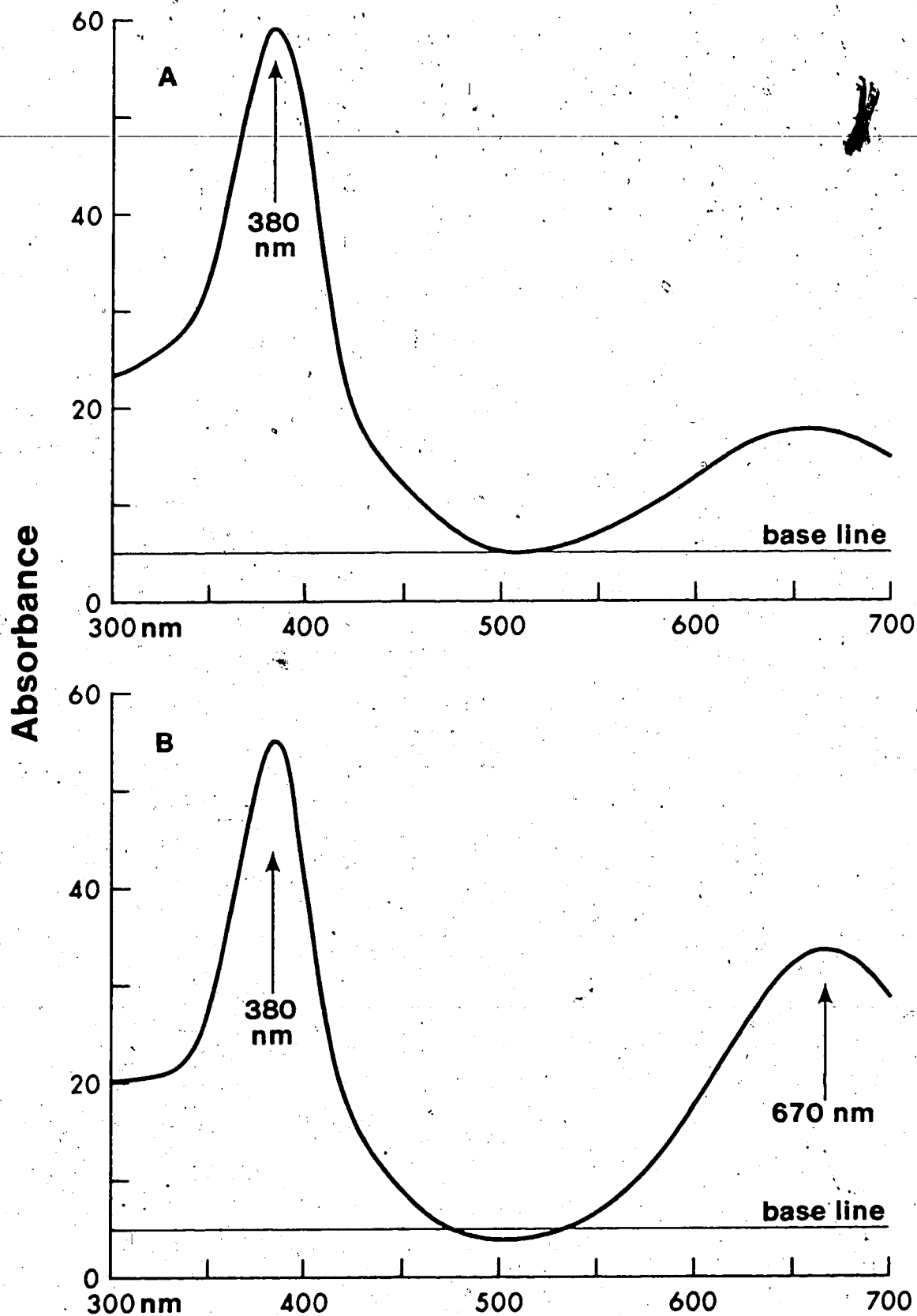
Figure 28

Spectral changes of biliverdin when acid is added to the solution. A) DMF solution of biliverdin without acid   B) in presence of 0.5 mM acid

Figure 28B shows a shift in the 650 nm peak to 670 nm while the peak at 380 nm remains unchanged.

4.4 SMACRS

Figure 29 shows R(ωt) at various wavelengths for a SMACRS experiment recorded during a linear potential sweep through the first two oxidation waves of a 0.50 mM bilirubin solution. The dc sweep rate was 0.005 V-s^{-1}. The ac conditions were 45 Hz and 0.03 V$_{p-p}$. The bipolar shape indicates first the appearance of some bilirubin oxidation product (negative R($\overline{\omega t}$)), and then the removal of some absorbing species from the electrode surface (positive R(ωt)). A plot of the 0.04 V peak (A) and the 0.15 V peak (B) as a function of wavelength of light is shown in Figure 30. This spectra consists of 20 separate SMACRS experiments.

Figure 31 and 32 show the SMACRS and voltammetry for 0.50 mM bilirubin from 0.00 V to 0.50 V at 546 nm as a function of base and acid additions respectively. The magnitude of the ac reflectance was noted to decrease as base was added. The voltammetry indicates that with additional amounts of base the first oxidation wave disappears. When acid was added to the solution, the voltammetry shows a positive shift in the peak potentials of both oxidation waves. The SMACRS results showed an

SMACRS peak height as a function of wavelength
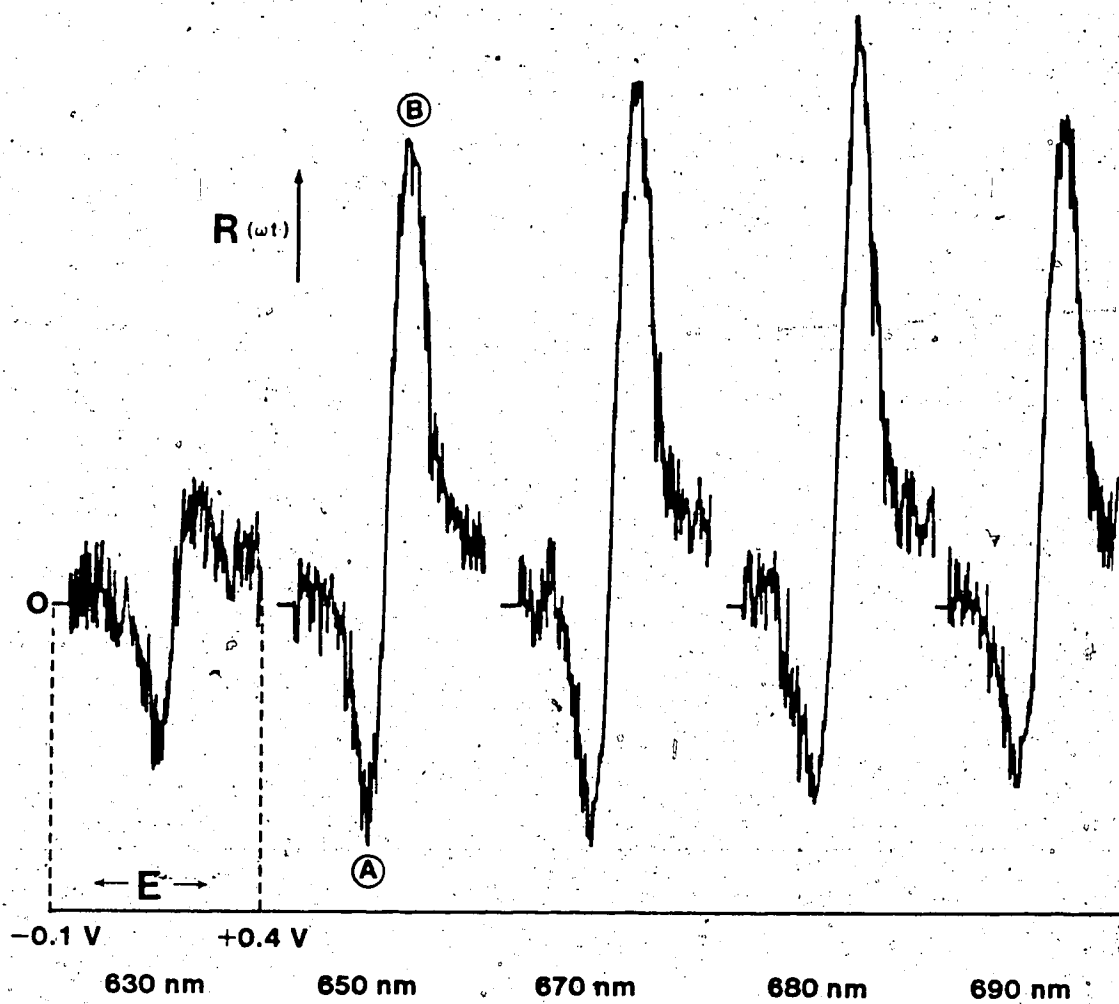
0.5 mM Bilirubin in DMF Ag/Ag+ ref.
Ⓐ 0.04V peak   Ⓑ 0.15V peak

Figure 29

SMACRS Dependence on Wavelength
Peak Height for 0.04 V and 0.15 V Peaks
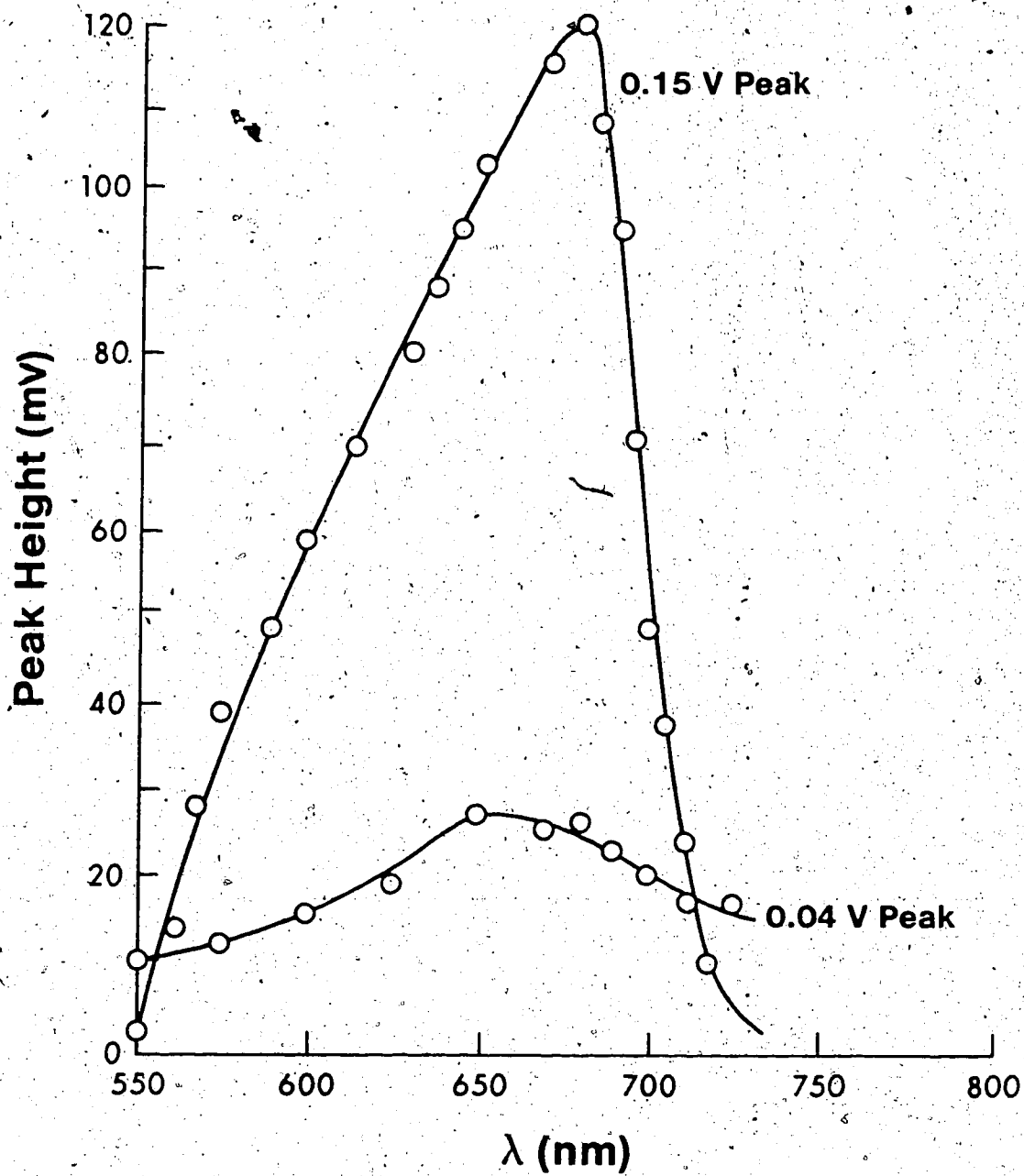
Figure 30
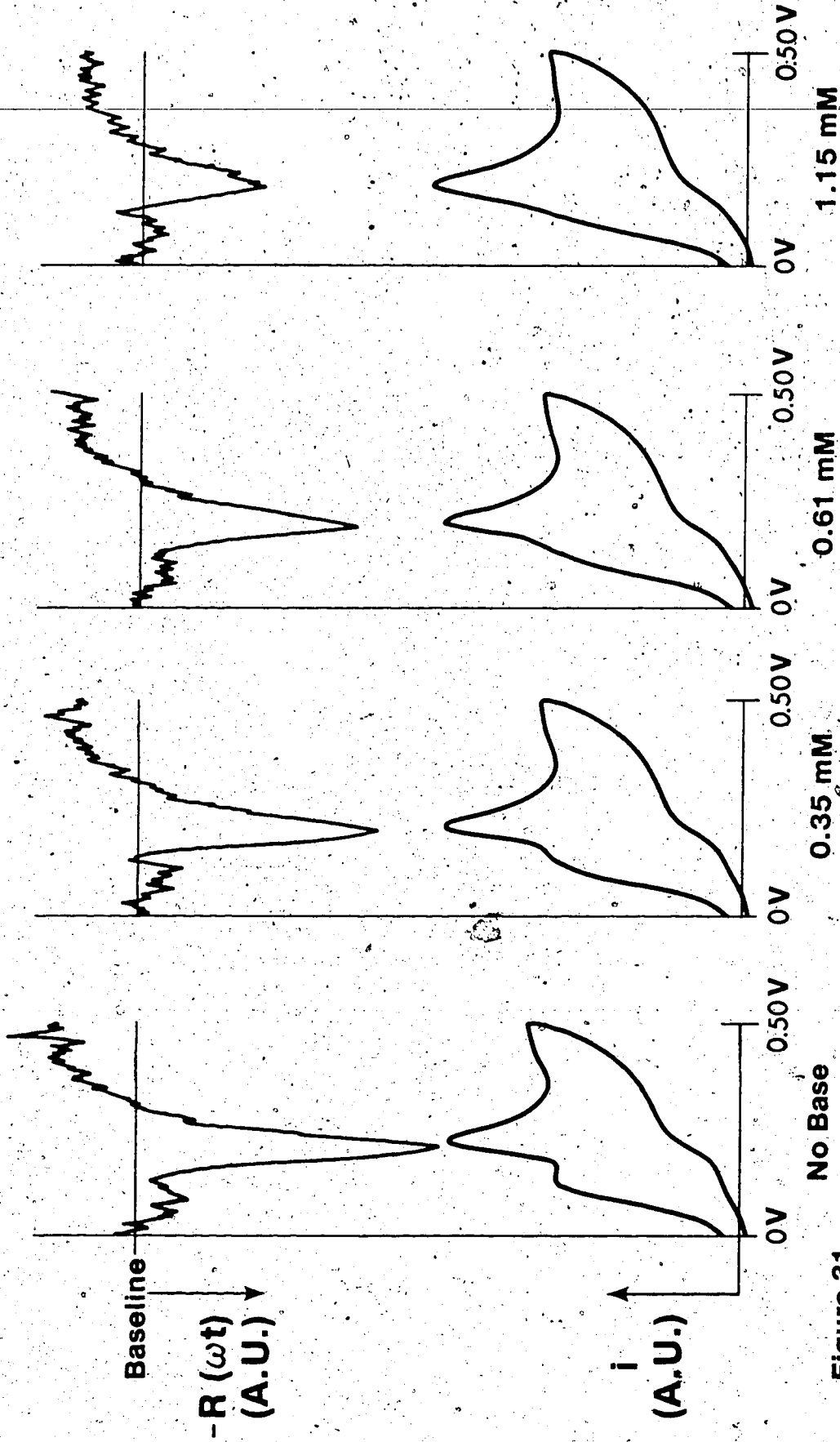
Figure 31

CV & SMACRS for 0.6 mM bilirubin in DMF as a function of base additions (2, 6 lutidine) to the solution. Ag/Ag$^+$ (0.1 M) reference. Voltammogram sweep rate 0.05 V s^{-1}. SMACRS dc 0.005 V s^{-1}, ac 0.03 V p-p at 40 Hz. λ = 546 nm.

Figure 32   No Acid   0.28 mM   0.54 mM   1.06 mM
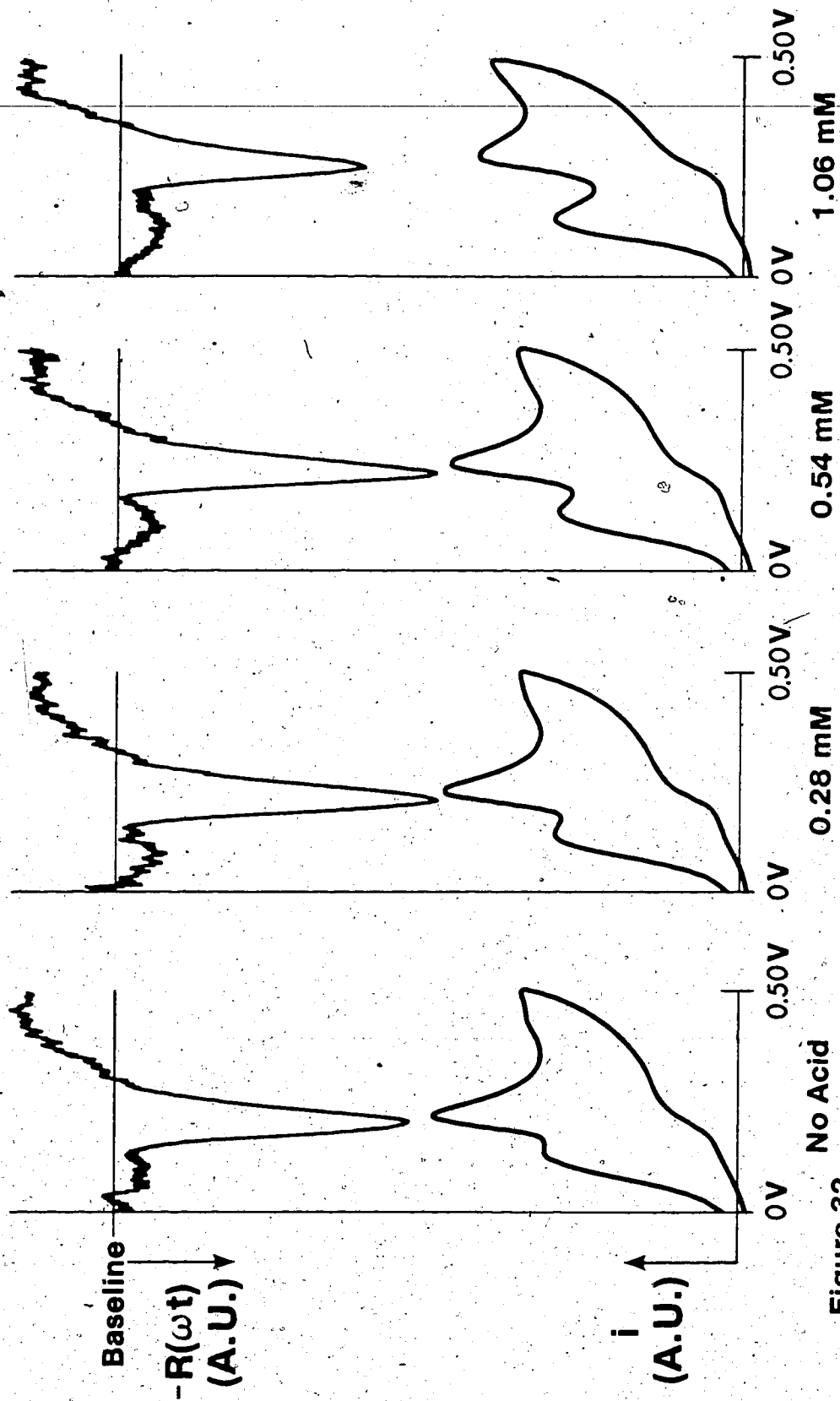
CV & SMACRS For 0.6 mM BR in DMF as function of acid additions (tetrafluoroboric acid). Experimental conditions are identical to those on Figure 31.

optimum concentration of protons (0.28 mM) above which

R(ωt) decreased. For both Figures 31 and 32 the acid and

base concentrations reported represent the net amount

added and not the actual concentration in the solution

since the small amount of basic impurities in the solvent

will effect the pH of the solution.

If R(ωt) was measured over a more extended potential

range two further oxidative processes can be identified.

These are shown in Figure 33A. The reflected light was

held constant at 546 nm. When acid was added to the

solution (trifluoromethylsulfonic acid (0.5 mM)) the first

SMACRS peak (I) increases in height, the second peak (II)

remains essentially unchanged, while (III) and (IV)

increase in height. The voltammetry of these solutions

are shown below each SMACRS scan on the same potential

scale.

4.5 MSRS

Figure 34 shows the MSRS response for a potential

modulation between -0.50 V and 0.20 V. A weak signal at

675 nm was recorded. Figure 35 gives the MSRS response

when the modulation limits are extended (-1.20 V to 0.20

V). A very strong signal was recorded. Peaks were

present at 636 nm and 675 nm. When the modulation

frequency was increased to 80 Hz the peak at 675 nm was
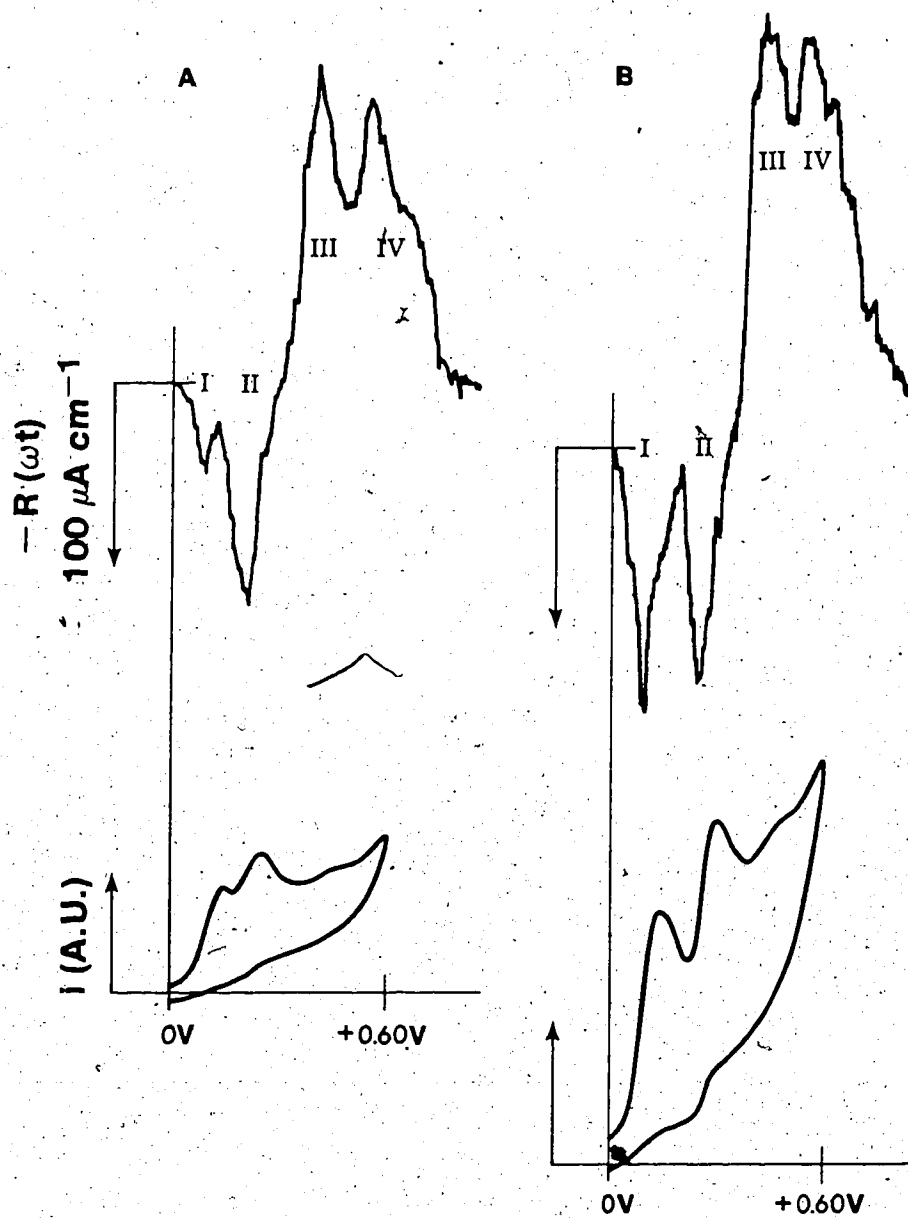
SMACRS and corresponding voltammetry for 0.5 mM bilirubin at 546 nm. Voltammetry: 0.10 V s^{-1}. SMACRS: dc 0.003 Vs^{-1}, ac 36 Hz 0.03 V p-p A) neutral solution B) acidic (0.05 mM) acid

Figure 33
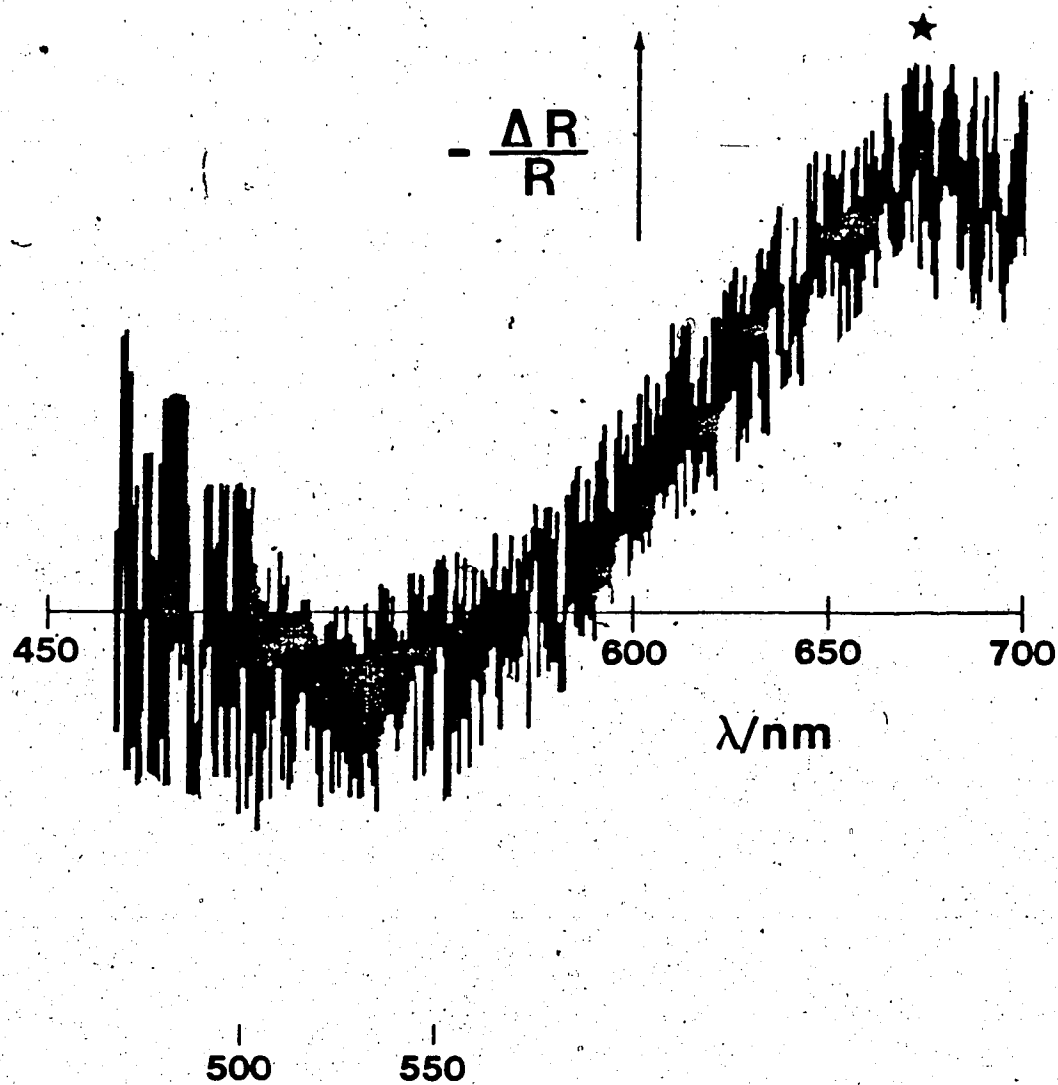
MSRS recorded at 40 Hz with potential limits −0.50V−+0.20V, slit width 2000Å, scan rate 5Å sec⁻¹, 0.5 mM bilirubin in DMF and 0.15 M TBAF Ag/Ag⁺ (0.1M) reference electrode.

Figure 34

$$-\frac{\Delta R}{R}$$

500   550   600   650   700

λ/nm
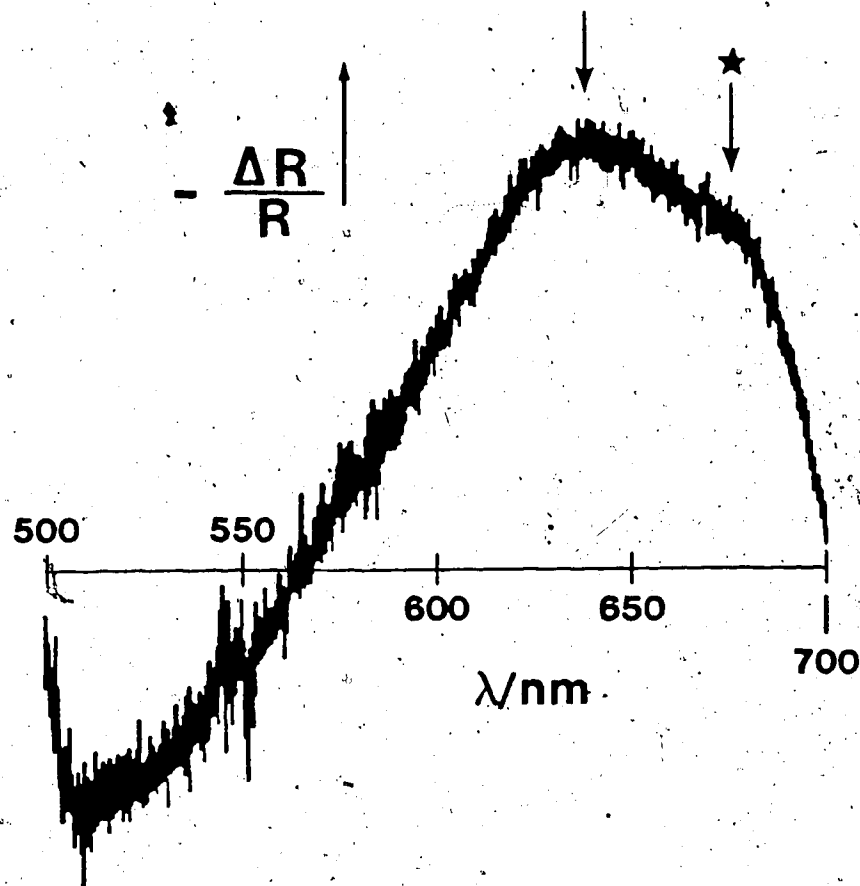
MSRS recorded at 40 Hz, with potential limits
−1.20V to +0.20V , Other parameters
identical to Figure 17. —

Figure 35

severely attenuated, while the peak at 636 nm was only

slightly affected. Below 500 nm excessive noise was

evident since the large bilirubin absorbance begins there,

and the feedback system tries to divide ΔR by a very small

number.

4.6 TRANSIENTS

Figure 36 shows absorbance-time transients recorded

at 625 nm, 636 nm and 675 nm. The solution was 0.5 mM

bilirubin in DMF with 0.15 M TBAF, and the reference

electrode was Ag/Ag$^+$ (0.1 M). The electrode was pulsed

from -1.10 V (800 ms) to 0.20 V (100 ms), and 64 scans

were collected and averaged. The recorded transient con-

sisted of 512 10 bit data points obtained at 500 μs-pt^{-1}.

4.7 PHOTO-CHEMISTRY

Figure 37 shows the changes in voltammetry which

occur when light (350-700 nm) was incident on a solution

of 0.5 mM bilirubin in DMF containing 0.15 M TBAF. The

voltammograms were taken at various photolysis times with

a sweep rate of 0.10 V-s^{-1}. As the time was progressively

increased wave (I) was observed to decrease in height

while wave (II) increased in height.

Absorbance – Time Transients
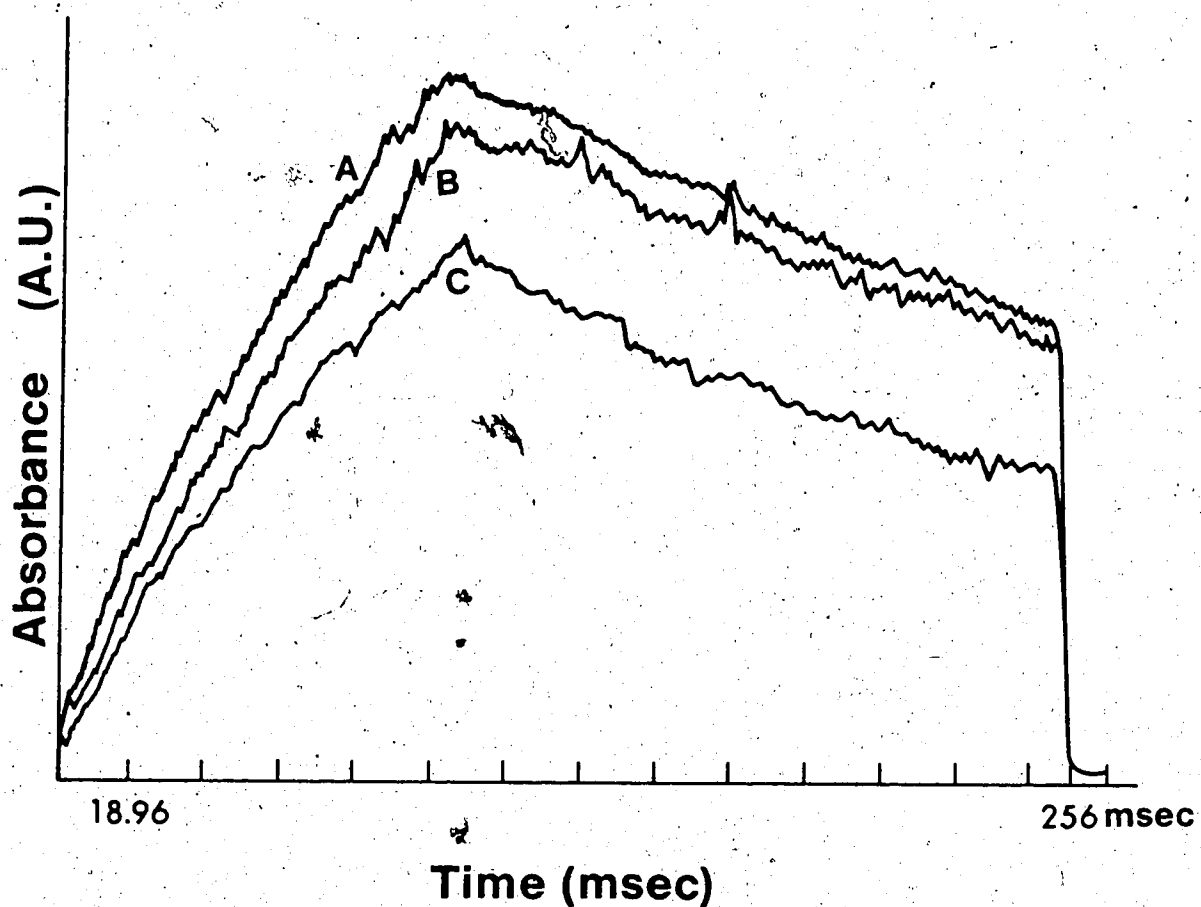
Absorbance-time transients recorded at (A) 636 nm, (B) 625 nm and (c) 675 nm 0.5 mM Bilirubin in DMF with 0.15 M TBAF, Ag/Ag$^+$ (0.1 M) reference,Slit width 1000 Å

Figure 36
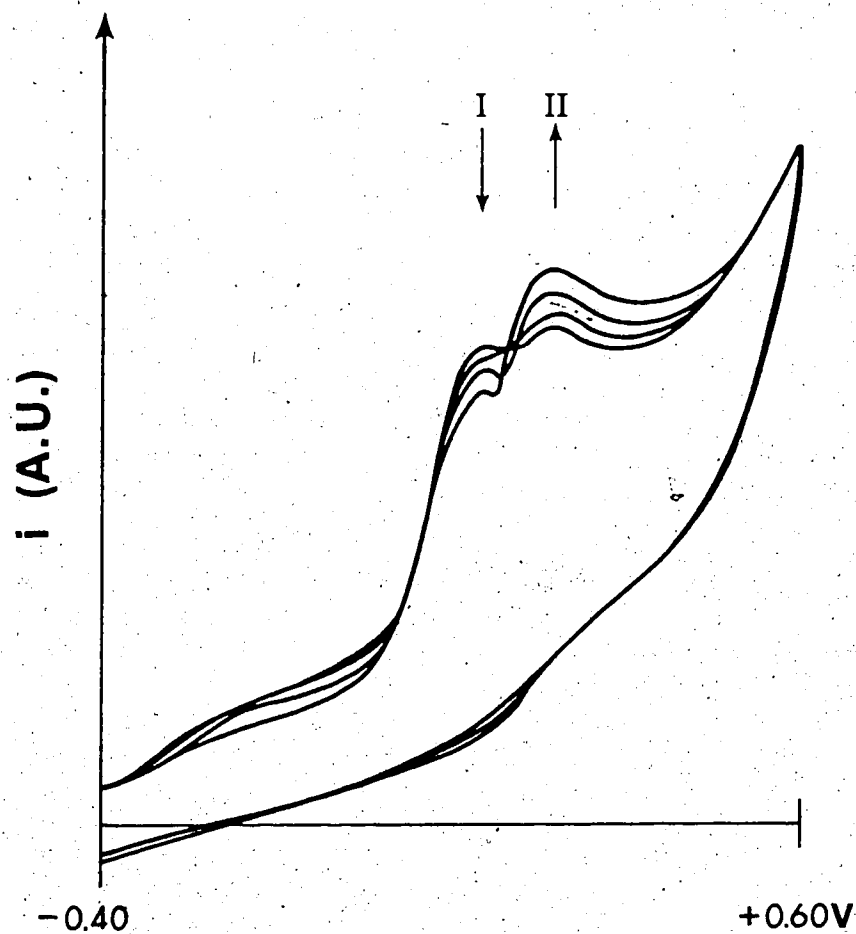
Voltammetric changes as a function of photolysis time

Broad band visible light was employed. 0.5 mM bilirubin solution in DMF with 0.15 M TBAF was used. Sweep rate was 0.10 V s^{-1}. Potentials are referenced to Ag/Ag$^+$ (0.1 M).

Figure 37

Table 2 displays the compiled results of current
monitoring during photo-oxidation. The electrode
potential was maintained at -1.30 V such that any
biliverdin produced (via photo-oxidation of bilirubin)
would be electrochemically reduced at the Pt working
electrode. The cell employed is shown in Figure 15. The
current which resulted from the electrochemical reduction
of biliverdin was integrated for 100 seconds. Background
current was measured by turning off the light and
measuring the resultant current for 100 seconds. The
electrode surface and solution were thoroughly refreshed
between runs.

Table 2. Photocurrent obtained during the photo-oxidation
of bilirubin with broadband light.

Background (100 s)		With Light (100 s)	
V-s	#e$^-$/10^{15}	V-s	#e$^-$/10^{15}
.1215	1.56	.1630	2.03
.1104	1.37	.1510	1.87
.1226	1.52	.1467	1.82
.093	1.36	.1400	1.74
.1178	1.46	.1428	1.77
.1178	1.46	.1400	1.74
.1204	1.50	.1340	1.67
.1105	1.37	.1391	1.73
.1073	1.33	.1462	1.82
.1081	1.34	.1438	1.79

Solution concentration   - .73 mM

Volume of solution upon
 which light was incident   - 1.57 × 10^{-3} cm^3

Integration time   - 100 s

Light wavelength   - 400 - 550 nm

CHAPTER 5

DISCUSSION

5.1 BILIRUBIN OXIDATION MECHANISM

Figures 18-21 show the typical voltammetric behavior

of bilirubin and biliverdin in DMF during oxidation and

reduction. To assist in the discussion of the

voltammetric response, a composite voltammogram displaying

all of the oxidation and reduction waves for bilirubin is

given in Figure 38. Wave (I) has been previously

identified [37] as the two electron oxidation of bilirubin

to biliverdin. Oxidation waves (II) and (III) have not

been discussed previously and are absent at sweep speeds

greater than 0.30 V-s^{-1}. Wave (II) appears at the same

potential as that of the oxidation potential of pure

biliverdin and was thus assigned to biliverdin

oxidation. According to the Gmelin sequence (Figure 7)

the oxidation of biliverdin leads to the production of

purpurin. Wave (III) was therefore suspected to be the

oxidation of purpurin. To confirm this assignment, pure

purpurin was prepared by the electrochemical oxidation of

biliverdin. A voltammogram of the purpurin showed an

oxidation wave at the same potential as wave (III).

101
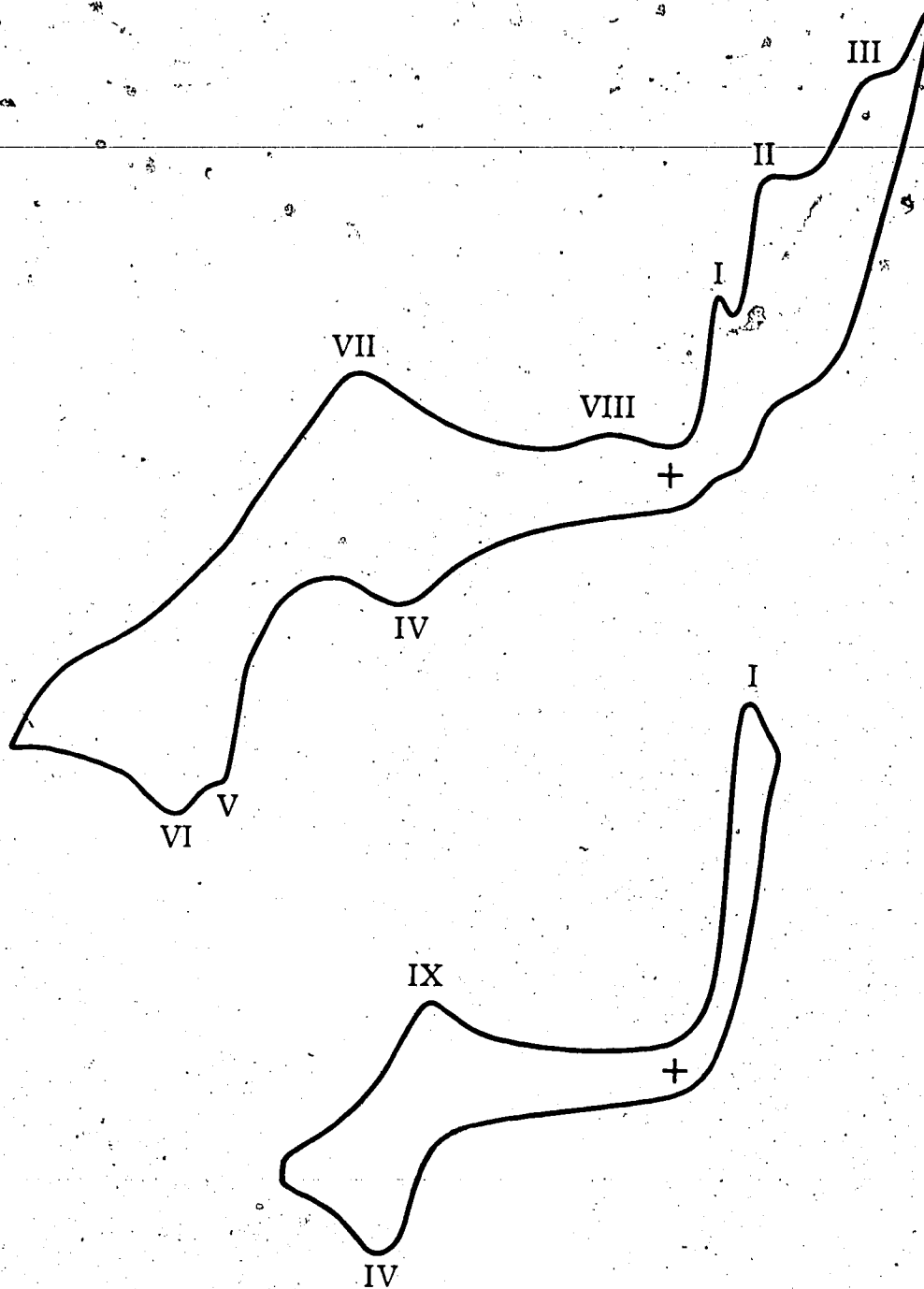
A composite of all oxidation-reduction waves
for discussion purposes.

Figure 38

A most significant voltammetric result concerning
bilirubin oxidation was appearance of the new redox couple
(waves (IV) and (IX) in Figure 38). These waves only
appear after wave (I), and are observed (Figure 24) to be
accompanied by the regeneration of bilirubin since the
peak current (i_p(I)) remains virtually constant upon
continued cycling between -1.20 V and 0.15 V vs Ag/Ag$^+$.
When the negative switching potential was reduced such
that the potential limits are -0.50 V to 0.15 V, the
bilirubin oxidation wave height falls rapidly. There
exists the possibility that wave (IV) was simply the
reduction of protons which are generated during the
oxidation of bilirubin. Protons reduce at this potential
in DMF on Pt vs Ag/Ag$^+$ (see for example Figure 20 – the
reduction of biliverdin dihydrochloride). However, when
the same potential cycling experiment (-1.20 V to 0.15 V)
was carried out on a vitreous carbon electrode, on which
the hydrogen overpotential was large, the same results as
shown in Figure 25 are obtained. It can be concluded that
some intermediate species produced during bilirubin
oxidation at peak (I) was being reduced and oxidized in
waves (IV) and (IX). The overall oxidation of bilirubin
involves the loss of two electrons and two protons. The
small size of the biliverdin oxidation wave, especially at
higher sweep rates leads to the conclusion that at least

one of the deprotonation steps was slow. Also, the inability to ever see a reverse wave for bilirubin oxidation or a transition from $n=2$ to $n=1$ at high sweep speeds indicates that the second electron transfer takes place simultaneously with, or immediately after the first. This implies that if a deprotonation step separates the electrochemical steps it must be extremely rapid.

Waves (V) and (VI) are observed to be the reduction of biliverdin and bilirubin respectively. Figure 19B confirms this. Initially the solution was pure bilirubin and as expected only one reduction wave (-1.55 V) was present. However, upon sweeping positive to 0.15 V biliverdin was produced at the electrode surface. With a subsequent potential sweep in the negative direction, the reduction of both biliverdin and bilirubin occurs. The negative potential sweep of pure biliverdin (Figure 20B) further substantiates these peak assignments.

Wave (VII) was the oxidation of some bilirubin reduction product. This wave does not appear if the negative switching potential was more positive than the halfwave potential of the bilirubin reduction wave. The final oxidation wave (VIII) was assigned to oxidation of the dianion of bilirubin [38].

Figure 22 shows the quantitative conversion of bilirubin to its dianion. As tetrabutylammonium hydroxide was added, the wave at -0.21 V increases and the 0.10 V bilirubin oxidation wave decreases. We have found that when DMF was stored in tightly sealed containers in the dark for more than two days, sufficient amounts of basic amine impurities are formed such that a noticeable chemical reaction occurs leading to formation of the dianion. While this was a nuisance and has prompted distillation of the DMF over barium oxide before use, it also has the attribute of providing us with a means of checking that the solution was indeed pure before an experiment was performed.

The effect of acid on wave (I) is shown in Figure 23. The slope decreases as the acid concentration increases but the linearity as a function of sweep rate does not deviate. It can be concluded that the rate of electrochemical oxidation was slowed by the addition of acid. From Le Chatlier's principle this was exactly what we would expect since two electrons and two protons are lost during the reaction. The observation that the biliverdin oxidation wave disappears at high sweep rates, coupled with the fact that the slope never changes from n=2 to n=1 allows us to conclude that the last step in the overall oxidation of bilirubin must be a deprotonation step.

From the six mechanistic possibilities which
initially existed as shown in Figure 39 we are now able to
eliminate the three which do not have deprotonation as the
final step. We are left with EECC, CEEC, and ECEC, where
E deontes electron transfer, and C denotes a homogeneous
chemical reaction. With this information it was now
possible to elucidate the rest of the mechanism by
employing MSRS, SMACRS, and ac voltammetry.

Because of the close relationship between $R(\omega t)$ and
$I(\omega t)$ as shown in Equation 20, ac measurements were
utilized as a complementary tool. This choice was made
for two reasons: 1) a greater signal to noise ratio may
be obtained with $I(\omega t)$, 2) $|I(\omega t)|$ increases with ω
whereas $|R(\omega t)|$ decreases. Figure 26 shows some linear
sweep ac voltammograms recorded during a potential sweep
through waves (I) and (II). While the biliverdin current
wave increases with frequency as expected, the bilirubin
wave actually gets smaller at higher frequency.

Van Norman and Szentirmay [92] have shown that
titration of bilirubin with TMG (base) has two inflection
points. They occur when one and two equivalents of TMG
per mole of bilirubin has been added. However,
electrochemically only two oxidation waves have ever been
observed, i.e. wave (I) believed to be oxidation of
neutral bilirubin and wave (VIII) oxidation of the
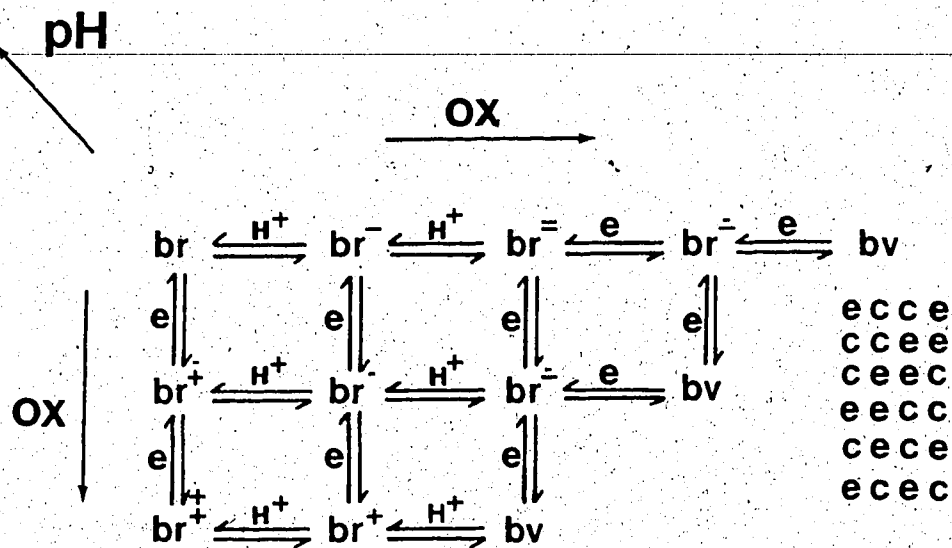
Possible mechanisms for bilirubin oxidation

Figure 39

dianion. It appears that wave (I) in Figure 38 is
actually oxidation of the anion of bilirubin which was in
equilibrium with the neutral bilirubin molecule. The
neutral, closed, hydrogen bonded molecule appears
electrochemically inert over the potential range
studied. Observation of only two bilirubin oxidation
waves (Figure 22) along with the low frequency response
leads us to suspect that the bilirubin oxidation process
must be preceeded by a chemical equilibrium between the
neutral molecule and its anionic form. This pre-
equilibrium was denoted as (P).

Figure 29 shows $R(\omega t)_{650\ nm}$ recorded during a linear
potential sweep through waves (I) and (II). Repeating
this potential sweep at twenty different wavelengths gives
the spectra shown in Figure 30. The large difference in
spectral response between the two waves indicates that
while the species being removed (B) at 0.15 V was
biliverdin as might be expected, the initially generated
species (A) at 0.04 V was something different. The
spectra shown in Figure 28B confirms that the species
being removed (B) was protonated biliverdin (the protons
residing on the nitrogens). If we recall that at the
electrode surface the solution was highly acidic due to
the rapid release of two equivalents of proton per mole of
biliverdin produced, the absorption maxima at 675 nm
(protonated biliverdin) was expected.

It was observed that the addition of acid or base causes a potential shift in both the bilirubin and biliverdin oxidation waves. In basic solutions the two waves begin to coalesce and it was impossible to determine the relative sizes of $i_p(I)$ and $i_p(II)$. From the dc voltammograms in Figure 31 it is evident that the current represents a mixed process. However, by using SMACRS, $R(\omega t)_{547\ nm}$ can be used to "track" the biliverdin ac response independently of the bilirubin oxidation process. The wavelength specific SMACRS response is shown above each voltammogram as base (Figure 31) and acid (Figure 32) were added. Voltammetry showed that a potential shift in the biliverdin oxidation wave occurs (0.065 V per decade of base added from another experiment). Clearly the oxidation of biliverdin was pH dependent. The ac reflectance shows that there exists an optimum pH at which $R(\omega t)_{547\ nm}$ was a maximum.

If $R(\omega t)_{547\ nm}$ was measured over a greater potential range (Figure 33) two further oxidation processes can be identified. Peak (II) represents the formation of some biliverdin oxidation product. Peak (III) represents subsequent purpurin oxidation (a removal peak: note positive value of $R(\omega t)$). Peak (I) was again some intermediate species produced during bilirubin oxidation. Peak (IV) was suspected to be the oxidation of

choletellin, i.e. the third oxidation product of bilirubin, as given in the Gmelin reaction (Figure 7). Due to the large background current present at this potential, it was not possible to resolve this process using voltammetric experiments.

By oxidizing bilirubin at the potential of peak (III) in the thin layer/optical cell, the spectra of the resulting species was recorded as shown in Figure 27D. This spectra confirms the identity of the species being removed at peak (III). Since peaks (I) and (II) are creation peaks (-R(ωt)) their magnitude was sensitive to the time scale of the experiment. On the ac time scale of the SMACRS experiment peaks (I) and (II) represent oxidation intermediates. However, if the solution was fully electrolyzed at the potential of peaks (I) and (II), the resultant spectra (Figure 27B-C) shows only the overall dc time scale products of biliverdin (I) and purpurin (II) oxidation.

Modulated reflectance spectra for a solution of bilirubin recorded about wave (I), (-0.50 V to 0.20 V) gave a very weak signal with $\lambda_{max} = 675$ nm as shown in Figure 34. This MSRS signal was thus due to biliverdin. Just as in the SMACRS experiment, the strongly acidic region near the electrode surface leads to the observed bathochromic shift of the biliverdin absorption maximum

from 650 nm. When the modulation limits are extended

& (-1.20 V to 0.20 V) to include wave (IV) (Figure 38) a

very strong MSRS signal was observed (Figure 35) showing

the removal of bilirubin, and the generation of a new

species with λ_{max} at 636 nm. A small shoulder at 675 nm

was still present indicating some residual protonated

biliverdin formation. At a modulation frequency of 80 Hz

the size of the 675 nm band relative to the 636 nm band

was very small.

The characteristics of wave (IV) imply that the

potential for the second electron transfer E_2 (during

bilirubin oxidation) was negative of that for the first

E_1. During the recording of the MSRS spectrum, whatever

species was generated at the upper potential 0.20 V was

reduced at the lower potential -1.2 V. Since we know that

the final proton transfer step must be slow, it was

reasonable to assign the 636 nm absorption peak to the

carbonium ion of bilirubin. This was formally the same as

the protonated biliverdin molecule. We therefore assign

the potential for E_2 as the $(Br^+ \rightarrow Br^\bullet)$ reduction

potential, where Br denotes bilirubin.

Figure 36 displays a transient recorded in a

bilirubin solution which was pulsed from -1.10 V (800 ms)

to 0.20 V (100 ms) and then back to -1.10 V. For this

study the system was not open-circuited at the conclusion

of the main (positive) pulse. It was evident from the
SMACRS and voltammetry results that we are pulsing between
potentials where creation of the bilirubin cation (upper
potential) and degradation to the bilirubin radical (lower
potential) occur. Interpretation of the transient was
complicated by the fact that Br^+ has the ability to
undergo concerted proton rearrangement producing
protonated biliverdin which does not reduce at -1.10 V,
and additionally has a greater extinction coefficient than
Br^+ at the wavelengths of interest. The sum of these two
absorbing species explains why the transient rises faster
than $t^{1/2}$.

For a conventional experiment where A ⇄ B was
reversible and only B absorbs at the wavelength
investigated, a plot of $-\log(1-\Delta R/R)$ vs $t^{1/2}$ will be
linear. When this plot was made for the transient in
Figure 36, a superlinear curve resulted. This deviation
occurs since this system has the form A ⇄ B $\xrightarrow{k}$ C where A
represents $Br^{\bullet}$, B represents Br^+ and C represents
protonated biliverdin which forms at some characteristic
rate k. Additionally, C was a greater absorber than B.
The superlinearity results from the fact that species B
forms as $t^{1/2}$ (linear) but superimposed on this rising
absorbance was the contribution of absorbance from species
C which was kinetically controlled and forms as a function

of time. The sum of these two absorbances leads of the observed response. If species C had an extinction coefficient less than species B then a sublinear curve would be observed for the plot of $-\log(1-\Delta R/R)$ vs $t^{1/2}$ [93]. The rate constant for this homogeneous complication has been shown to be [93]

$$k = \frac{A_k^T(t) - A_0^B(t)}{\int_0^t \left\{(1 + \frac{\Delta \epsilon}{\epsilon_B}) A_0^B(t) - A_k^T(t)\right\} dt} \qquad (29)$$

where $A_k^T(t)$ is the total absorbance of both species as a function of time, $A_0^B(t)$ is the absorbance of species B as a function of time in the absence of any chemical complications, and $\Delta \epsilon = \epsilon_C - \epsilon_B$ where ϵ_C and ϵ_B represent the extinction coefficients for C and B respectively. From this equation a value of $k = 0.61$ s^{-1} was obtained for the reaction.

As demonstrated earlier the spectrum of a given species can be built from a series of transients. Even in the presence of homogeneous complications, this remains qualitatively true. From Figure 36 we see that the greatest absorbance occurs at 636 nm. From the MSRS experiments we observe Br$^+$ to have $\lambda_{max} = 636$ nm, thus the spectral response of these transients supports the fact that we are initially producing Br$^+$.

When the pulse was terminated at $t = 100$ ms, species
C continues to form from residual B and absorbs light
while most of species B was being reduced back to A at
-1.10 V. This process was manifested in the second
portion of the transient where the absorbance $(-\Delta R/R)$ is
noted to decrease at a far slower rate than expected for
an A $\updownarrow$ B system.

Slifstein and Arial [39] have suggested an EECC
mechanism for bilirubin oxidation on the grounds that the
two nitrogens are oxidized at the same potential
simultaneously. The observation of wave (IV) however, was
conclusive evidence that the electron transfer steps are
separated, with $E_2 < E_1$. This fact, together with the
strong pH dependence of wave (I) leads us to discount EECC
as a likely mechanism.

The low frequency ac voltammetric response supports
CEEC as a likely mechanism, i.e. the deprotonation step
might preceed the first electron transfer. This may occur
since the carboxylic protons are quite labile and it was
possible that a N-H proton was shared with a CO_2^- group.
We feel however, that the above argument was weakly
supported, especially since we observe a SMACRS signal
during the oxidation of bilirubin; because of the
selectivity toward reversible process inherent in SMACRS,
it is unlikely that we would see an irreversible electron

transfer as would be the case for EE with $E_2 < E_1$. It is more likely that the SMACRS signal reflects E_1 of an ECE type mechanism. This possibility was supported by the pH dependence of the bilirubin $R(\omega t)$ wave shown in Figure 33. At high proton concentrations the deprotonation step is inhibited so that we see an enhanced (more reversible) $R(\omega t)$ for the first electron transfer $Br \rightarrow Br^{\bullet+}$ (Figure 33B peak I). It is clear that the enhancement of $R(\omega t)$ was not due to the biliverdin formation process. In fact, the opposite was true as evidenced by the reduced biliverdin dc oxidation wave under acidic conditions.

The low frequency ac response must therefore have another cause. The most likely possibility is intramolecular hydrogen bonding between the carboxylic acid and amino groups, causing distortion of the molecule [38] and inhibiting charge transfer. Since hydrogen bonding does not take place if the carboxylic protons are lost, a pre-equilibrium must exist in which the positioning of the carboxylic group acts as the opening or closing of a gate, i.e. non-hydrogen bonded or hydrogen bonded.

To confirm this proposed ECEC mechanism for the oxidation of bilirubin, the sweep rate dependence of i_p (I, IV, IX) in Figure 38 was examined in terms of the Nicholson and Shain theory for an ECE process [94]. A

plot of $i_p/\sqrt{v}$ vs v for each wave allows for the differentiation of the four possibilities inherent in this mechanism (I-I, I-R, R-I, R-R) where I represents an irreversible heterogeneous charge transfer step and R represents a reversible heterogeneous charge transfer step. The sweep rate was varied from 0.10 V-s^{-1} to 3.5 V-s^{-1}. The results allow for the exclusion of I-I and R-I. However, it was not possible to discriminate between R-R and I-R. From consideration of the SMACRS experiment (Figure 29) R-R is the probable mechanism (inherent sensitivity to reversible processes).

In consideration of the above results we assign wave (I) to the oxidation of Br $\rightarrow$ Br$^{•+}$, followed by deprotonation of Br$^{•+}$ and a second electron transfer yielding Br$^+$, probably in its protonated form because of the local low pH. Wave (IV) was the reduction of Br$^+$ $\rightarrow$ Br$^•$. The Br$^•$ was then reoxidized to Br$^+$ (wave (IX)), or may be protonated to form Br$^{•+}$, which was then rapidly reduced to the parent molecule Br at this potential.

These conclusions are further supported by the voltammetric results obtained in acidic solutions where wave (IX) was absent and wave (IV) enhanced, i.e. in acid solutions the protonation of Br$^•$ was accelerated. The decrease in wave (I) at higher sweep speeds was a consequence of the reversible nature of the Br$^+$ reduction

under these conditions (no bilirubin was being
regenerated).

The complete oxidation scheme was therefore proposed
to be:

$$
\begin{array}{ccccccccc}
 & -e^- & & -H^+ & & -e^- & & -H^+ & \\
Br & \rightleftarrows & Br^{\bullet+} & \rightleftarrows & Br^\bullet & \rightleftarrows & Br^+ & \rightleftarrows & Bv \\
\updownarrow -H^+ & & \updownarrow -H^+ & & \updownarrow -H^+ & & \updownarrow -H^+ & & \updownarrow -H^+ \\
 & -e^- & & -H^+ & & -e^- & & -H^+ & \\
\underline{Br} & \rightleftarrows & \underline{Br}^{\bullet+} & \rightleftarrows & \underline{Br}^\bullet & \rightleftarrows & \underline{Br}^+ & \rightleftarrows & \underline{Bv}
\end{array}
$$
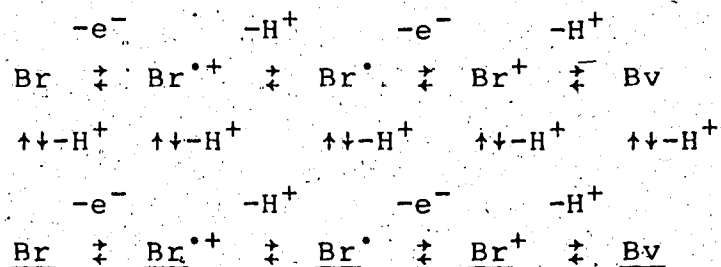
where $\underline{Br}$ means Br with a deprotonated carboxylic group.
It should be noted that the observed protonation of Bv
leading to λ_{max} = 675 nm was likely due to protonation of
the basic amine groups. Because of the low pH at the
electrode the 636 nm band was Br^+ rather than $\underline{Br}^+$ and the
broad absorption observed in the SMACRS experiment (Figure
30) was $Br^{\bullet+}$. The $Br^\bullet$ was too short lived to ever be
observed in these experiments (equilibrium concentration <
10^{-11} mol/cm^3).

Figure 40 displays a possible molecular mechanism for
bilirubin oxidation. The molecule was initially held in a
rigid twisted configuration by the hydrogen bonds between
the carboxylic groups and the pyrrole N-H groups. A
hydrogen bond-nonhydrogen bond equilibrium exists. In

Proposed mechanism for bilirubin oxidation (PECEC)

$$BR \xrightarrow{p} BR \xrightarrow[\textcircled{1}]{-e^-} BR^{\cdot+} \xrightarrow[\textcircled{2}]{-H^+} BR^{\cdot} \xrightarrow[\textcircled{3}]{-e^-} BR^+ \xrightarrow[\textcircled{4}]{-H^+} BV$$
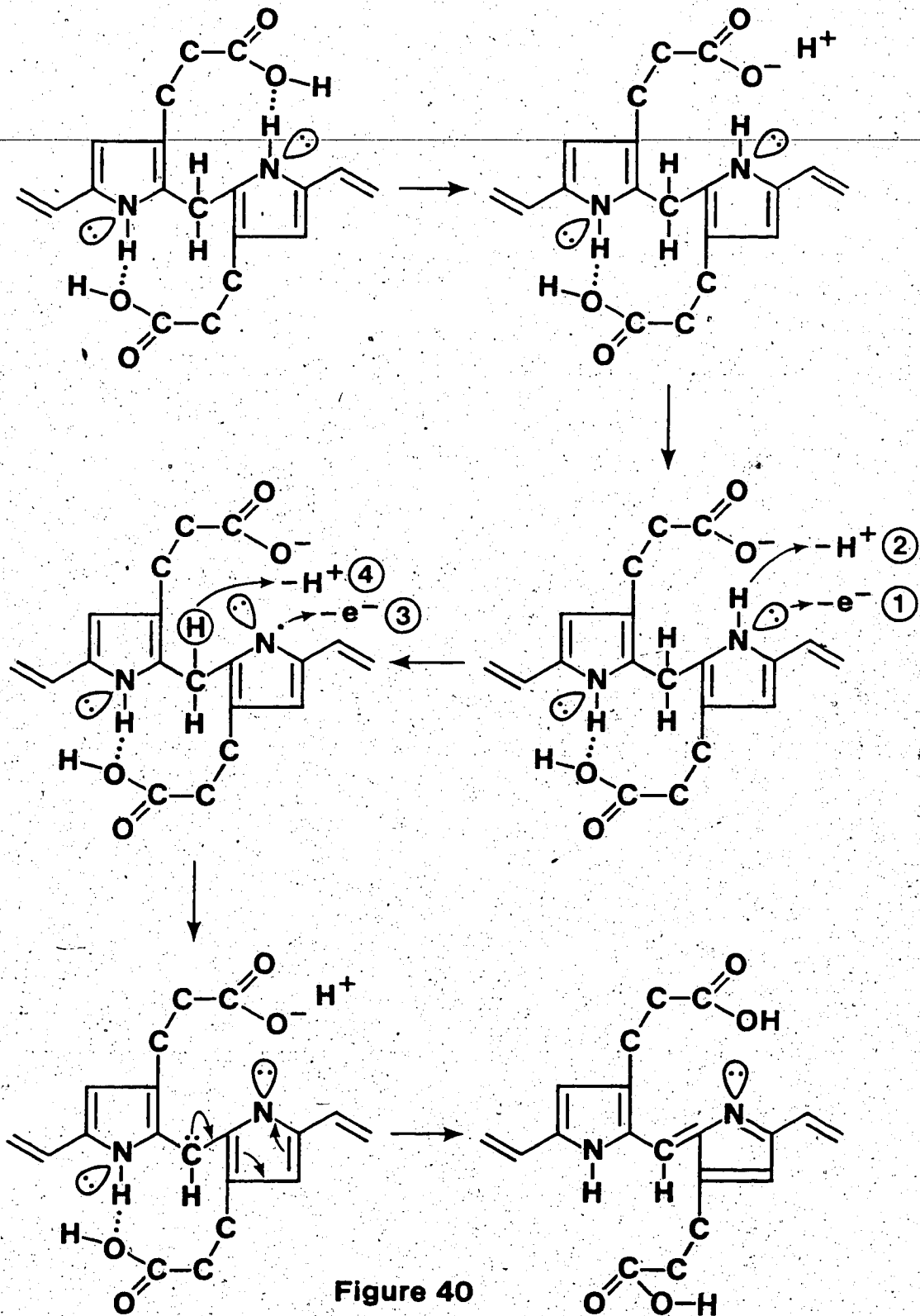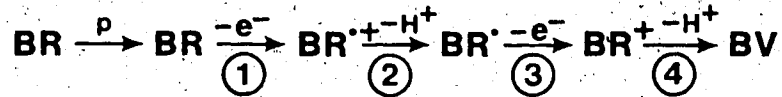
Figure 40

order for electron transfer to occur the hydrogen bond
must be broken. Once this occurs, loss of an electron and
proton at the pyrrole nitrogen takes place, leading to
formation of the radical. Another electron was
subsequently lost followed by a proton at the methane
bridge position. Upon rearrangement of electrons the new
rigid, linear tetrapyrrole exists as biliverdin, with
fully protonated carboxylic acid groups.

5.2 PHOTOCHEMISTRY

Figure 38 shows the qualitative changes observed in
the voltammetry of a bilirubin solution as a function of
photolysis time. Although numerous products are formed
during bilirubin photolysis, we are only interested in
determining the relative percent of photo-oxidation, i.e.
the percent of biliverdin produced compared to the percent
of bilirubin photolyzed. As the duration of photolysis
was increased the peak height of bilirubin was noted to
decrease. Likewise, the peak height of the biliverdin
oxidation wave increased with photolysis time.

Before proceeding with this experiment, an additional
experiment was performed to confirm that the voltammetric
response observed during photolysis indeed represented
biliverdin production. Using the cell shown in Figure 15,
the working electrode potential was fixed at -1.30 V

(biliverdin reduction potential) such that any biliverdin formed photochemically would be reduced electrochemically. The current which resulted during photolysis was monitored. Clearly biliverdin was formed (Table 2) as evident by the larger current at this potential when the light was incident upon the solution. After correcting for background and determining the volume of solution upon which the light was incident, it was found that 1.84×10^{15} molecules were photo-oxidized in a volume of solution which contained 6.9×10^{20} molecules of bilirubin. This efficiency of conversion was comparable to that previously found [6].

Returning to the original photolysis experiment (Figure 38) we note that the current can be expressed as simply a constant multiplied by C_r^b as shown in Equation 25 for an irreversible reaction, where C_r^b represents the bulk concentration of the reduced species - namely bilirubin. From this relationship it was observed that the changes in peak height directly relates to the changes in concentration of the two species. A decrease in peak height implies a decrease in concentration; an increase in peak height - an increase in concentration. By using the peak height for the bilirubin and biliverdin oxidation waves, converting them into units of current, dividing by their respective heights at photolysis time t = 0, and

plotting these absolute changes as a function of time, we obtain two lines with different slopes. The slope of these lines represents the changes in concentration of the two species as a function of photolysis time. If the photo-oxidation of bilirubin to biliverdin was 100% efficient then the slope of the two lines should be identical assuming that the diffusion coefficients and the charge transfer coefficients are identical. Dividing the slope of the biliverdin line by the slope of the bilirubin line will reveal the percent of bilirubin which was photo-oxidized to biliverdin. Following this procedure a value of 17% was calculated for the amount of biliverdin being formed during the photolysis of bilirubin.

5.3 CONCLUSIONS

The oxidation of bilirubin in DMF has been observed to be consistent with a PECEC mechanism where P is a preceeding equilibrium, E is an electrochemical step, C a chemical step and E_2 in the above-mechanism was less than E_1. Spectra are reported for Br^+ ($\lambda_{max} = 636$ nm), $Br^{\bullet+}$ (broad $\lambda_{max} = 625-700$ nm), Bv ($\lambda_{max} = 650$ nm) and protonated Bv ($\lambda_{max} = 675$ nm). Oxidation potentials for $\underline{Br^{\bullet}/Br^{\bullet+}}$ and $Br^+/Br^{\bullet}$ are reported as E = 0.10 V and -0.90 V $\underline{vs}$ Ag/Ag$^+$ (0.10 M) respectively. Through voltammetry, it has been possible to perform $\underline{in\ situ}$ monitoring of

biliverdin formation during the photo-oxidation of bilirubin. For photolysis times less than two minutes, 17% of the bilirubin has been shown to be photo-oxidized to biliverdin. From the insight which voltammetry provides along with the spectroelectrochemical selectivity of MSRS and the recently described SMACRS technique, it has been possible to elucidate the electro-oxidation mechanism of bilirubin IX-α in DMF.

REFERENCES

1. P. Manitto and D. Monti, J.C.S. Chem. Comm., 123 (1976).

2. R. Bonnett, J.E. Davies, and M.B. Hursthouse, Nature 262, 326 (1976).

3. B.T. Newbold and G. Leblanc, Can. J. Biochem. 42, 1697 (1964).

4. R. Tenhunen, H. Marver, and R. Schmid, Biochemistry 61, 748 (1968).

5. R. Tenhunem, H. Marver, and R. Schmid, J. Bio. Chem. 244, 6388 (1969).

6. L. Indyk, "Birth Defects Vol. XII #2", Editor D. Bergsma, S.H. Blondheim, American Elsevier Publishing Co. Inc., 1976, New York, pp. 23.

7. A.F. McDonagh, Biochem. Biophys. Res. Comm. 48, 408 (1972).

8. J.D. Ostrow and R.V. Branham, Gastroenterology 58, 15 (1970).

9. A.F. McDonagh and L.A. Palma, J. Am. Chem. Soc. 104, 6865 (1982).

10. P. Manitto, Specialia 15, 1147 (1971).

11. D.A. Lightner and G.B. Quistad, Nature New Biology 236, 203 (1972).

12. L. Stern, B. Doray, G. Chan, and D. Schiff, "Birth Defects Vol. XII #2", Editor D. Bergsma, S.H. Blondheim, American Elsevier Publishing Co., Inc., 1976, New York, pp. 255.

13. D. Bratlid, ibid, pp. 184.

14. E.A. Garry and T.C. Argerich, J. Lab. & Clin. Med. 62, 141 (196).

15. J.D.H. Cooper, Clin. Chem. 17, 1180 (1971).

16. H.T. Malloy and K.A. Evelyn, J. Bio. Chem. 119, 481 (1937).

17. R. Zetterstrom and L. Ernster, Nature 178, 1335 (1956).

18. H. Nakajima, J. Biol. Chem. 238, 3797 (1963).

19. H. Nakajima, T. Takemura, O. Nakajima, and Yamaoka, J. Biol. Chem. 238, 3784 (1963).

20. R. Schmid, The Metabolic Basis of Inherited Disease, 2nd Ed., McGraw-Hill, New York, 1966, p. 871.

21. T.O. Cockayne, Leechdoms, Wartcunning and Starcraft of Early England, The Holland Press, 1961, V. II, p. 107.

22. G. Stadeler, Ueber die Farbstoffe der Galle, Justus Liebigs Anal. Chem. 132, 323 (1864).

23. W. Siedel and H. Fisher, Hoppe Seylers Z. Physiol. Chem. 214, 145 (1933).

24. H. Fisher and H. Plieninger, Hoppe Seylers Z. Physiol. Chem. 274, 231 (1943).

25. H. Fisher and H. Orth, The Chemistry of Pyrrole, Vol. I,II, Akad. Verlagsges., Leipzig, 1934.

26. A.F. McDonagh and F. Assisi, FEBS Lett. 18, 315 (1971).

27. J. Fog, Scand. J. Clin. Lab. Invest. 16, 49 (1964).

28. A.F. McDonagh and F. Assisi, Biochem. J. 129, 797 (1972).

29. Z. Petryka, Ann. NY Acad. Sci. 206, 701 (1973).

30. Ibid. 707.

31. A.W. Nichol and D.B. Morell, Biochim. Biophys. Acta 177, 599 (1969).

32. R. Bonnett and A.F. McDonagh, J. Chem. Soc. D. (Chem. Commun.), 238 (1970).

33. T.K. With, Bile Pigments, New York, Academic Press, 1968, pp. 25.

34. Ibid. 25.

35. D.A. Lightner and G.B. Quistad, FEBS Lett. 25, 94 (1972).

36. A.F. McDonagh, Biochem. Biophys. Res. Commun. 44, 1306 (1971).

37. J.D. Van Norman, Anal. Chem. 45, 173 (1973).

38. J.D. Van Norman and R. Szentirmay, Anal. Chem. 46, 1456 (1974).

39. C.H. Slifstein and M. Ariel, Electroanalyt. Chem. & Interfac. Electrochem. 48, 447 (1973).

40. C.H. Slifstein and M. Ariel, J. Electroanal. Chem. 75, 551 (1976).

41. P. Longhi, P. Manitto, D. Monti, T. Mussini and S. Rondinini, Electrochimica Acta 26, 541 (1981).

42. J.F. Lucey, Seminars in Hematology 9, 127 (1972).

43. E.W. Callahan, M.M. Thaler, M. Karon, Pediatrics 46, 841 (1970).

44. J.D. Ostrow, J. Clin. Invest. 50, 707 (1971).

45. H.T. Lund and J. Jacobsen, Acta Paediatr. Scand. 61, 693 (197).

46. S.H. Blondheim, D. Lathrop, J. Zabriskie, J. Lab. Clin. Med. 60, 31 (1962).

47. J. Kapitulnik, S.H. Blondheim, A. Grunfeld, and N.A. Kaufmann, Clin. Chim. Acta 47, 159 (1973).

48. A.F. McDonagh and L.A. Palma, unpublished observations.

49. E. Garbagnati and P. Manitto, J. Pediatr. 83, 109 (1973).

50. D.A. Lightner, D.C. Crandall, S. Gertlers, and G.B. Quistad, FEBS Lett. 30, 309 (1973).

51. R. Bonnett and J.C.M. Stewart, J. Chem. Soc. Chem. Commun., 596 (1972).

52. J.S. Bellin, Photochem. Photobiol. 8, 383 (1968).

53. D.A. Lightner and G.B. Quistad, Science 175, 324 (1972).

54. R. Bonnett and J.C.M. Stewart, Biochem. J. 130, 895 (1972).

55. J.W. Sargent and R.J. Sieffl, Red. Proc. 29, 1699 (1970).

56. H. Mark and E. Randall, Symp. of the Faraday Soc. 4, 157 (1970).

57. D. Laser and M. Ariel, J. Electroanal. Chem. 35, 405 (1972).

58. A. Trifanov and I. Schopov, ibid., 415.

59. J. Robinson, Ph.D. Thesis, U. of Southampton, 1976.

60. W. Heineman and T. Kuwana, Anal. Chem. 43, 1075 (1971).

61. J. Strojek and T. Kuwana, J. Electroanal. Chem. 35, 471 (1968).

62. G. Grant and T. Kuwana, ibid., 24, 11, 1970.

63. M. Petek, T. Neal and R. Murray, Anal. Chem. 43, 1069 (1971).

64. R. Archer, J. Electrochem. Soc. 104, 619 (1957).

65. A. Bewick, J. Mellor and S. Pons, Electrochem. Acta 23, 77 (1978).

66. A. Bewick and A. Tuxford, Symp. Faraday Soc. 4, 116 (1970).

67. D. Schwab, unpublished results.

68. H. Mark and S. Pons, Anal. Chem. 38, 119 (1966).

69. S. Pons, J. Mattson, L. Winstrom and H. Mark, ibid., 39, 685 (1967).

70. R. Vonbenken and T. Kuwana, ibid., 42, 1114 (1970).

71. A. Bewick, J. Mellor and S. Pons, Electrochimia. Acta 25, 931 (1980).

72. S. Pons and S.B. Khoo, J. Am. Chem. Soc. 104, 3845 (1982).

73. S. Pons, T. Davidson and A. Bewick, J. Am. Chem. Soc. 105, 1802 (1982).

74. B.S. Pons, private communication.

75. N. Winograd, H.N. Blount and T. Kuwana, J. Phys. Chem. 73, 3456 (1969).

76. A.W. Aylmer-Kelly, A. Bewick, P.R. Cantrell and A.M. Tuxford, Dis. Faraday Soc. 56, 96 (1973).

77. A.S. Hinman, J.F. McAleer and B.S. Pons, J. Electroanal. Chem., in press.

78. D.E. Smith, "Electroanalytical Chemistry, Vol. 1", A.J. Bard, Editor, Marcel Dekker, New York, 1966, pp. 1-155.

79. A.M. Bond, R.J. O'Halloran, I. Ruzic and D.E. Smith, Anal. Chem. 50, 216 (1978).

80. A.J. Bard and L.R Faulkner, "Electrochemical Methods", John Wiley and Sons, New York, 1980, p. 219.

81. Ibid, pp. 222.

82. A.M. Bond, R.J. O'Halloran, I. Ruzic, and D.E. Smith,
     Anal. Chem. 48, 872 (1976).

83. D.T. Sawyer and J.L. Roberts, "Experimental
     Electrochemistry", John Wiley & Sons, Inc., 1974, pp.
     347-349.

84. Cell designed by Dr. J.F. McAleer.

85. T.K. With, Bile Pigments, Academic Press, New York,
     1968, pp. 28.

86. H.W. Siegelman, D.J. Chapman and W.J. Cole,
     Porphyrins and Related Compounds, Academic Press,
     London, New York, 1968, pp. 107.

87. J.J. Lee and M.L. Cowger, Res Commun. Chem. Path.
     Pharmac. 5, 505 (1973).

88. D.A. Lightner and D.C. Crandall, FEBS Lett. 20, 53
     (1972).

89. A.F. McDonagh and R. Bonnett, J. Chem. Soc. Chem.
     Commun., 238 (1970).

90. P. Manitto and D. Monti, Specialia 35, 9 (1979).

91. H. Lund and P. Iverson, "Organic Electrochemistry",
     M. Baizwer, Editor, Marcel Dekker, New York, 1973.

92. J.D. Van Norman and R. Szentirmay, Bioinorganic Chem.
     4, 37 (1974).

93. J.F. McAleer, B.S. Pons and J.R. Pradko, in
     preparation.

94. R.S. Nicholson and I. Shain, Anal. Chem. <u>36</u>, 707
     (1964).